TOXICOLOGICAL CHARACTERISTICS OF PARTICULATE MATTER IN AN URBAN ENVIRONMENT AND THEIR LINKAGE TO THE SOURCE-SPECIFIC CONSTITUENTS

by

Vishal Verma

A Dissertation Presented to the
FACULTY OF THE USC GRADUATE SCHOOL
UNIVERSITY OF SOUTHERN CALIFORNIA
In Partial Fulfillment of the
Requirements for the Degree
DOCTOR OF PHILOSOPHY
(ENVIRONMENTAL ENGINEERING)

May 2011

Dedication

To my Anjalu
for her persistent love, motivation, and faith in my abilities
&
To my mother
for her unconditional love and support throughout my life

Acknowledgements

I would like to take this opportunity to express my sincere thanks to all those people who made it possible for me to complete this thesis. It is my great pleasure to convey my sincere gratitude to all of them with my humble acknowledgement.

To begin with, I am deeply indebted to my graduate advisor Prof. Constantinos Sioutas, who gave me an opportunity of working under his guidance and also his whole hearted support, interest and encouragement, that made this work possible. His thoughtful discussions on technical aspects, deep interest and enthusiasm in aerosol research and pragmatic approach towards problem solving have helped me to develop the scientific acumen.

I express deep sense of gratitude to the members of my guidance committee, Prof. Ronald C Henry and Prof. Nicos A Petasis for providing thoughtful and insightful suggestions on my research work as well as dissertation.

I would also like to thank my previous and current lab mates and friends both in the group at USC and in collaborative institutions. I want to thank the post doctors in our group: Dr. Zhi Ning, Dr.Subhasis Biswas, Dr. Markus Sillanpaa, and also Debbie and Emma from UCLA who have provided valuable advice in science discussion and guidance in the papers writing. Special thanks also go to Dr. Andrea

Polidori. It is his advice and exceptional experience that have helped me during the initial days of my study at USC. I also extend my thanks to Payam Pakbin, Neelakshi Hudda, Kalam Cheung, Winnie Kam, Nancy Daher, Zhen Xu, Diana, Niloofar, Shruthi, and Risabh Jain and for their valuable support.

Last but not the least, I would like acknowledge my wife (Geetanjali), my parents (Savitri Devi and Inder Kumar Verma), my friends (Satya Da, Babu, Harish Bhai) who helped me directly or indirectly throughout the work.

Table of Contents

Dedication ii

Acknowledgements iii

List of Tables viii

List of Figures ix

Abstract xii

Chapter 1: Introduction 1
  1.1 Background 1
    1.1.1 Characteristics and Sources of Particulate Matter (PM) 1
    1.1.2 Health Effects of Particulate Matter 3
  1.2 Rationale for the Present Study 4
  1.3 Thesis Layout 7

Chapter 2: Physicochemical and Toxicological Properties of PM Emissions from Heavy-Duty Diesel Vehicles 10
  2.1 Introduction 10
  2.2 Experimental Methods 11
    2.2.1 Vehicles 13
    2.2.2 Equipment and Instruments 16
    2.2.3 Sample Analysis 18
  2.3 Results and Discussion 19
    2.3.1 Size Distribution 19
    2.3.2 Size Segregated Mass Emission Factors 25
    2.3.3 Particle Volatility 28
    2.3.4 Emission Factors (EF) of Inorganic Ions and Total Carbon (TC) 30
    2.3.5 Size Segregated Chemical Speciation 35
    2.3.6 DTT Activity 38
    2.3.7 Water Soluble Organic Carbon and DTT 45
    2.3.8 Correlation between Chemical Species and Oxidative Potential 46
  2.4 Conclusions 47

Chapter 3: Toxicity Profiles of Ambient Particles Influenced by Vehicular, Woodsmoke and Secondary Photochemical Sources 49
3.1 Oxidative Activity Profiles of Ambient Particulate Matter from Primary and Secondary Sources 49
3.1.1 Introduction 49
3.1.2 Experimental Methods 51
3.1.2.1 Sampling Location 51
3.1.2.2 Sampling Protocol 52
3.1.2.3 Sample Analysis 54
3.1.3 Results and Discussion 55
3.1.3.1 Physical Parameters 55
3.1.3.2 Chemical Parameters 58
3.1.3.3 Oxidative Activity 66
3.1.3.4 Correlation of Oxidative Activity with Chemical Constituents of PM 71
3.1.4 Conclusions 77
3.2 Oxidative Activity Profiles of Ambient Particulate Matter Influenced by Woodsmoke Emissions from Wildfires 78
3.2.1 Introduction 78
3.2.2 Experimental Methods 79
3.2.2.1 Sampling Location 79
3.2.2.2 Sampling Protocol 80
3.2.2.3 Sample Analysis 81
3.2.3 Results and Discussion 81
3.2.3.1 Particulate Matter Characteristics 81
3.2.3.2 Gaseous Pollutants 84
3.2.3.3 Water Soluble Trace Elements 85
3.2.3.4 Water Soluble Organic Carbon (WSOC) 87
3.2.3.5 Organic Constituents 88
3.2.3.6 PM Oxidative Activity 91
3.2.4 Conclusions 97

Chapter 4: Contribution of Semi-Volatile Organic Compounds and Non-Volatile Transition Metals in the PM Oxidative Activity 98
4.1 Contribution of Semi-Volatile Organic Compounds in the Oxidative (DTT) Activity of Ambient Particles 98
4.1.1 Introduction 98
4.1.2 Experimental Methods 100
4.1.2.1 Sampling Location 100
4.1.2.2 Sampling Protocol 100
4.1.2.3 Sample Analysis 104
4.1.3. Results and Discussion 104
4.1.3.1 Physical Parameters 104
4.1.3.2 Chemical Parameters 110

4.1.3.3 Oxidative Potential 118
4.1.3.4 Association of Oxidative Potential with PM Chemical Composition 120
4.1.4 Summary and Conclusions 122
4.2 Contribution of Transition Metals in the Reactive Oxygen Species Activity of PM Emissions from Retrofitted Heavy-Duty Vehicles 123
4.2.1 Introduction 123
4.2.2 Experimental Methods 124
4.2.2.1 Sampling Protocol 124
4.2.2.2 Sample Analysis 125
4.2.3 Results and Discussion 127
4.2.3.1 Water Soluble Metals 127
4.2.3.2 Macrophage ROS Activity 132
4.2.3.3 Chelex Treatment 135
4.2.3.4 Statistical Association between ROS Activity and Metals 138
4.2.4 Summary and Conclusions 145

Chapter 5: Conclusions and Future Research Directions 147
5.1 Summary and Conclusions 147
5.2 Recommendations 149

Bibliography 154

Appendix 170

List of Tables

Table 2.1:	Details of test fleet	14
Table 2.2:	Size fractionated mass EFs of test fleet	26
Table 2.3:	Correlation coefficient (R) and significance level (p) for oxidative potential (measured by DTT) and selected chemical species from test fleet	46
Table 3.1:	Average concentrations of water-soluble elements in ambient quasi-ultrafine particles at the USC sampling site during morning and afternoon periods	61
Table 3.2:	Summary of the regression analysis for select species with DTT and ROS levels of ultrafine particles at USC sampling site.	73
Table 3.3:	Average fractional concentration of water soluble elements (ICP-MS) in ambient particles collected at the USC site during and after the fire event	86
Table 3.4:	Coefficients of statistical determination (R^2) and associated levels of significance (p-value) for the correlations between selected water soluble PM constituents and redox activities (as measured by the DTT and ROS assays) for PM samples collected during and after the fire period.	96
Table 4.1:	Summary of the regression analysis between major PM chemical constituents and DTT activity of the ambient and thermodenuded ultrafine particles.	121
Table 4.2:	Pearson correlation coefficients and associated levels of significance for the univariate regression between ROS activity and major water-soluble metals of PM from the test fleet	139
Table 4.3:	Parameters of the multivariate regression analysis between ROS activity and water-soluble metals of PM from the test fleet	144

List of Figures

Figure 2.1: Experimental set-up (Dynamometer) 12

Figure 2.2: Particle (exhaust) number size distribution of the test fleet 21

Figure 2.3: Number (DMS) and mass emission factors (nano-MOUDI) for exhaust particles from the test fleet 27

Figure 2.4: Size distribution of thermo denuded aerosols for cruise driving mode of the test fleet 29

Figure 2.5: Emission factors of integrated chemical species (from the test fleet) measured by MOUDI-NanoMOUDI 31

Figure 2.6: EC, WSOC and WIOC emission rates from the test fleet 33

Figure 2.7: Emission rates of size-resolved PM chemical species from the test fleet 36

Figure 2.8: Oxidative potential (DTT consumption in n-moles min^{-1} μg^{-1} of PM) of thermo-denuded and undenuded PM from the test fleet 40

Figure 2.9: Relationship between oxidative activity and semivolatile PM fraction at 150 °C for the PM emitted from test fleet 42

Figure 2.10: DTT consumption rate (for the exhaust particles) per unit distance traveled by vehicles 43

Figure 2.11: DTT consumption in relation to the water-soluble organic carbon (WSOC) of PM from the test fleet 45

Figure 3.1: Diurnal profile of the average particle number concentration of quasi-ultrafine particles measured at the USC sampling site and the average particle number size distribution in “morning” and “afternoon” periods 57

Figure 3.2: Average concentration of the major inorganic ions in quasi-ultrafine particles collected in the morning and afternoon periods at the USC sampling site 58

Figure 3.3: Average concentration of the various organic species measured at the USC sampling site during the morning and afternoon periods 62

Figure 3.4: Oxidative activity (DTT) of quasi-ultrafine particles collected at the USC sampling site during the morning and afternoon periods 68

Figure 3.5: Oxidative activity (ROS) of quasi-ultrafine particles collected at the USC sampling site during the morning and afternoon periods 70

Figure 3.6: Evolution of the particle number size distribution from days characterized by wildfire emissions to periods not directly affected by fire 83

Figure 3.7: 24-hr averaged concentration of NO, NO2, CO and O3 at North Main Street (Los Angeles) and Particle Number Concentration at the USC (also 24-hr average) before, during and after the fire period 84

Figure 3.8: Fractional concentration of the organic constituents in PM samples collected at the USC site, during and after the fire events 89

Figure 3.9: Oxidative activity of PM samples collected at the USC site during and after the fire period 92

Figure 4.1: Experimental setup for sampling ambient semi-volatile particles 102

Figure 4.2: Particle size distributions (number and volume based) of the concentrated ambient and thermodenuded particles at 50, 100 and 200 ^{o}C 107

Figure 4.3: Concentration of water soluble inorganic ions in the concentrated ambient and thermodenuded particles at different TD temperature configurations – 50, 100, 200 ^{o}C 112

Figure 4.4: Concentration of elemental and organic carbon in the concentrated ambient and thermodenuded particles collected at three TD temperature configurations (50, 100 and 200 ^{o}C) 114

Figure 4.5: Concentration of PAHs in concentrated ambient and thermodenuded aerosols collected at three TD temperature configurations – 50, 100 and 200 °C 117

Figure 4.6: Percentage loss in oxidative potential, measured by DTT activity on heating the ambient aerosols at 50, 100 and 200 °C 118

Figure 4.7: Distribution of water-soluble metals in the exhaust PM from various vehicle-configurations, under three driving cycles, i.e. cruise, UDDS and idle 128

Figure 4.8: Water-soluble content (µg/g) of major redox active metals in the exhaust PM from various vehicle-configurations 131

Figure 4.9: Reactive Oxygen Species (ROS) activity of PM from the tested vehicles 133

Figure 4.10: Percent removal (average of all vehicle-configurations) of major water-soluble elements using Chelex treatment of the exhaust PM samples 136

Figure 4.11: Percent removal of ROS activity in relation to that of aggregate water soluble metals after Chelex treatment of the exhaust PM samples from test vehicle-configurations under different driving cycles 137

Figure 4.12: Correlation of measured and reconstructed ROS activity with successive inclusions of different species in the multivariate regression model 142

Abstract

A number of population based epidemiological studies as well as recent toxicological and clinical studies indicate a strong association between particulate matter (PM) exposure and adverse health outcomes. Despite commendable progress in particle-related toxicological research for the last few decades, the exact mechanisms by which PM inflicts health injuries are still largely unknown and constitute a subject of great interest for the scientific community. An increase in the abundance of reactive oxygen species (ROS) in biological systems after PM exposure and the resulting oxidative stress has been hypothesized to be mostly responsible for the initiation of inflammatory cascades.

The core objective of this work is to determine the toxicological characteristics of particulate matter in an urban environment and to investigate their associations with the source-specific particle constituents. This objective has been accomplished by evaluating the oxidative potential of particles collected from various sources such as exhaust tail pipe of the heavy-duty diesel vehicles, wood-smoke and ambient particles in segregation to their primary and secondary sources. The role of semi-volatile organic compounds in the oxidative activity of PM was assessed by their removal using thermodenuder and measuring the resultant oxidative potential by DTT assay. Similarly, the contribution of transition metals was quantified by their chelation using Chelex® chromatography. The use of statistical tools (bivariate and multivariate regression techniques) further supported in identification of the specific PM constituents responsible for major variability in the responses of toxicological assays. The results demonstrate the importance of both semi-volatile (organic compounds) and non-volatile (transition metals) species of particulate matter in stimulating the generation of different oxidizing species in biological systems, measured by DTT and ROS assay. These findings are useful in elucidating the health risks related to the PM exposure from different sources and ultimately in promulgating the effective control strategies to protect public health.

Chapter 1: Introduction

1.1 Background

1.1.1 Characteristics and Sources of Particulate Matter (PM)

Particulate matter is a general name given to the solid particles and/or liquid droplets, and when suspended in air, is also known as aerosol. Particulate matter is a mixture of many subclasses of chemical species - both organic and inorganic, most of which are potentially hazardous to human health. Particulate matter can be divided into three broad categories based on their aerodynamic diameters. These modes are: coarse mode (2.5-10 μm), accumulation mode (0.1-2.5μm) and the ultrafine mode (0.01-0.1 μm). Particles with aerodynamic diameter larger than 10 μm are usually not the point of interest in environmental and health studies because of their short life time in the atmosphere. The aerodynamic diameter of particles is an important property because it determines majority of its behavior in the atmosphere such as residence time and deposition characteristics in the human respiratory system.

The sources of airborne particulate matter can be divided into two broad categories: primary and secondary. Primary sources include combustion sources (heavy and light duty vehicles, woodsmoke, industries), and construction activities. The particles emitted from these primary sources may undergo photochemical processing in the presence of various atmospheric oxidants to yield secondary particles. The physical and chemical characteristics of these secondarily formed particles are distinctly different compared to their primary precursors. The secondary photochemical reactions in addition to the vehicular emissions constitute the most prominent sources of ultrafine particles in an urban metropolis like Los Angeles (Fine et al., 2004).

Another important property of the particulate matter which governs its existence either in particle or gas phase is the volatility. Thus, particulate matter can be considered as a complex mixture of semi-volatile (most organic compounds and the major inorganic ions – ammonium, sulfate and nitrate) and non-volatile (metals, elemental carbon and few organic compounds) species (Seinfeld and Pandis, 2006). The semi-volatile compounds exist simultaneously in the gas and particle phases at equilibrium. The vapor pressure of these compounds is a strong function of temperature, which determines the extent of their partitioning into particulate and gaseous phase at a given concentration. Recent studies have indicated that the organic compounds volatilized and subsequently photo-oxidized from the semi-volatile fraction of the particles substantially contribute to the formation of secondary organic aerosol (SOA) (Robinson et al., 2007). This contribution far exceeds that from the photo-oxidation of primary volatile organic compounds (VOCs).

Heavy-duty diesel trucks constitute only a small fraction of the total fleet in California but have an important contribution to the emissions of fine and ultrafine particles. Efforts from both the regulatory and the manufacturing communities have been devoted to the reduction of emissions from diesel-powered engines. US EPA 2007 emissions standards enforce to reduce the diesel PM mass emissions from heavy-duty engines ten fold from the old 0.1 g bhp^{-1} h^{-1} PM limit to 0.01 g bhp^{-1} h^{-1} (Merrion, 2003). These new emission standards motivated the development of several after-treatment devices for in-use heavy-duty diesel vehicles (HDDVs), e.g. diesel particulate filter (DPF) and selective catalytic reduction (SCR) retrofits to reduce the PM and NO_x emissions, respectively. Although, these after-treatment devices significantly reduce the mass emission rates (McGeehan et al., 2005) of DEPs, but not necessarily the number-based particle emissions. Several studies have shown that under certain conditions, enhanced formation of ultrafine particles occurs by heterogeneous nucleation for the vehicles equipped with after-treatment devices (Kittelson et al., 2006; Vaaraslahti et al., 2004).

1.1.2 Health Effects of Particulate Matter

Both epidemiological and clinical research have demonstrated strong links between atmospheric aerosols and adverse health effects, including premature deaths (Hoek et al., 2002; Samet et al., 2000), respiratory and cardiovascular diseases (Gauderman et al., 2007; Riediker et al., 2004; Stayner et al., 1998), and neurodegenerative disorders (Peters et al., 2006). Particles deposit in different parts of the lung according to their aerodynamic diameter, resulting in varying degree of toxic potency. *In-vitro* and *in-vivo* experiments have linked particle exposure to airway inflammation, mitochondrial damage and lung cancer (Castranova et al., 2001; Garshick et al., 2004; Kumagai et al., 1997; Li et al., 2003; Saldiva et al., 2002; Yin et al., 2007). Chronic exposure of DEPs may lead to exacerbation of pulmonary diseases such as asthma and bronchitis as well as lung cancer (Garshick et al., 2004; Rusznak et al., 1994). Alveolar macrophages (AM), which are responsible for the defense of susceptible cells, release pro-inflammatory cytokines in the presence of PM constituents, such as polycyclic aromatic hydrocarbons (PAHs), and may experience alteration in their gene expressions (Koike et al., 2002). A few studies have also described negative impacts of PM on reproductive systems (Watanabe and Oonuki, 1999), liver functions (Folkmann et al., 2007) and brain activity (Cruts et al., 2008).

1.2 Rationale for the Present Study

The exact mechanisms by which particulate matter inflicts health injuries remain largely unknown; however, PM-associated reactive oxygen species (ROS), and the resulting oxidative stress induced in human tissues is believed to be implicated in inflammatory effects. In healthy biological systems, natural generation of ROS as a result of aerobic metabolism is balanced through scavenging by endogenous antioxidants (Halliwell and Cross, 1994); oxidative stress results when ROS concentrations exceed the capacity of the antioxidant systems to maintain ROS levels within physiologically normal ranges. Toxicological studies have confirmed the oxidative activity of particulate matter and its ability to stimulate cellular generation of ROS (Donaldson et al., 1996; Donaldson et al., 2002; Donaldson et al., 2003; Kunzli et al., 2006). A few investigations have also linked PM toxicological characteristics to their chemical composition, most notably to organic species and transition metals (Chen and Lippmann, 2009; Cho et al., 2005; DiStefano et al., 2009; Ntziachristos et al., 2007; Shafer et al., 2010). Most of these studies indicate a consistently higher oxidative potential on a per PM mass basis of quasi-ultrafine particles (e.g. ≤250 nm) compared to the fine and coarse particles (Cho et al., 2005; Donaldson et al., 2002; Ntziachristos et al., 2007).

Both molecular and cellular assays have been used to examine PM-induced oxidative stress. In molecular (cell-free) assays, chemical method such as consumption of dithiothreitol [DTT; (Cho et al., 2005)] has been used. The DTT assay determines in quantitative terms the capacity of a test sample to transfer electrons from dithiothreitol (DTT) to oxygen – a reaction analogous to the cellular redox reaction involving NADPH and oxygen. The electron transfer is monitored by the rate at which DTT is consumed under a standardized set of conditions, and the rate is proportional to the concentration of the redox-active species in the PM sample. To assess the relevance of this assay to cellular effects, studies have been conducted in which the DTT based redox activity of a sample has been compared with its capacity to induce the stress protein, hemeoxygenase-1 in two cell lines – RAW264.7 and BEAS-2B. RAW 264.7 is a murine macrophage cell line that mimics the oxidative stress response of pulmonary alveolar macrophages (Hiura et al., 1999; Li et al., 2002), and BEAS-2B is a transformed human bronchial epithelial cell line, which mimics the oxidative stress response of primary bronchial epithelial cells (Li et al., 2002). DTT activities of PM samples were found to correlate with the induction of hemeoxygenase-1 in both cell lines (Li et al., 2003). These data suggest that redox activity measured by this procedure is a reasonable predictor of oxidative stress status in cells.

Fluorescent probes such as 2′,7′- dichlorofluorescein diacetate (DCF) (Becker et al., 2005) has been extensively employed to study the cellular generation of ROS. The macrophage ROS assay is a fluorogenic cell-based method to examine the production of reactive oxygen species and is performed in rat alveolar macrophages (NR8383, American Type Culture Collection), which are exposed to aqueous suspensions of PM. The ROS probe used in this method – DCFH-DA (2,7-dichlorodihydrofluorescein diacetate) is a non-fluorescent, membrane permeable compound. Upon entering a cell, it is de-acetylated by cellular house-keeping esterases, yielding 2,7-dichlorodihydrofluorescein (DCFH). Non-fluorescent DCFH can then be converted by free radicals and other oxidants within the cell into the highly fluorescent 2,7-dichlorofluorescein (DCH) which can be easily monitored using a fluorescence plate reader. Further details of this assay are given in Landreman et al., (2008).

While each of these assays was putatively considered a germane tool for measurement of net PM oxidative activity in biochemical systems, an increasing body of evidence, discussed in literature (Cho et al., 2005; DiStefano et al., 2009; Shinyashiki et al., 2009) suggests that the various toxicity assays are selective in their response to different PM constituents. It is thus generally believed that knowing particle chemical composition along with their physical attributes and source of emissions may be the critical starting point in understanding the fraction within PM that drives the health effects.

The primary objective of this study is to evaluate the toxicological characteristics of particulate matter in an urban environment and their linkages to the source-specific particle constituents. This objective is carried out by collecting both ultrafine and fine particles from an array of diverse emission sources, i.e. primary (heavy-duty diesel vehicles, and ambient PM influenced by vehicular and woodsmoke emissions), and secondary photochemical sources. Both cell-free (DTT) and cell-based (macrophage ROS) assays were used to evaluate the oxidative activity of the collected particles. In addition, physicochemical characteristics of the sampled particles, such as particle number distribution, elemental and organic carbon, water soluble organic carbon, water soluble elements, inorganic ions and organic species were also analyzed. The associations of PM chemical constituents with their oxidative characteristics were investigated by mechanistic (physicochemical segregation of PM constituents) and statistical (bivariate and multivariate regression) techniques. This study offers a novel and informative perspective on the relationship between composition and sources of atmospheric particles to their relative toxicity potential.

1.3 Thesis Layout

This thesis is divided into five chapters:

Chapter 1 is the introduction and gives an overview of the particulate matter along with their sources, characteristics and health effects. It also sets up the rationale for the present study.

Chapter 2 describes the physicochemical and toxicological characteristics (i.e. size distribution, volatility, size-resolved chemical components, and DTT activity) of PM emitted from heavy-duty diesel vehicles retrofitted with state-of-the-art after-treatment devices. Apart from assessing the potency of semi-volatile species to induce oxidative stress, the results are useful in assessing the efficacy of these control technologies and in establishing the future needs for additional measures to control these PM species.

Chapter 3 discusses the physicochemical and toxicological characteristics of ambient particles from different primary and secondary sources (e.g. vehicular emissions, woodsmoke, and secondary photochemical reactions) at an urban site near downtown Los Angeles.

Chapter 4 explores the linkages between chemical constituents of PM with their toxicological profiles. Both mechanistic (physicochemical segregation of PM constituents) and statistical (bivariate and multivariate regression) analyses have been performed to quantify the contribution of these species in oxidative activity of the particles.

Finally, Chapter 5 of the thesis is the concluding chapter which summarizes the findings of the present investigation. It also identifies the limitations associated with the current methodologies and provides recommendations to improve upon. The chapter thus paves the road for future investigations aimed at a better assessment of the role of different PM constituents in the observed health effects.

Chapter 2: Physicochemical and Toxicological Properties of PM Emissions from Heavy-Duty Diesel Vehicles

2.1 Introduction

Diesel exhaust particles (DEPs) are normally agglomerates of hundreds of volatile/semi-volatile species adsorbed onto its refractory carbonaceous core (Bayona et al., 1988). As general perception has emerged towards the potential risks of diesel particulate matter, policy makers are promulgating stricter emission control rules and regulations. To effectively meet such stringent emission standards, various advanced engine design and control technologies are being considered and rigorously evaluated for the newer fleet of heavy duty trucks. While these after-treatment devices (such as DPF) have been highly efficient in removing refractory solid particles (>50nm), some of the potentially harmful volatile and semi volatile species (such as PAHs), originally emitted in the vapor phase at high plume temperature, may penetrate through (Kittelson, 1998; Matter et al., 1999). As the exhaust temperature decreases drastically at the tail pipe exit, these vapor phase species condense and form fresh nucleation mode particles (Kittelson, 1998).

There has been a limited number of papers in the literature reporting the chemical composition of PM emissions from diesel vehicles equipped with DPF and SCR retrofits (Grose et al., 2006), especially for newer vehicles meeting the US 2007 emission standards. To a certain degree, these studies are limited by the insufficient PM mass of the exhaust that poses a challenge for detailed chemical analysis. Nevertheless, PM emissions from a diesel engine with advanced after-treatment devices are fundamentally different than that from an uncontrolled diesel engine with respect to particle size, morphology, and chemical composition.

The primary objective of this collaborative study between the California Air Resources Board (CARB) and the University of Southern California is to evaluate the physicochemical (size distribution, volatility, size-resolved chemical composition) and toxicological characteristics of the volatile and non-volatile fractions of particles emitted from a variety of different engines, fuels and emissions control, each operating under different driving conditions using a dynamometer set-up. Comparisons within heavy-duty vehicle types and driving cycles and also with respect to a baseline vehicle (without any control technology) are discussed.

2.2 Experimental Methods

Experiments were carried out at the California Air Resources Board's (CARB) heavy-duty diesel emission testing laboratory (HDETL) in downtown Los Angeles. Ayala et al., (2002) described the dynamometer specifications in details. Figure 2.1 shows the schematic of the experimental setup. The sampling train includes heavy-duty chassis dynamometer, constant volume sampling (CVS) dilution tunnel and aerosol samplers. Diesel vehicle exhausts were transported by a stainless steel hose pipe and diluted with filtered air through the CVS. Measurements were taken 18 diameter lengths downstream of the exhaust introduction in the CVS. Three driving cycles, i.e. steady state cruise (50mph), transient [EPA urban dynamometer driving schedule (UDDS)] and idle were tested to simulate various real-world driving conditions. The fuel used to run the engines was CARB ultra-low sulfur diesel (ULSD) with sulfur content less than 15 ppm. Tunnel blank levels were measured and vehicles were conditioned (warmed up) everyday before the start of official runs. The CVS was cleaned prior to starting the project.

Figure 2.1: Experimental setup

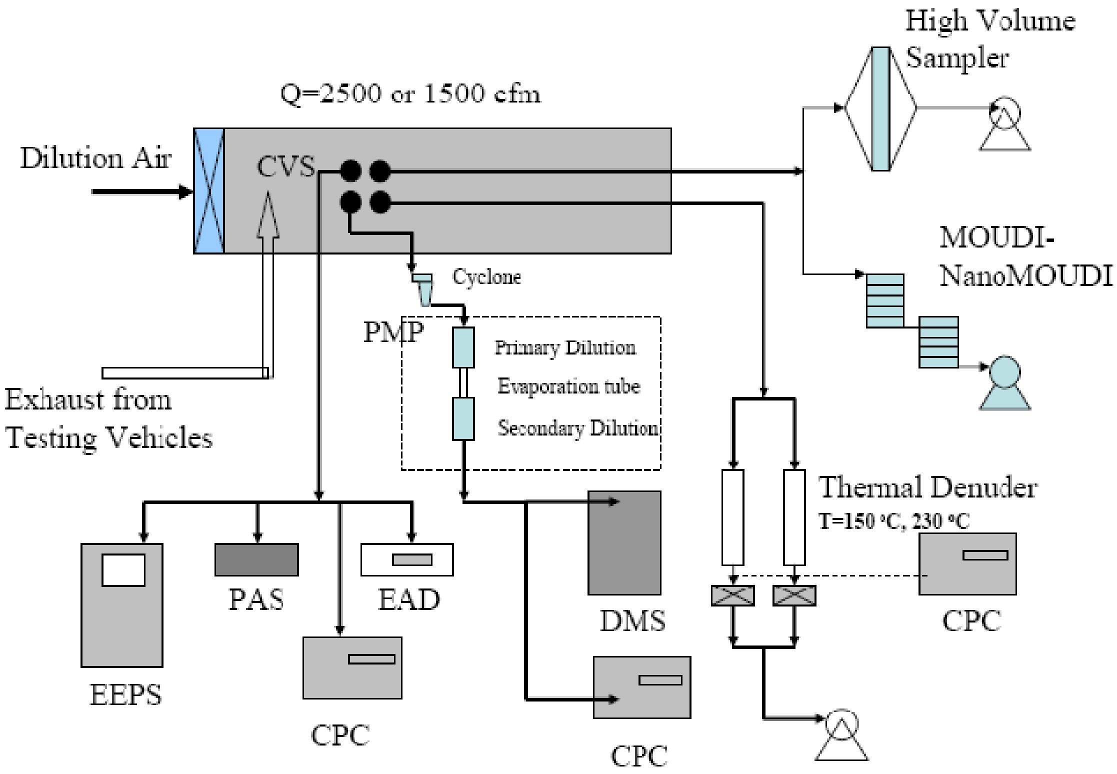

2.2.1 Vehicles

The test fleet comprised of four heavy-duty diesel vehicles in seven configurations (Table 2.1). A 1998 Kenworth truck served as a baseline vehicle, without any emission control technology. The same Kenworth truck was also tested with three different control technologies: a Continuously Regenerating Technology [CRT], consisting of a diesel oxidation catalyst (DOC) followed by an uncatalyzed trap; CRT in combination with a selective catalytic reduction system [Zeolite or vanadium based SCRTs]. The other three test vehicles were a diesel hybrid electric bus, a school bus, and a Caltrans truck.

Table 2.1: Details of test fleet

Vehicle		**Engine**		**After treatment (AT)**		**Dilution**
Make	**Nomenclature**	**Model**	**Size [L]**	**Type**	**Miles on AT**	**Approximate Dilution Ratio in CVS**
Kenworth	**V-SCRT**	Cummins M11, reflashed	11	Vanadium based SCRT®	50,000	9.2 Cruise 6-30 UDDS 14 Idle
Kenworth	**Z-CERT**	Cummins M11, reflashed	11	Zeolite based SCRT®	0 on SCR, 50,000 on CRT	9.2 Cruise 6-30 UDDS 14 Idle
International	**DPX**	International DT466E	7.6	Engelhard DPX	30,000	6.2 Cruise 5-25 UDDS 22 Idle
Gillig (35ft) with Alison Hybrid	**Hybrid-CCRT**	Cummins	5.9	CCRT®	1000	5-50 UDDS
Thompson-School Bus	**EPF/School Bus/Horizon**	Cummins	5.9	Cleaire - Horizon	32,000	8.3 Cruise 8-80 UDDS 25 Idle
Kenworth	**CRT**	Cummins M11, reflashed	11	Continuously Regenerating Technology	64,000	9.2 Cruise 6-30 UDDS 14 Idle
Kenworth	**Baseline**	Cummins M11, reflashed	11	None	NA.	9.2 Cruise 6-30 UDDS 14 Idle

The two SCRT technologies consist of a wall-flow particulate trap (CRT) followed by a SCR section. The CRT was the same in each configuration. The difference between them lies in the choice of catalysts (vanadium or Zeolite) for the SCR to control oxides of nitrogen (NOx). The Caltrans truck, with a smaller engine (7.6 L) than the Kenworth truck (11 L, Table 2.1), is retrofitted with an Engelhard DPX filter. The DPX filter is comprised of a diesel particulate trap with a catalytic wash-coat. The diesel hybrid electric bus (San Joaquin Valley RTD) is equipped with a catalyzed continuously regenerative trap, or CCRT, consisting of a DOC followed by a catalyzed trap, which was virtually brand-new, with only 1000 miles on the odometer. The last test vehicle was an Elk Grove school bus, equipped with an electric particle filter (EPF). The EPF (Horizon) consists of a non-catalyzed silicon carbide substrate for PM control, coupled with an electric heating element and a small blower. The trap is regenerated periodically using electricity from the grid (plug in configuration) during non-operational periods—mostly at night. Hereafter, the test fleet is referred as baseline, CRT, V-SCRT, Z-SCRT, DPX, hybrid-CCRT and EPF/School Bus/Horizon.

The dilution air flow rate at CVS was 2600 cfm (74 m^3 min^{-1}) for cruise and UDDS cycles, and 1600 cfm (45.4 m^3 min^{-1}) for the idle. For EPF and Hybrid-CCRT, the flow rates were maintained at 1600 cfm for all cycles. These flow-rates result in approximate dilution ratios of 6-9 for cruise, 5-80 for UDDS, and 15-25 for idle.

2.2.2 Equipment and Instruments

Specific descriptions of some of the instruments and equipment used for this study are provided in this section.

Nano-MOUDI

Size-resolved samples were collected using a micro-orifice uniform deposited impactor (MOUDI) upstream of a nano-MOUDI (MSP Corporation, Minneapolis, MN) loaded with pre-cleaned aluminum foil substrates. Particles were classified in the following aerodynamic size ranges: 10-18nm, 18-32nm, 32-56nm, 56-100nm, 100-180nm, 180nm-2.5µm and >2.5µm. The MOUDI-Nano MOUDI tandem was operated for multiple runs in order to accumulate sufficient mass for chemical analysis for each vehicle and driving cycle.

DMS/ EEPS

Size distribution of engine exhausts from the CVS was monitored every second by two multiple channel differential mobility spectrometers: a DMS500 (Cambustion) and an engine exhaust particle sizer (EEPS 3090, TSI Inc.). Both DMS and EEPS classify particles on the basis of their mobility diameter. The cut-off size ranges of EEPS and DMS are 5.6-523 nm and 4.5- 1000 nm, respectively. With high time resolutions, they are both capable of tracking transient particle behavior, especially during UDDS cycles. With few exceptions (V-SCRT, Z-SCRT only), in which the DMS was placed downstream of the particle measurement program (PMP) sampler, both instruments were connected directly to CVS.

PMP

A particle measurement program (PMP) protocol was developed in Europe to measure the solid particle emissions from light duty vehicles. The sampling train of PMP contains a volatile particle remover (VPR) and a particle counter. The VPR provides two stage dilution connected by an evaporation tube (ET). The temperature for the primary dilution, ET and secondary dilution is 150, 300 and ~35 ^{o}C, respectively. Detailed information for the PMP can be seen in Herner et al.,(2007a).

Thermodenuder

Particle volatility was determined by two thermodenuders (Model ELA-230, Dekati Ltd) sampling in parallel, each heating the entering aerosol to 150 and 230 ^{o}C, respectively. The thermodenuder consists of a heating section, followed by an adsorption/cooling unit. As aerosol stream was drawn from the CVS and passed through the heating tube, part of its volatile/semi-volatile components was sheared off. These labile species adsorb onto a layer of activated charcoal placed on the walls of the thermodenuder, leaving the non-volatile PM fraction to be collected on Teflon filters (47mm, PTFE, Gelman) placed downstream of the thermodenuders. Multiple runs were integrated to achieve desired sample mass loadings on these filters to perform various chemical and toxicological analyses. Solid particle number concentrations and size distributions were monitored intermittently by a condensation particle counter (CPC 3022 A, TSI Inc., MN) and a differential mobility particle sizer (DMA, TSI 3085).

High Volume Sampler

The high volume sampler is a specially designed filter holder [Hi-Q Environmental Products Co., CA; (Misra et al., 2002)] to collect particles on 20x25 cm filters at a relatively high flow rate (450 l/min). Integrated PM samples from the CVS were collected using this sampler on Teflon coated glass fiber (GF) filters (Pallflex, Fiberfilm T60A20 – 8x10 inch, Pall Corp., East Hills, NY).

2.2.3 Sample Analysis

Aluminum substrates from MOUDI-NanoMOUDI stages were pre and post-weighed during the sampling to determine the mass loadings. The elemental and organic carbon (EC, OC) content of deposited PM was analyzed by thermal-optical method (Kleeman et al., 1999). The ion concentrations were derived by ion chromatography (IC) technique. The water-soluble organic carbon (WSOC) content extracted from Teflon coated GF filters were analyzed by Shimadzu TOC-5000A liquid analyzer (Zhang et al., 2008). The oxidative potential of PM was measured by the DTT assay. The DTT assays were performed for denuded and undenuded PM collected on Teflon filters and undenuded PM on Teflon-coated glass fiber filters.

2.3 Results and Discussion

2.3.1 Size Distribution

Figure 2.2 presents tunnel blank- subtracted mean particle size distributions for vehicles at different operating conditions. These distributions derived from DMS/EEPS measurements are grand averages of multiple runs for each driving cycle. The data are reported in terms of number per vehicle kilometer traveled for cruise and UDDS cycles, and number per hour for idle. The primary focus here is to give a brief overview in order to provide meaningful insights and support to some of the findings described in subsequent sections.

While performing preliminary quality assurance – quality control (QA/QC) of real time data for SCRTs (V-cruise, UDDS, Z-Cruise), we noticed that few EEPS sizes channels (10-20nm) were almost always saturated due to particle over-loadings. These size bins were subsequently replaced with corresponding secondary dilution-corrected DMS data (the DMS was placed downstream of the PMP secondary dilution with the ET off) to obtain more accurate size distributions. For rest of the test fleet [except CRT], we used data from the DMS, which was directly connected to the CVS. We have added a tunnel blank distribution in Figure 2.2f (Baseline vehicle).

Size distribution patterns for both SCRTs are quite similar with sharp modes (Figure 2.2 a,b) at ~ 10nm. The distinguishable feature is the less prominent nucleation mode for UDDS runs especially for the Z-SCRT-UDDS cycle. This may be due to the fact that the

Zeolite-SCRT requires much higher temperature to trigger and sustain nucleation than the vanadium based SCRT catalysts (Herner et al., 2007b). Moreover, in general the zeolite catalysts have lot more catalytic surface area than vanadium catalysts and the Z-SCRT system used for this study is completely new (Table 2.1). These provide higher storage sites for sulfate generated by the upstream DOC and DPF during transient and low temperature testing.

Figure 2.2 a, b, c, d, e, f: Particle number size distribution

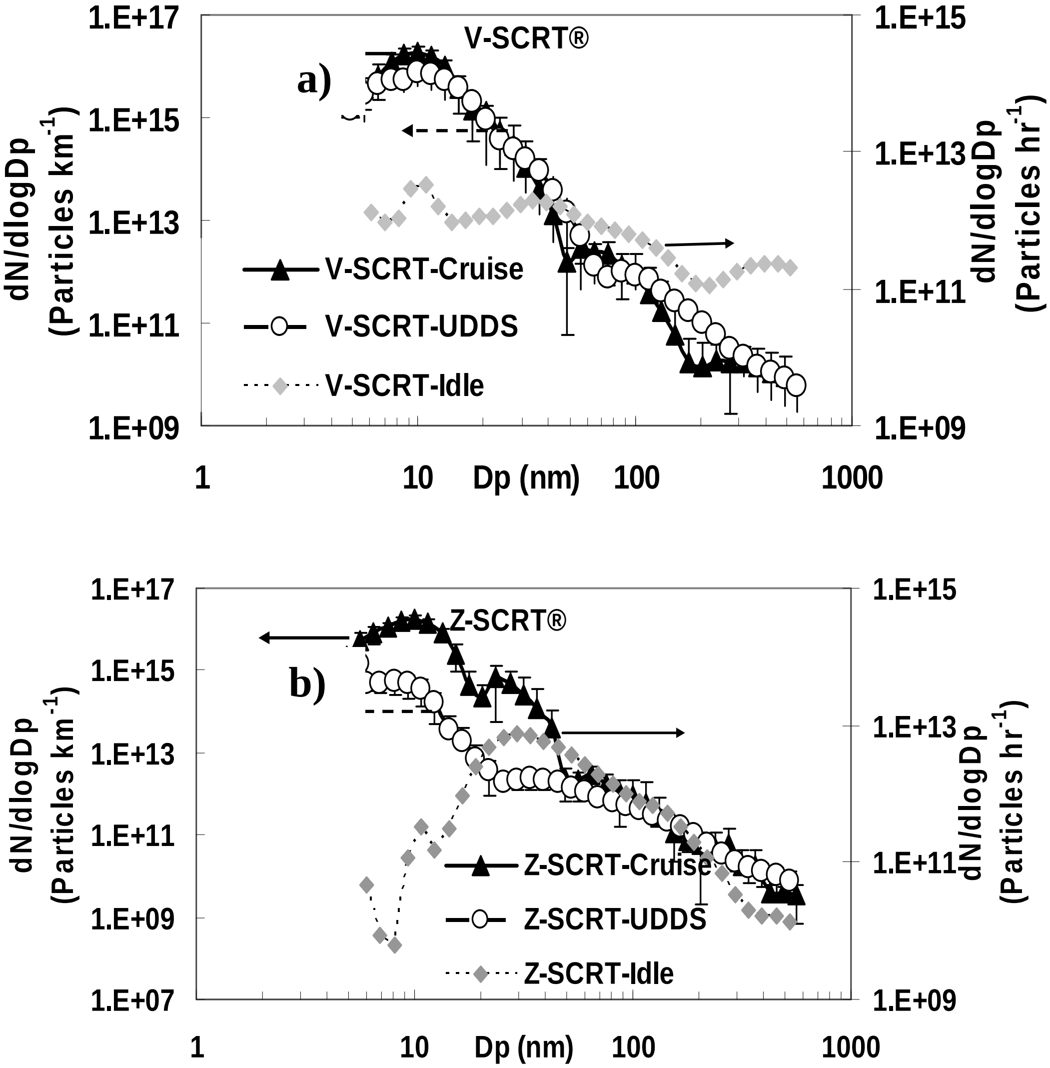

Figure 2.2 (Continued)

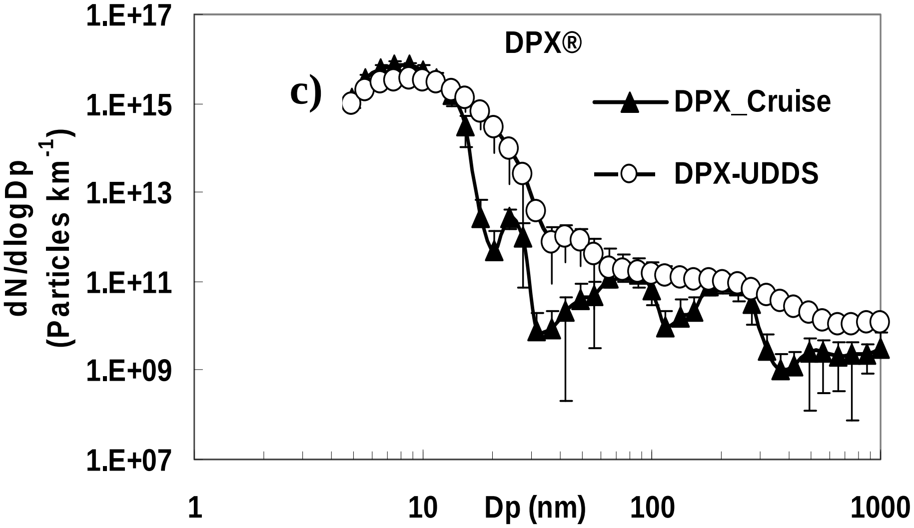

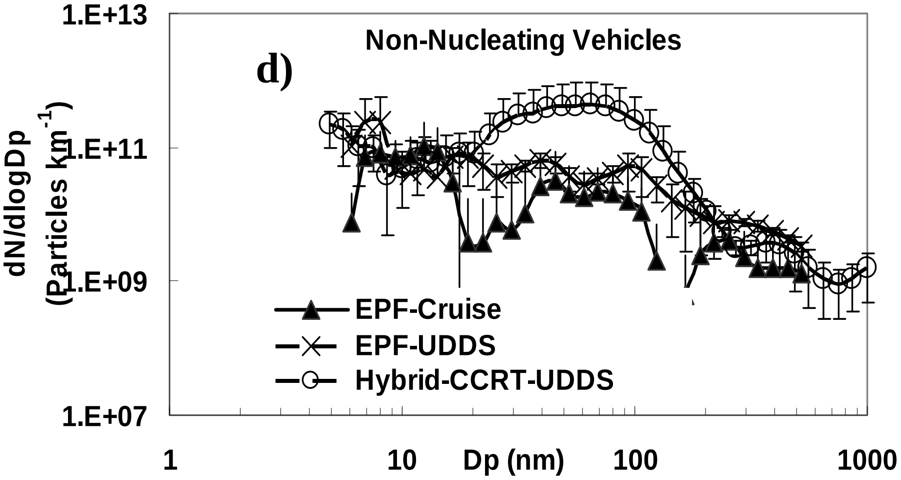

Figure 2.2 (Continued)

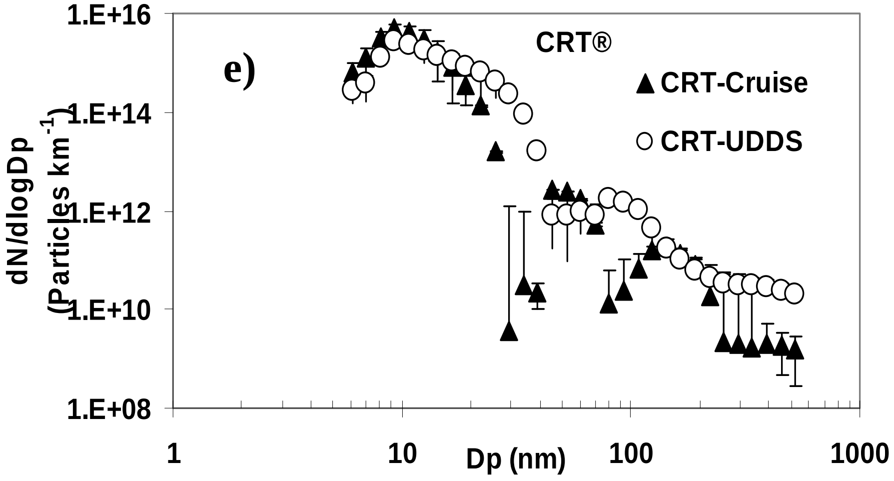

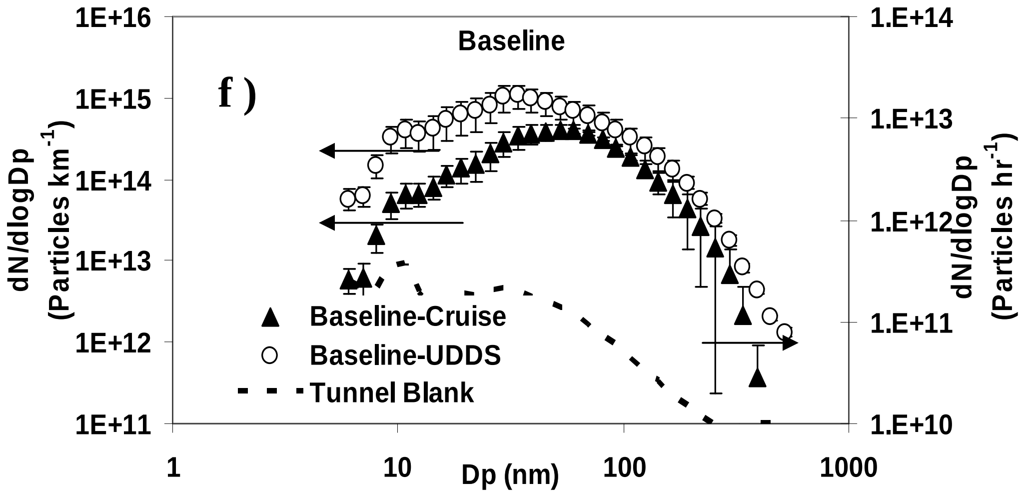

Although the main purpose of SCR technologies is to reduce NOx by ammonia, at elevated temperatures, their in-built catalysts may encourage the formation of sulfate, an important component acting potentially as seed aerosol for particle formation by condensation of semi-volatile organic vapors. For a brief sampling period, we bypassed the SCR portion from exhaust after-treatment system (SCRT) just to investigate the impact of the SCR catalysts. Although, this modification did not result in visible alteration of the shape (on log scale) of the distributions (CRT, Figure 2.2e), number concentration decreased by a factor of 2-3 from the V-SCRT and Z-SCRT cruise cycles - suggesting SCR catalysts's role on nucleation. Unlike cruise or UDDS cycles, idle runs are characterized with remarkably low particulate number emission rates, coupled with broad size distributions (Figure 2.2a, b). The second test engine, Engelherd-DPX (Figure 2.2c) displays a dominant nucleation mode, almost identical to the SCRTs/CRT. It has been hypothesized that the catalyst wash-coat on DPF (if saturated) may be enhancing the conversion of SO_2 to SO_3/sulfate and partially stimulates the nucleation process (Hansen et al., 2001).

Contrary to the general notion that particulate filters augment nucleation, the hybrid vehicles [with a CCRT] and the school bus [with an EPF] were found to be highly efficient in suppressing if not eliminating this PM mode. The Hybrid-CCRT vehicle (Figure 2.2d) resulted in concentrations (CVS) in the range of $\sim 10^4$ particles cm^{-3}, thus a 1,000-fold improvement over the previously tested vehicles ($>10^7$ particles cm^{-3}). We hypothesize that the initial capacity of its relatively new trap (with only 1000 miles on it) to store sulfur has significantly suppressed the formation of nuclei mode particles. Once all the storage sites are saturated, nucleated sulfate particles are expected. For this vehicle only a few odd large particles are left downstream (Figure 2.2d). The school bus (Figure

2.2d), however, was the cleanest amongst the entire test fleet with number emissions less than 1500 particles cm^{-3}measured in the CVS. It is important to note here that this vehicle is equipped only with an uncatalyzed filter (EPF) which is least likely to enhance the nucleation process. Thus, nucleation is not only control device specific but also a function of age and operating conditions e.g. temperature of the catalysts.

The baseline truck, on the other hand, represents the older genre of vehicles and was found to emit substantial amounts of larger particles (Figure 2.2f) with modes in the 60-100 nm range. Because of their large surface area, these accumulation mode particles act as adsorption sites and thus perfect sinks for organic vapors, leading to suppression of nucleation mode (Liu et al., 2007).

2.3.2 Size Segregated Mass Emission Factors

Size fractionated mass emissions factors (in mg km^{-1} or mg hr^{-1}) are calculated based on the loadings on the MOUDI-nano-MOUDI impaction plates. The mass loadings on the individual substrates are generally low for retrofitted vehicles and depending on size ranges variation in the order of 20-40% (*Standard Deviation/Mean*; from few duplicate measurements) are observed.

Although a direct correspondence of mobility and aerodynamic diameters is not accurate without establishing some conversion factors, we can utilize the information from Table 2.2 to complement the mobility size distributions (Figure 2.2) described before. Number and mass based size distributions are found to be in reasonable agreement with each other in terms of their trends.

Table 2.2: Size fractionated mass EFs (mg km $^{-1}$ for Cruise and UDDS, mg hr^{-1} for Idle)

Size (nm)		**10--18**	**18-32**	**32-56**	**56-100**	**100-180**	**180-2500**	**>2500**
V-SCRT	**UDDS**	0.73	1.44	2.46	1.36	0.86	1.07	0.83
	Idle	3.18	2.48	1.77	4.25	12.03	7.78	6.37
Z-SCRT	**Cruise**	0.9	1.48	1.6	1.15	0.53	0.97	0.5
	UDDS	0.17	0.34	0.32	0.17	0.62	0.55	0.66
	Idle	1.06	3.54	1.42	0.35	3.54	0	3.18
DPX	**Cruise**	0.65	0.29	0.3	0.11	0.27	0.21	0.2
	UDDS	0.56	0.46	1.25	0.6	0.41	0.2	0.35
	Idle	4.91	1.89	12.45	3.4	7.92	3.02	5.66
Hybrid (CCRT)	**UDDS**	0.26	0.12	0.22	0.33	0.17	0.57	0.35
CRT	**Cruise**	1.35	0.86	0.98	0.49	0.57	1.15	0.37
	UDDS	1.25	1.52	3.19	0.55	1.52	2.63	0.83
EPF	**Cruise**	0.04	0.22	0.12	0.14	0.07	0.15	0.12
	UDDS	0.05	0.08	0.16	0.1	0.05	0.29	0.17
	Idle	5.92	3.48	5.92	4.53	3.13	8.71	7.66
Baseline	**Cruise**	1.02	1.96	5.96	9.98	29.4	31.1	1.03
	UDDS	1.39	2.54	10.7	19.6	86.8	192	3.41
	Idle	19.363	60.241	565.83	600.26	2327.9	6049.9	346.39

Figure 2.3: Number (DMS) and mass emission factors (nano-MOUDI)

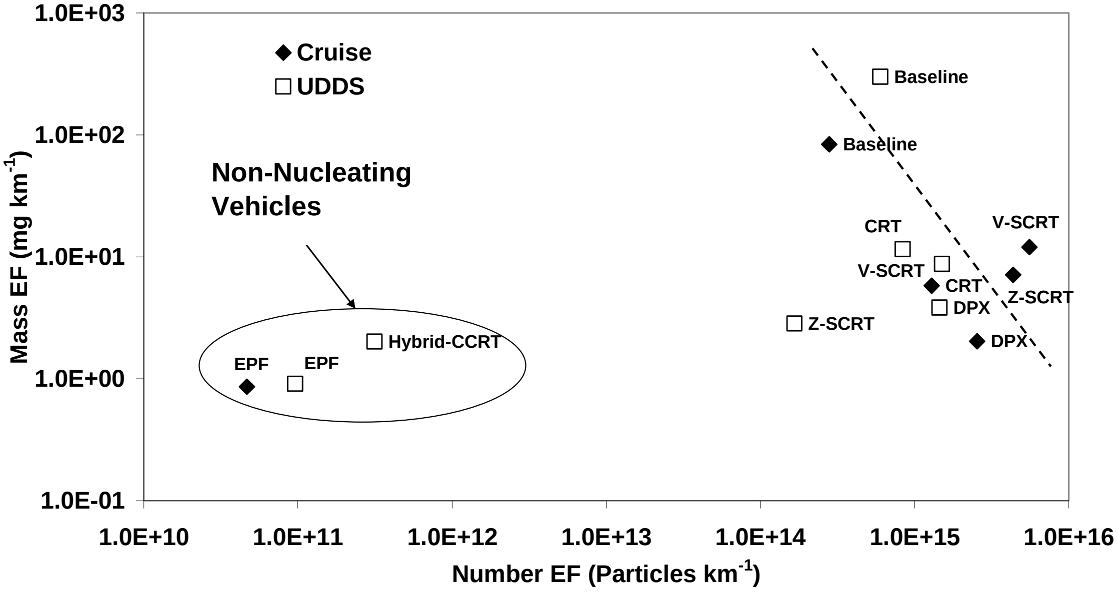

The emission factors are remarkably low (~1-12 mg km^{-1}) for the fleet operated with control technologies compared to the baseline vehicle (~80-316 mg km^{-1}). While the majority (>95%) of PM mass is concentrated between 100nm-2.5µm for the baseline truck, nuclei modes are clearly visible for vehicles retrofitted with control devices. Significant reduction (>90%) of the mass is achieved for vehicles retrofitted with control devices.

Some general trends and inferences can be drawn from Figure 2.2 and Table 2.2. Consistent with a previous study (Vaaraslahti et al., 2004), the majority of the control technologies evaluated here have promoted bulk production of nano-size (nucleation) particles during steady state and high speed segment of transient running cycles. The cruise cycles on average generate higher nucleation and lesser accumulation mode particles than the UDDS cycles. The differences between these driving cycles are even more pronounced in mass distributions (Table 2.2): significant shifts towards larger sizes are apparent in UDDS runs due to increased emission of accumulation mode particles during the acceleration processes (Polidori et al., 2008). Aerosol formation mechanism, poorly understood till date, seems to be a function of vehicle type and driving conditions and retrofit design.

Figure 2.3 is an informative graph showing a plot of number EFs vs. Mass EFs (nano-MOUDI, except V-SCRT-Cruise) for each vehicle and driving cycle. Each data point corresponds to a cruise or an UDDS cycle for a given vehicle. The graph shows that for several of the after-treatment devices tested, particle number emissions increase with reduced mass emissions. There are some outliers or exceptions observed for Z-SCRT at UDDS cycle, Hybrid-CCRT, EPF and Idle (not shown) for which both number and mass EFs are relatively low. Thus, most of the new after-treatment devices appear to be highly efficient in reducing mass emissions but some are not effective in controlling number concentrations due to the formation of nuclei mode particles.

2.3.3 Particle Volatility

Particle volatility was measured at 150 and 230^{o}C except in few occasions (Hybrid-CCRT, EPF) when both the thermodenuders were operated at 150^{o}C to maximize our capability to collect mass of non-volatile particles. For the majority of the cases, volatility at 230°C is at least an order of magnitude higher than their counterparts at 150°C, indicating complete disappearance of large fraction of particles within this temperature window.

The significant particle number loss between 150 to 230°C, especially for cruise cycles, may be elucidated by the evaporation profiles shown in Figure 2.4. The majority of particles in the 7-20 nm size range for DPX and CRT have disappeared as the aerosol stream is heated from 150°C to 230°C. This is in total contrast to the baseline vehicle, where no noticeable shift in size spectrum is observed. Matter et al., (1999) reported very similar thermal desorption trends between 172 and 204°C for particles sampled downstream of a DPF.

Figure 2.4: Size distribution of thermo denuded aerosols for cruise mode
Note: Available only for DPX®, CRT® and Baseline

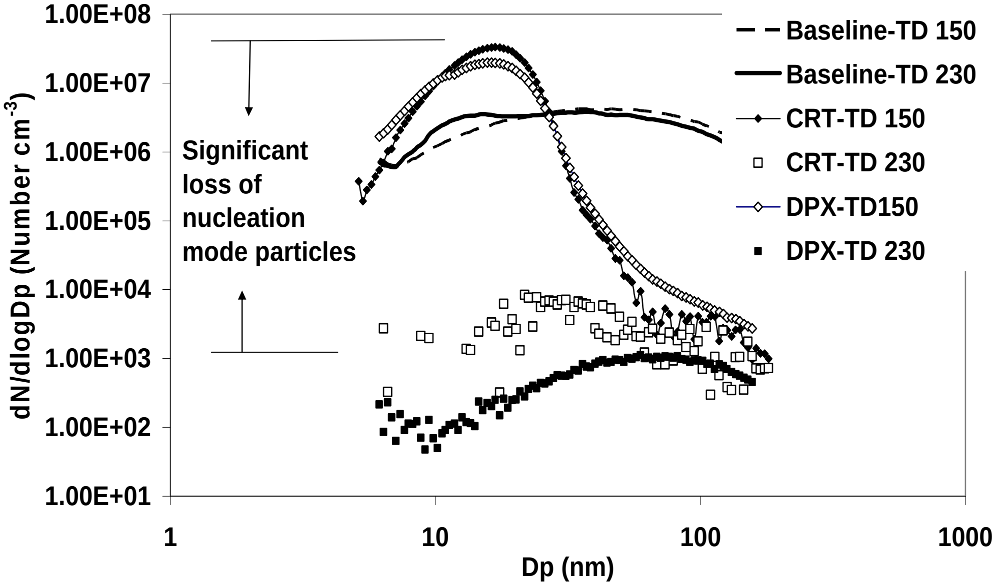

2.3.4 Emission Factors (EF) of Inorganic Ions and Total Carbon (TC)

Figure 2.5 shows the EFs (expressed in mg of PM species per kilometer driven) of chemical species integrated over the MOUDI-NanoMOUDI stages from 0.01- 2.5 μm. The low emission vehicles pose a challenge for PM chemical analysis due to very low mass loadings on individual substrates. The analytical uncertainties are shown by the error bars.

Figure 2.5: Emission factors of integrated chemical species measured by MOUDI-NanoMOUDI. a). Cruise 50 mph b). Transient UDDS

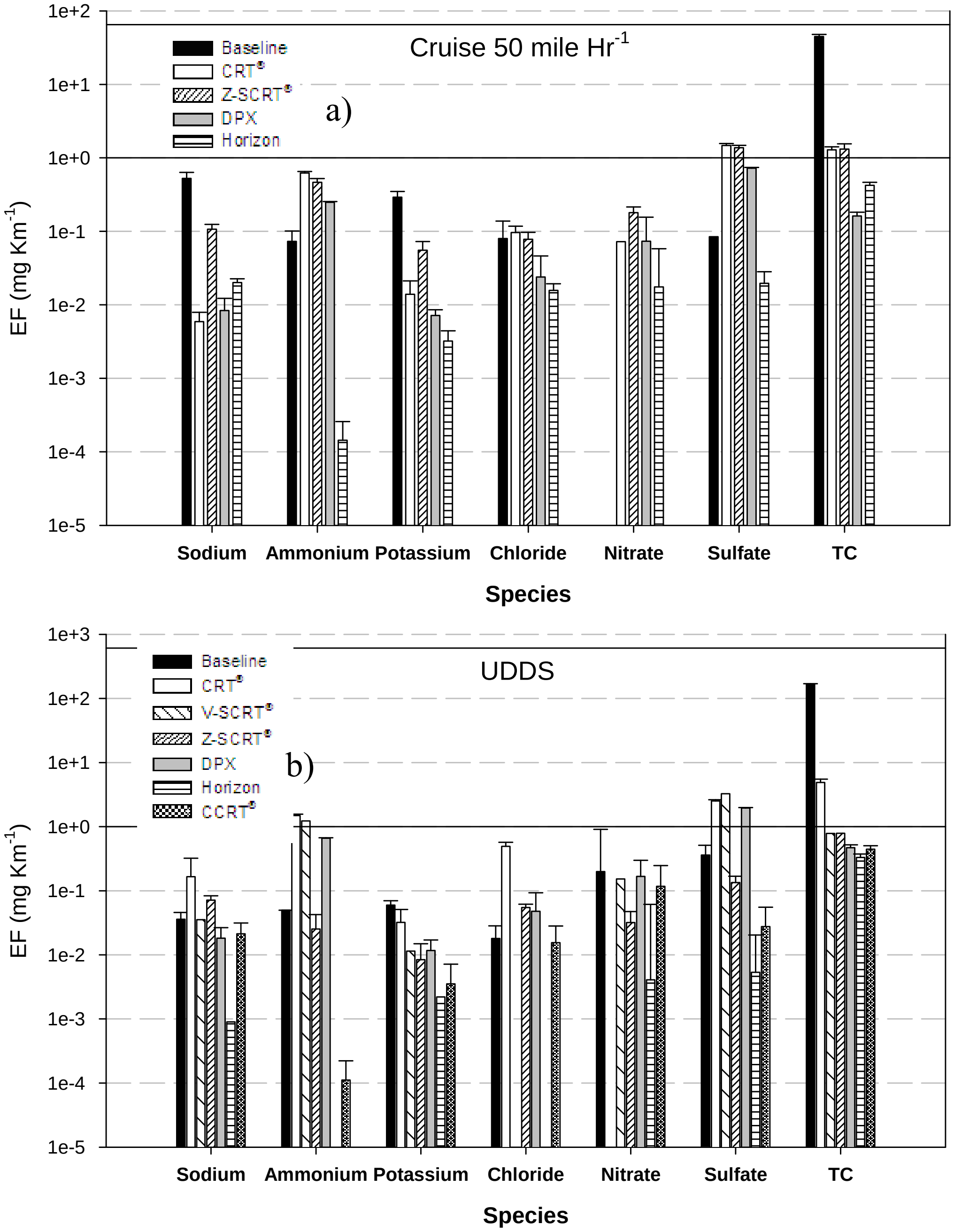

At both cruise and UDDS cycles, significant reductions in the emission of TC were observed for the retrofitted vehicles compared to the baseline vehicle. However, elevated emission rates of sulfate and ammonium were observed for vehicles and-or driving cycles that have a substantial fraction of nucleation mode particles, i.e. CRT, V-SCRT (measurements only available for UDDS cycle), Z-SCRT-cruise and DPX, compared to the baseline vehicle. The school bus retrofitted with an electric particulate filter (Horizon) was consistently the cleanest vehicle with the lowest emissions of inorganic ions and TC. This is also in agreement with the emission rates of PM based on gravimetric mass measurement.

The emission factors of TC were further split into EC, water-soluble and water-insoluble OC (WSOC and WIOC, respectively) and shown in Figure 2.6. The baseline vehicle (shown on secondary axis) not only emits considerable amount of EC (Cruise: 13.8 mg km^{-1}, UDDS: 65.9 mg km^{-1}) but also elevated levels of WIOC (Cruise: 28.2 mg/km; UDDS: 88 mg/km) and WSOC (Cruise: 2.7 mg km^{-1}; UDDS: 14 mg km^{-1}). The low EFs of WIOCs (~0.1-0.4 mg km^{-1}) and WSOC (0.05-0.95 mg km^{-1}) for the retrofitted vehicles suggest that these control devices are also effective (65-99%) in reducing the major fraction of organic carbon in addition to EC. However, it is important to note here that only the baseline, V-SCRT, Z-SCRT and CRT configurations (same vehicle) are directly comparable and caution should be exercised while comparing with other vehicle configurations (DPX, Horizon, CCRT).

Figure 2.6: EC, WSOC and WIOC emission rates at a) Cruise 50mph and b) Transient UDDS c) Proportion of WSOC to OC.
Note: V-SCRT cruise and CCRT-Cruise cycles are not available

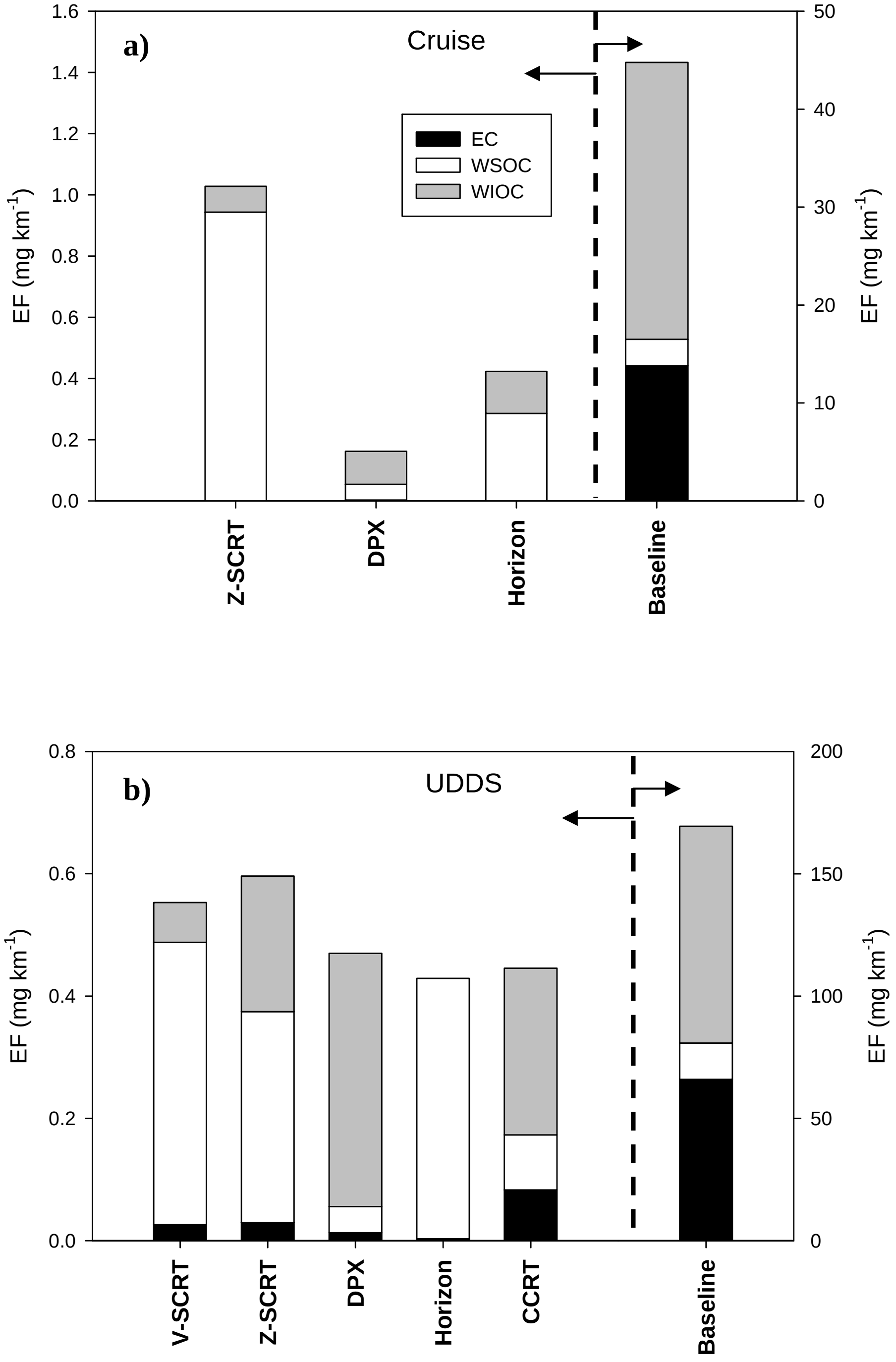

Figure 2.6 (Continued)

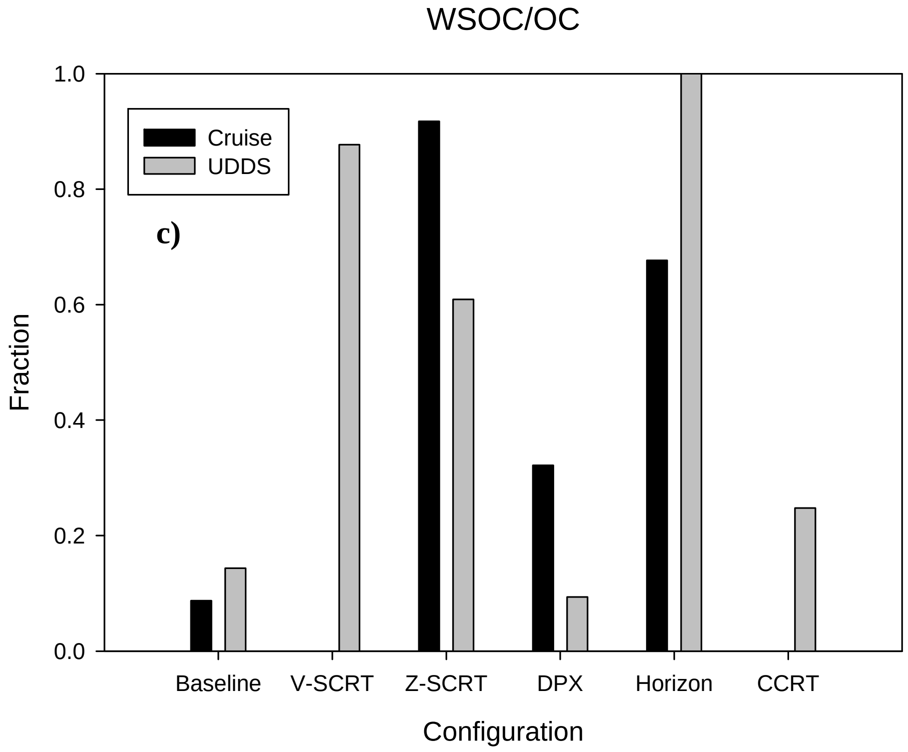

In addition to the overall reduction of OC, the proportion of WSOC to OC, illustrated in Figure 2.6c varies with vehicle configurations and running cycles. The baseline vehicle shows the lowest OC solubility (WSOC/OC =0.08-0.13) during both cruise and UDDS cycles, suggesting freshly emitted primary OC. By comparison, OC emitted from Horizon and SCRTs consists primarily of WSOC. DPX and CCRT WSOC contents are intermediate between the baseline and other retrofitted vehicles. An earlier study by Hameri et al., (2001) indicated higher water solubility of OC in the nucleation/UF mode than the accumulation mode. This may explain, to a certain extent, the higher WSOC/OC ratio of SCRTs and Horizon, where significant fraction of OC is observed in the nucleation mode. In contrast, OC dominates in accumulation mode for the baseline vehicle. In addition to size distribution of OC, control technologies seem to have major influences on the percentage of WSOC emitted by vehicles. The DPF of Horizon and SCRTs (higher WSOC/OC) are uncatalyzed, while DPX and CCRT (lower WSOC/OC) have catalyzed filters. Although SCRTs and CCRT both have DOCs upstream of the DPF, the results suggest that DOCs, in comparison to DPF types (catalyzed or uncatalyzed) have a minimal effect on the WSOC/OC ratio. This conclusion, however, does not imply that the DOCs have not contributed in reducing OC from the total vehicle emissions.

2.3.5 Size Segregated Chemical Speciation

The ion and total carbon emission data reported in Figure 2.7 a,b,c are further segregated into three size ranges, i.e. 10-56nm, 56-180nm and 180-2500nm. The V-SCRT-UDDS, Z-SCRT cruise, CRT and DPX have displayed the highest content of sulfate in the nucleation mode. This finding is consistent with the conclusions of recent emission studies that nuclei mode particles from DPF equipped vehicles are predominantly sulfates (Grose et al., 2006). However, significant levels of TC were also present in these vehicles. During the analysis of the physical PM properties, we observed that nucleation is suppressed in CCRT and Horizon, which have both a higher mass fraction of total carbon concentrations in all size ranges and less sulfate in nucleation mode PM. Unlike the SCRT cruise cycles, the UDDS cycles for Z-SCRT are unique in the sense that the emission rates of TC dominate those of sulfate. This may be again due to higher activation temperature of Zeolite catalysts, which may impede the conversion of SO_2 to sulfate during transient cycles, for which the exhaust temperature fluctuates continuously. Herner et al., (2007b) reported that the critical temperatures (post after-treatment temperatures) required for Z-SCRT and V-SCRT to trigger nucleation are 373^{o}C and 330 ^{o}C, respectively.

Figure 2.7: Emission rates of size-resolved PM chemical species. a) Cruise 50 mph, b) Transient UDDS c) Baseline vehicle
Note: Nucleation (Nuc, 10-56 nm), UF: 56-180 nm and Acc: 180 nm – 2.5µm.

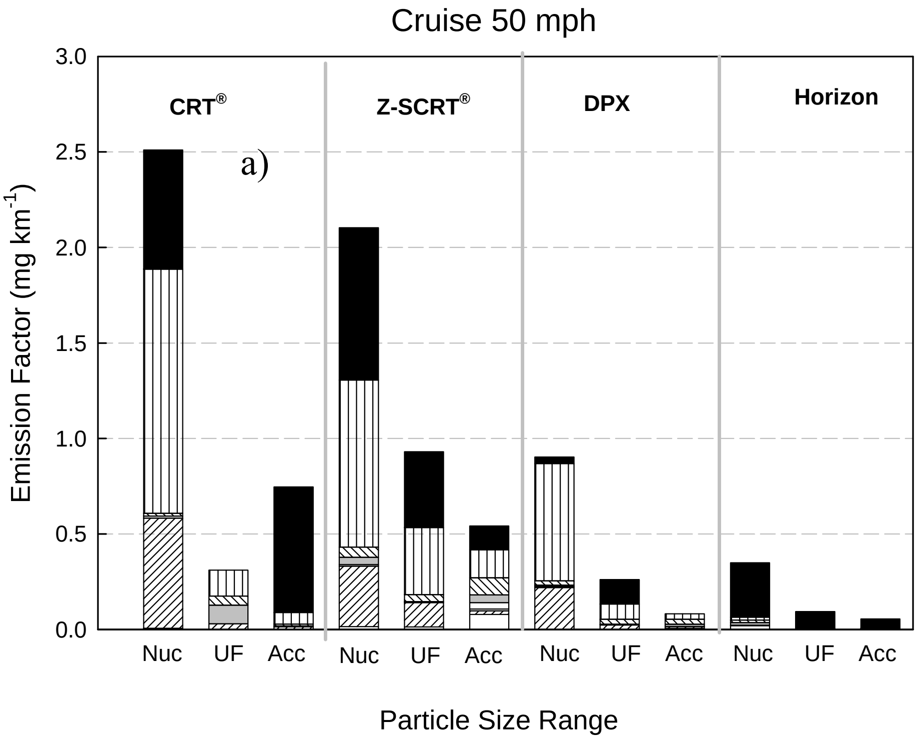

Figure 2.7 (Continued)

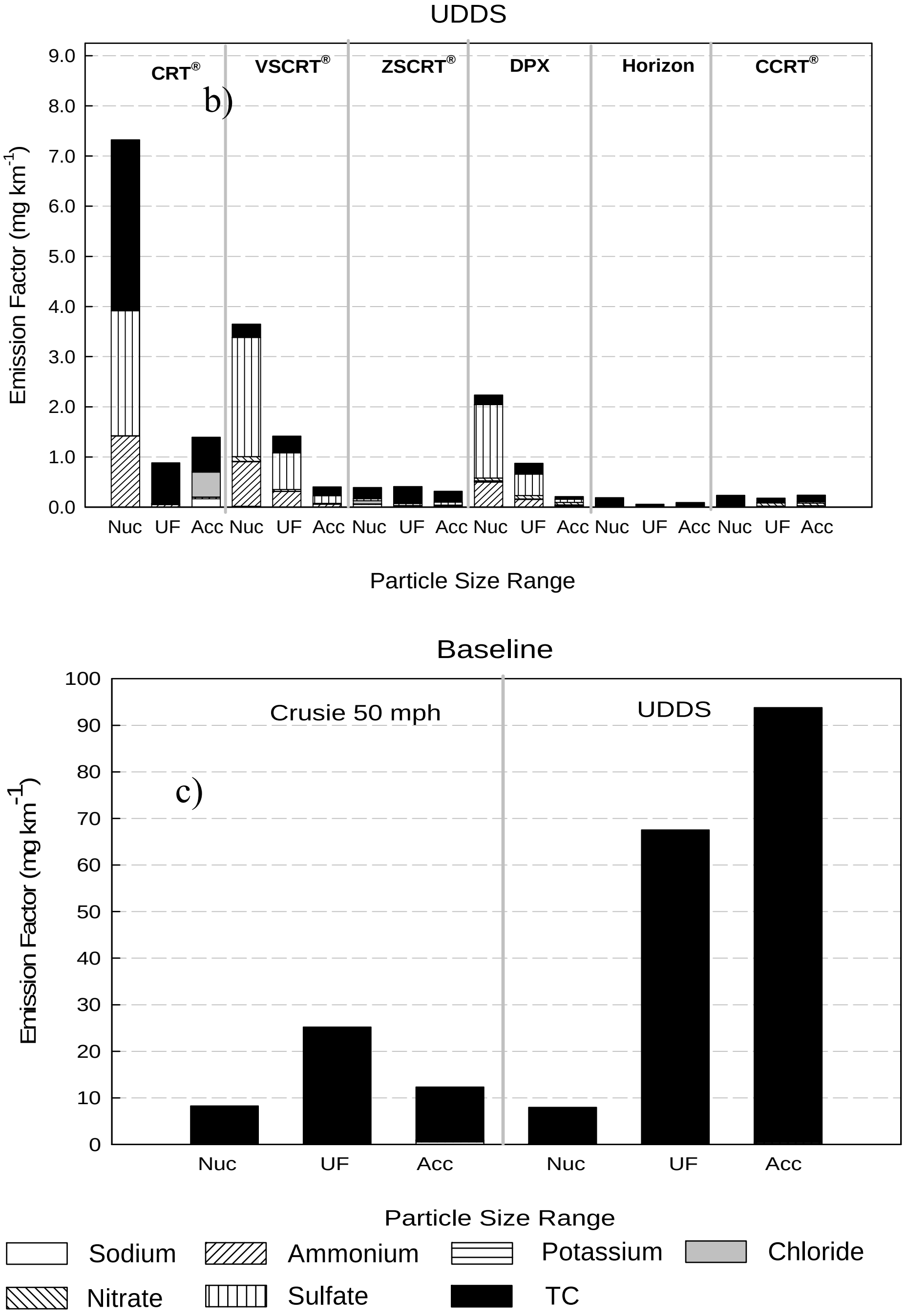

Figure 2.7c shows the mass size distribution of the chemical components of PM emissions from the baseline vehicle. Total carbon concentration outweighs any other species for the baseline vehicle (>99% of total PM mass concentration). Further, the UDDS cycle of Baseline vehicle emits almost 3-fold higher TC than the cruise cycle. This can be explained by the shift of TC peaks during cruise cycle in the 100-180nm (25mg km^{-1}) size rage to the even larger accumulation mode (180-2500nm, 90mg km^{-1}) during UDDS cycle. The higher emission of TC during the transient cycles, however, was not observed for Z-SCRT and Horizon (Figure 2.7a, b). The Z-SCRT-UDDS cycle emitted the least amount of PM mass among all the retrofitted cycles of Kenworth truck (CRT; SCRT cycles). This particular cycle also lacked a pronounced nucleation mode which was observed in CRT and other SCRT cycles. Higher activation temperatures for the Zeolite catalysts can inhibit the nucleation process (as mentioned before) especially during the fluctuating exhaust temperature of the UDDS cycle. Since a considerable fraction of TC (mostly OC for retrofitted vehicles) is associated with the nucleation mode, it is likely that the lack of nucleation can retard condensation of organics on these particles. Emissions of TC from both the Horizon cycles are low and comparable to the analytical limits of detection; therefore caution should be exercised in making inferences based on these data.

2.3.6 DTT Activity

Blank-subtracted (filter blank DTT~0-0.0005 n-mole μg^{-1} min^{-1}) DTT consumption rates, normalized per unit mass of PM are reported in Figure 2.8 a,b,c for various vehicle configurations. The vehicle with the Horizon trap had the highest per mass DTT activity (0.16-0.19 n-mole μg^{-1} min^{-1} for cruise and UDDS) irrespective of driving conditions. The DTT consumption rates from both Vanadium and Zeolite-based SCRTs are on the same order of magnitude (0.01-0.02 n-mole μg^{-1} min^{-1}). It is interesting to note that when the selective catalytic reduction (SCR) section from SCRT is removed from the exhaust stream and the vehicle is operated with only CRT (i.e., the DOC+ uncatalyzed filter), the DTT activity increased by a factor of almost 3, both for cruise and UDDS cycles. The CCRT (Catalyzed filter + DOC) is the most efficient among the test fleet with DTT rates as low as 0.006 n-mole μg^{-1} min^{-1}. Of particular note is the elevated level of activity for the DPX and Horizon vehicles. The baseline vehicle emitted PM with similar oxidative characteristics to those of newer vehicles with control technologies.

Figure 2.8 also reports the DTT values for the thermo denuded filters. There is a significant reduction (50-100%) in the activity as particles are heated to 150°C and their semi-volatile component is removed. The baseline vehicle, however, did not show any alteration in DTT response between denuded and undenuded exhaust stream, except while idling. This is because of the highly refractory nature (mostly soot) of these particles.

Figure 2.8 a, b, c: Oxidative Potential (DTT consumption in n-moles min^{-1} μg^{-1} of PM) of thermo-denuded and undenuded PM

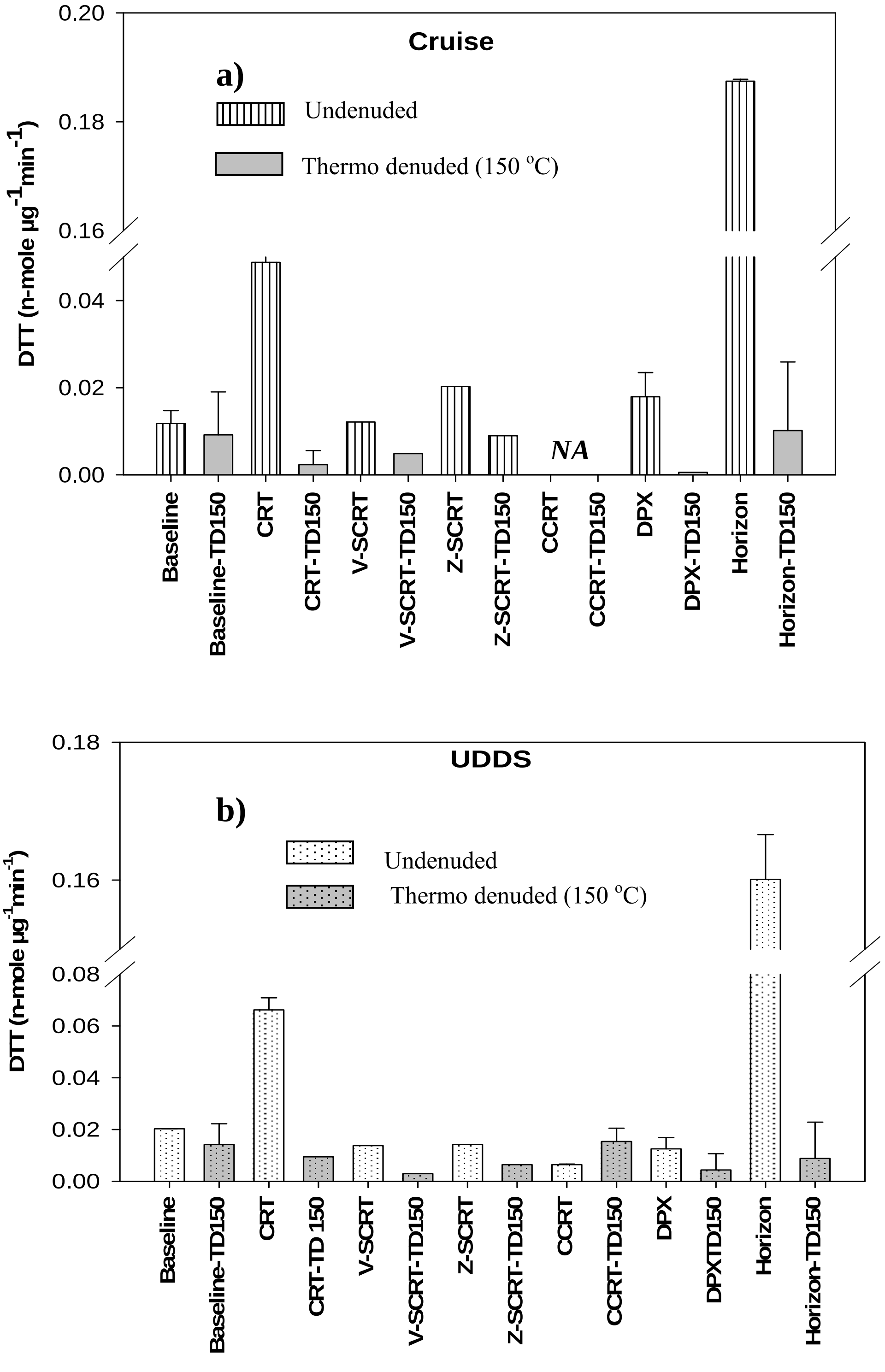

Figure 2.8 (Continued)

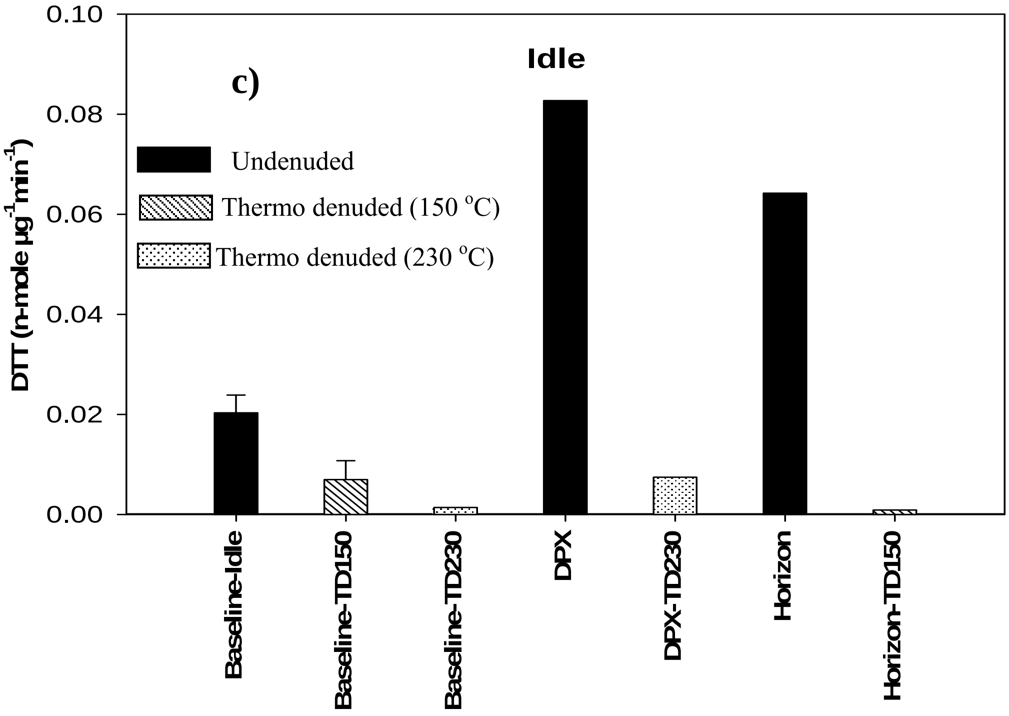

The increased DTT activity of the semi-volatile PM fraction is further highlighted by comparing with their corresponding semi-volatile PM mass and number fractions (Figure 2.9). For vehicles with (soot removing) control devices, the semi-volatile fraction contributed roughly 70-100% of the net oxidative activity compared to 20-30% for baseline vehicle. The sole exception is the CCRT vehicle, which hardly produced any oxidative activity from its semi-volatile fraction, despite emitting 45% of semi-volatile PM by mass and 37% by number. For this vehicle (CCRT) the relatively low level of OP has originated from its residual non-volatile fractions. In general, particle number-based volatility, which is predominantly driven by the evaporation of the sub-50 nm, so-called nucleation mode particles (Kittelson, 1998), followed the activity trends better than the PM mass volatility.

Figure 2.9: Relationship between oxidative activity and semivolatile PM fraction at 150 °C (Showing good correlation of DTT (filled circles) with particle number (hollow diamonds) and poor correlation with PM mass (bars)).

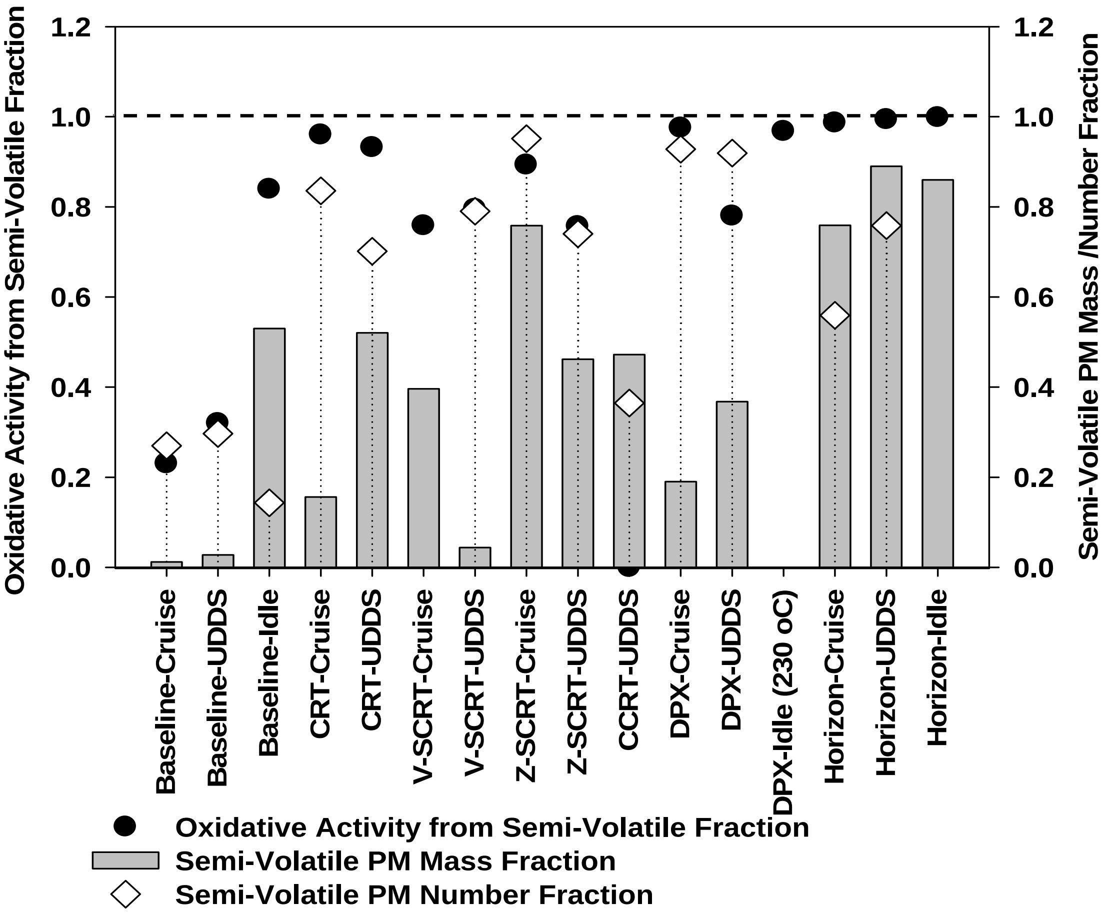

- - - ***Total Oxidative Activity (1): Sum of oxidative activity from semi-volatile and non-volatile fraction***

The DTT results (Figure 2.10 a,b,c) expressed per unit vehicle distance traveled provide a better idea of the total oxidative load imparted on the environment by these vehicles. They also provide a quantitative assessment of the effectiveness of these after treatment devices. While we observed a comparable or lower oxidative response of the baseline vehicle per unit mass of PM, its net DTT consumption (per km) is substantially higher (>3 times) than retrofitted vehicles.

Figure 2.10 a,b,c: DTT consumption per unit distance (in n-moles min^{-1} km^{-1}) traveled by vehicles for Cruise and UDDS cycles and per hour(in n-moles min^{-1} hr^{-1}) for Idle

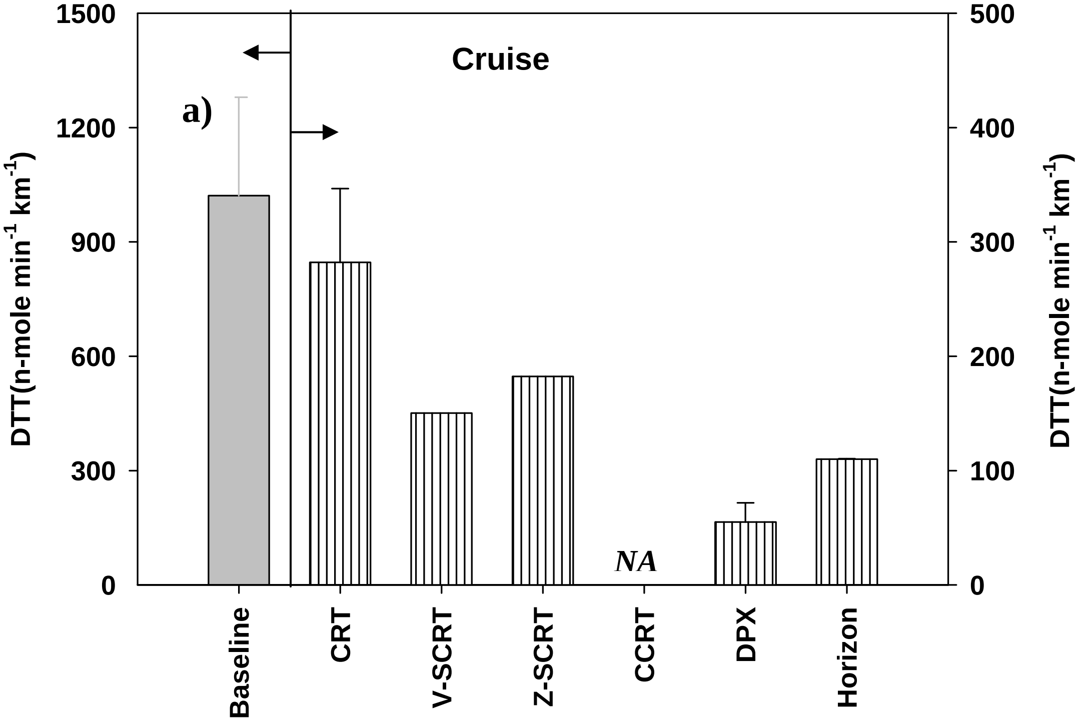

Figure 2.10 (Continued)

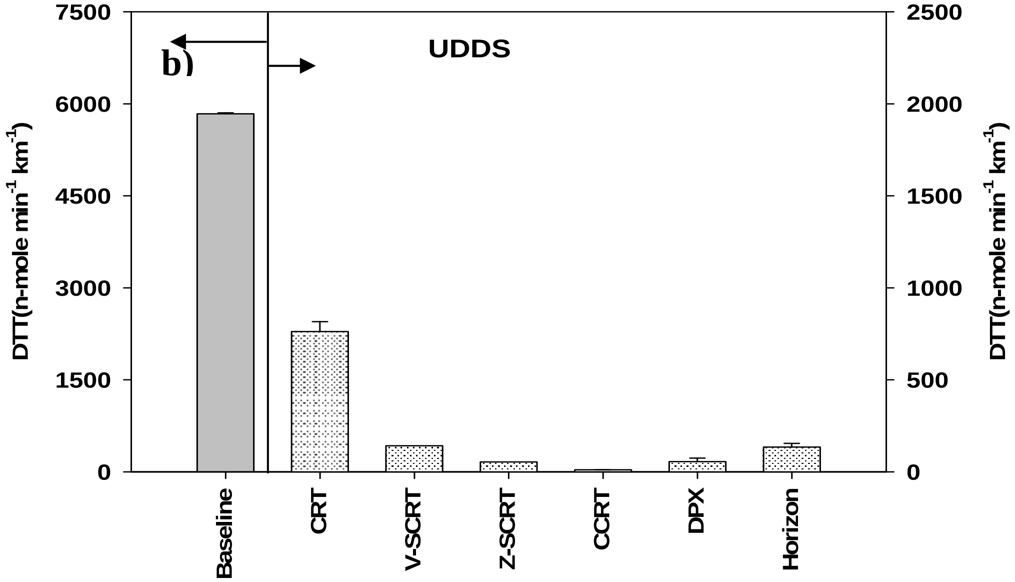

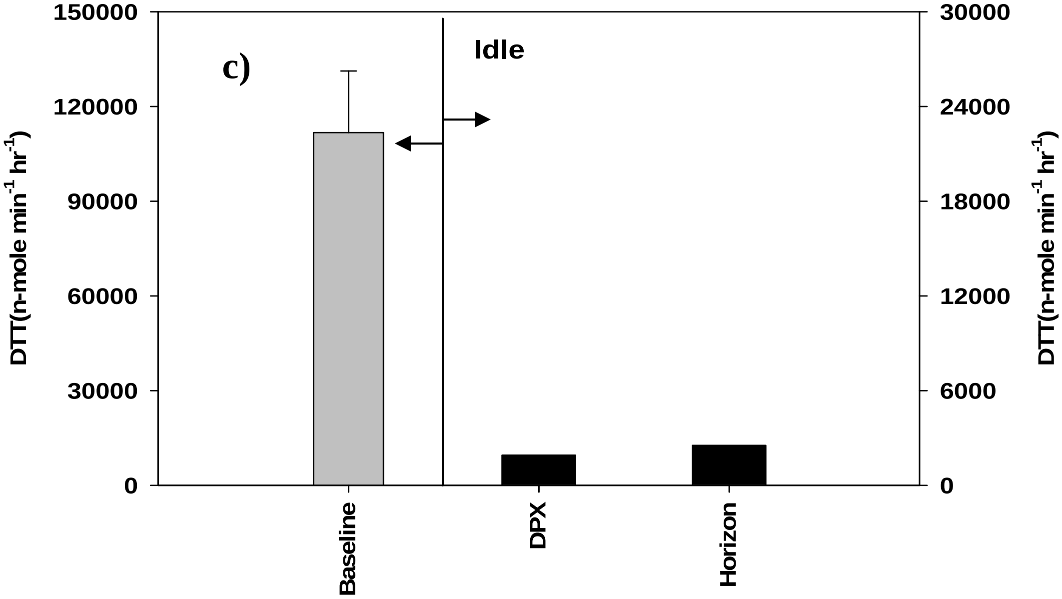

2.3.7 Water Soluble Organic Carbon and DTT

Figure 2.11 shows the WSOC (% of PM mass) and DTT consumption (per unit PM mass) for vehicle-configurations. DTT and WSOC followed the same trend, irrespective of driving condition or control devices. The school bus (Horizon), which exhibited the highest oxidative activity per unit mass, also emitted the highest fraction of soluble organics (35-83%). Similarly higher WSOC content was found for the higher DTT values of PM produced by the DPX-idle cycle.

Figure 2.11: DTT consumption (n-moles min^{-1} μg^{-1} of PM) in relation to the water-soluble organic carbon (WSOC) of PM from the exhaust

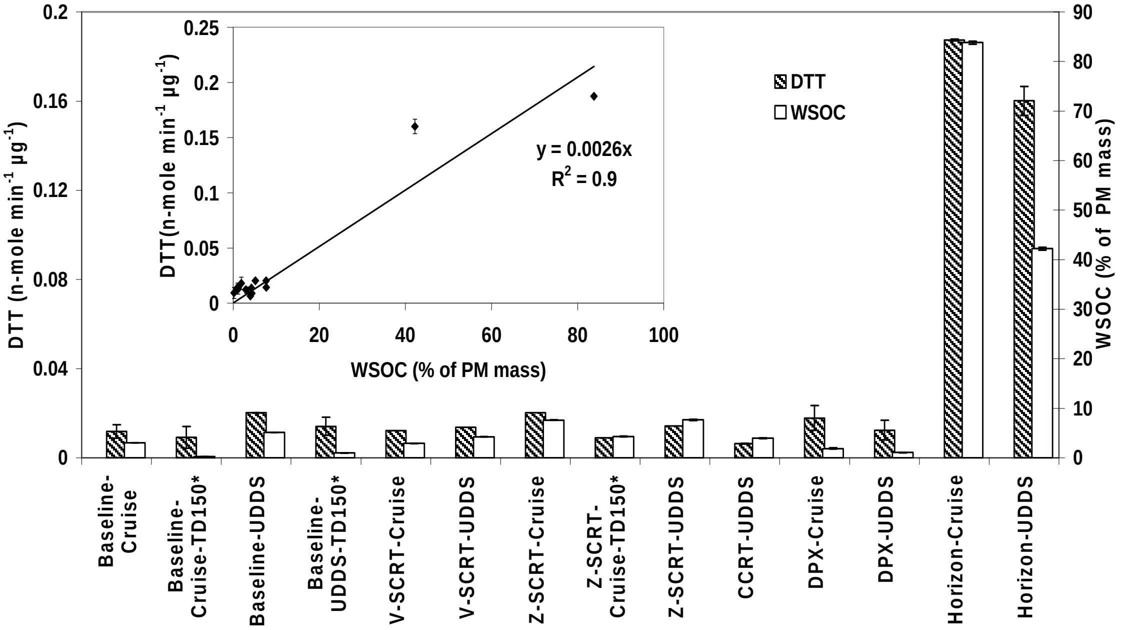

2.3.8 Correlation between Chemical Species and DTT Activity

To assess the contribution of various species to DTT activity, the Pearson's coefficient (R) and the associated significance levels (p-value) have been calculated and are shown in Table 2.3 for the correlation of different chemical constituents with DTT values. The DTT was significantly correlated with WSOC (R=0.94, p<0.01) and organic acids (sum, R=0.91; p<0.01) and moderately correlated with organic carbon (R=0.76, P=0.02). All other species, including inorganic ions, PAHs, EC, alkanes either have low or negative correlation. No correlation analysis was performed between metals and DTT. Although some of the transition metals (such as Cu) can actively participate in DHBA assay, their contributions are insignificant for DTT tests (Cho et al., 2005).

Table 2.3: Correlation coefficient (R) and significance level (p) for the DTT activity and selected chemical species

Species	**R**	**P**
EC	-0.35	0.37
OC	**0.76**	0.02
NO_3^-	-0.09	0.77
SO_4^{2-}	-0.32	0.27
NH_4^-	-0.25	0.26
K^+	0.43	0.20
Cl^-	0.34	0.15
WSOC	**0.94**	<0.01
Alkanes (Alk.)	0.03	0.54
PAHs	-0.26	0.75
Organic Acids (OA)	**0.91**	<0.01

2.4 Conclusions

This investigation presents some of the first detailed particle characterizations for advanced NOx and PM retrofits in heavy duty diesel vehicles. The test fleet includes a diesel hybrid electric with a DPF (Hybrid-CCRT), a continuously regenerating technology (CRT), a vanadium-based SCR catalyst with a CRT (V-SCRT), a Zeolite-based SCR catalyst with a CRT (Z-SCRT), a DPX, and an EPF (Horizon/School Bus). A HDDV vehicle without emission controls served as the baseline vehicle. The fleet was tested under three driving cycles: cruise at 50 mph, UDDS and idle.

While comparing with a baseline vehicle, significant reduction (>90%) in mass, EC, OC, WSOC emissions is achieved for vehicles with retrofits. However, enhanced nucleation mode particles were observed for some of the vehicles especially during cruise cycles. The Hybrid-CCRT and EPF vehicles were efficient in controlling both mass and number emissions. The vehicles with significant nucleation (CRT, V-SCRT, Z-SCRT and DPX) mode particles produced considerable amount of sulfates especially during steady state operations. On the contrary, the non-nucleating configurations (Horizon, CCRT, Z-SCRT-UDDS) were associated with higher amount of total carbon in the form of OC. Soluble fraction of OC was highest for Horizon followed by SCRTs, DPX and baseline.

Despite a general increase in the intrinsic DTT activity (per mass basis) of exhaust PM with use of most control technologies, the overall activity (expressed per km or per hr) was substantially reduced for retrofitted configurations compared to the baseline vehicle.

The semi-volatile fraction of the exhaust particles was observed to be highly oxidative in nature as demonstrated by a significant reduction in DTT activity (by 50-100%) observed for thermally-denuded PM. Correlation analysis performed between all the species, showed that DTT is moderately associated (R=0.76) with organic carbon (OC) and strongly associated (R=0.94) with the water soluble organic carbon (WSOC).

Chapter 3: Toxicity Profiles of Ambient Particles Influenced by Vehicular, Woodsmoke and Secondary Photochemical Sources

This chapter is divided into two sections, describing the oxidative activity profiles of ambient PM from vehicular and secondary photochemical sources (section 3.1), and from woodsmoke sources (wildfires; section 3.2). The major findings of both the studies have been summarized in the respective sections.

3.1 Oxidative Activity Profiles of Ambient Particulate Matter from Primary and Secondary Sources

3.1.1 Introduction

Atmospheric quasi-ultrafine particles (quasi-UFP) originate from two broad categories of sources: primary and secondary. Primary particles are directly emitted from combustion sources, including heavy and light duty vehicles, woodsmoke, and industries including, for example, power plants. In the presence of various atmospheric oxidants, primary particles may undergo photochemical processing yielding secondary particles with distinctly different physical and chemical characteristics compared to their precursor primary particles. Diurnal changes in physical properties (particle number size distribution and volatility) of the quasi-ultrafine particles at an urban location near downtown Los Angeles have been discussed in detail by Moore et al., (2007). In a companion paper, the chemical composition of ambient samples collected in two different time periods (morning and afternoon) at the same site was also presented (Ning et al., 2007). Results from both studies indicated a strong influence of commute traffic emissions during the morning hours as evidenced by elevated concentrations of nitrogen oxides (NO_x), carbon monoxide (CO), black carbon (BC) (Moore et al., 2007), alkanes, PAHs and hopanes (Ning et al., 2007). By contrast, the afternoon concentrations of oxygenated organic acids and sulfate rose, while other species were diluted by the increased mixing height or lost due to increasing temperature. These are clear indicators that secondary photochemical reactions are a major source of quasi-ultrafine aerosols in the afternoon.

The reaction mechanisms leading to the generation of secondary organic aerosols (SOA) have not been fully characterized due to the complex nature of organic compounds in the atmosphere. The differences in the physico-chemical characteristics of primary and secondary particles will likely lead to differences in their oxidative activities including their ability to induce cellular oxidative stress (Baltensperger et al., 2008; Delfino et al., 2009; Ntziachristos et al., 2007). Recent laboratory experiments also indicate that combining primary diesel particles with ozone (in order to mimic atmospheric photochemical transformation processes) substantially enhances the oxidative activity of the PM (Li et al., 2009); however, there are very few studies investigating this important issue using real world atmospheric aerosols.

The present section of the chapter focuses on comparing the oxidative activity profiles of the quasi-ultrafine particles (<180 nm in this study) at an urban site near downtown Los

Angeles collected during two different time periods of the day – morning and afternoon, representing particles characterized by primary emissions and secondary aerosols formation, respectively. The oxidative activity of the collected particles has been measured by two independent assays: 1) the DTT assay, and 2) the macrophage ROS assay. Detailed chemical analyses of the collected samples including water soluble elements, inorganic ions, organic species and water soluble organic carbon have been conducted to distinguish the chemical properties of the source specific particles, and also to investigate their correlation with the measured oxidative activities. Our goal was to contrast the toxicity profiles of ambient quasi-ultrafine particles emitted from primary vehicular sources with those produced from secondary processes and atmospheric aging.

3.1.2 Experimental Methods

3.1.2.1 Sampling Location

This study was conducted at the Particle Instrumentation Unit (PIU) of Southern California Particle Center (SCPC) on the campus of University of Southern California (USC) near downtown Los Angeles. The sampling site is located approximately 130 m to the NE of the I-110 freeway, near construction, parking facilities and other nominal sources of pollutant emissions. Pollutant sources near this site are predominantly from vehicular sources with traffic patterns consistent with a mixed-use urban environment. Light duty gasoline vehicles constitute the major fraction (>93%) of traffic at the stretch of freeway near the site, with the rest being heavy duty diesel vehicles. Studies indicate that the average monthly PM chemical composition in the quasi-ultrafine mode at the

USC and other similar Los Angeles-area sites is dominated by organic carbon, which varies from 40 – 90% depending upon the season and location (Fine et al., 2004; Hughes et al., 1998; Sardar et al., 2005). Additional sampling site information including the results of earlier investigations of the physical and chemical properties of the PM observed at the USC site can be found in Ning et al., (2007) and Fine et al., (2004).

3.1.2.2 Sampling Protocol

Sampling was conducted between June and August, 2008 over a period of 10 consecutive weeks (excluding weekends). Quasi-ultrafine particles (D_p<180 nm) were collected using a low pressure drop impactor on Zefluor PTFE Membrane Filters (Pall Life Sciences, 3 µm, 8"x10", 28139-597) seated in a specially designed 20x25 cm high volume sampler (HIQ Environmental Products Co., CA). The impactor has been designed primarily as a separator of quasi-ultrafine particles from accumulation mode (0.18 µm ≤ Dp ≤2.5 µm) particles at a flow rate of 400 L/min. The design and operating performance of the multi-slit impactor have been described in detail previously (Misra et al., 2002). Time integrated samples were collected during both "morning" (6:00-9:00 PDT) and "afternoon" (11:00-14:00 PDT) time periods and were grouped into three sample sets (S1, S2, S3). There were 18 days total for the S1 sampling set, while both the S2 and S3 sets were collected for 16 days each. As the samples were composited for each grouping period (i.e. particles were collected on the same filter); the total number of samples for the entire campaign was 6 - two samples (morning and afternoon) for each grouping period (S1, S2 and S3). Thus, each sample of set S1 encompassed 54 hrs (18 days multiplied by 3 hrs per day), while 48 hrs (16 days multiplied by 3 hrs per day) for each sample of sets S2 and S3. The "morning" period corresponds to rush hour traffic when the ambient aerosols at the sampling site are dominated by primary particles freshly emitted from vehicles on the nearby freeway (Moore et al., 2007). The "afternoon" period represents the mixture of primary and secondary particles undergoing physical and chemical changes (i.e., photo-oxidation, volatilization, dilution and possibly re-suspension) (Moore et al., 2007). The strong influence of secondary photochemical sources during the afternoon at the sampling site is evidenced by the concentration of ozone [(O_3); averaged over three time periods, i.e., S1, S2 and S3], which increased from 9±4 ppb in the morning period to 50±10 ppb in the afternoon period. Meteorological conditions were quite consistent during the entire study period, with higher temperature and lower humidity in afternoon (28 ±2^{o}C and 44 ±5 %) compared to the morning period (20 ±1^{o}C and 70 ±5 %). The wind direction was mostly from south-west at the site. A Scanning Mobility Particle Sizer (SMPS Model 3080 and DMA Model 3081, condensation particle counter Model 3022A, TSI Inc., St. Paul., MN) was also set up concurrently to measure the particle size distribution. The sampling flow rate was 1.5 L /min, with a scan up time of 150 s. The minimum and maximum sizes detectable at these settings are 7.64 and 225 nm, respectively. The mass concentrations of quasi-ultrafine particles in both the morning and afternoon periods were obtained using a parallel MOUDI (Micro-Orifice Uniform Deposit Impactor; MSP Corporation, Minneapolis, MN) measurement. The mass concentration of quasi-ultrafine particles measured by the

MOUDI and the multi-slit impactor has been demonstrated to be in agreement (R^2>0.85) (Misra et al., 2002).

3.1.2.3 Sample Analysis

All filter samples, along with field blanks and lab blanks, were extracted in high purity deionized water at ambient temperature using a shaking table. The water extracts were analyzed for water soluble organic carbon (WSOC), water soluble ions, and water soluble trace elements. Water soluble ions were analyzed using two Ion Chromatography (IC) analyses: 1) analysis for cations; and 2) analysis for anions (Zhang et al., 2008). Trace elements were analyzed from the water extracts using a high resolution Inductively Coupled Plasma-Mass Spectroscopy (ICP-MS) as described by Zhang et al., (2008). Water soluble organic carbon (WSOC) for all the samples was analyzed using a Shimadzu TOC-5000A liquid analyzer (Decesari et al., 2001). A separate section of the sample, field blank and lab blank filters was extracted with a solvent mixture of methylene chloride and methanol using Soxhelet extraction. The extracts were concentrated before gas chromatography/mass spectrometry analysis as described by Stone et al., (2008). All chemical analyses were conducted with check standards and multipoint calibration curves to assure accurate quantification. All results were blank subtracted using the field blanks processed and analyzed with the samples.

The oxidative activity of the collected particles was quantified by two different assays: 1) consumption of dithiothreitol in a cell-free system (DTT assay), and 2) macrophage ROS

- in vitro exposure to rat Alveolar Macrophage (AM) cells using Dichlorofluorescin Diacetate (DCFH-DA) as the ROS probe. High purity deionized water was used for the filter extraction technique for both the DTT and ROS assays.

3.1.3 Results and Discussion

3.1.3.1 Physical Parameters

Figure 3.1a shows the hourly average particle number concentration in the size range from 7.64 nm to 180 nm, measured by the SMPS during the sampling campaign. As shown in the figure, the diurnal profile displays a shoulder in the morning (6:00 to 9:00 AM) to the distinguishable peak in the afternoon (11:00 AM to 2:00 PM). This represents emissions from morning rush hour traffic and secondary photo-chemical reactions occurring in the afternoon at the site, respectively (Moore et al., 2007). Average particle number concentrations in the afternoon are 1.6±0.1 times those in the morning, suggesting secondary particle formation consistent with the observations by Moore et al., (2007) at the same site. Figure 3.1b shows the average particle number size distribution (dN/dlogDp) measured during the morning and afternoon periods, respectively. The size distributions in both the morning and afternoon are mono-modal; however, the afternoon period is distinguished by a smaller peak mode diameter (28.9±1.1 nm) compared to the morning period (peak mode diameter = 41.5±1.5 nm). The larger peak mode diameter in the morning period may be due to the combined effects of condensation of organic vapors co-emitted from traffic sources onto freshly emitted ultrafine PM, which would be result of the lower temperatures and atmospheric dilution that prevail during this time period, and possibly to coagulation of highly concentrated nanoparticles. Both of these processes will enhance the growth of the particles emitted from vehicular sources compared to the relatively freshly formed secondary aerosols in the afternoon period (Zhu et al., 2002). Average mass concentrations of quasi-ultrafine particles were also higher in the afternoon period (5.7±2.6 μg/m^3) compared to 3.8 ±1.7 μg/m^3 in the morning period, indicating the additional contribution of secondary aerosol formation to the total $PM_{0.18}$ (particles with aerodynamic diameter ≤ 180 nm) mass.

Figure 3.1: a) Diurnal profile of the average particle number concentration of quasi-ultrafine particles measured at the USC sampling site and (b) the average particle number size distribution of quasi-ultrafine particles in “morning” and “afternoon” periods.

Figure 3.1a

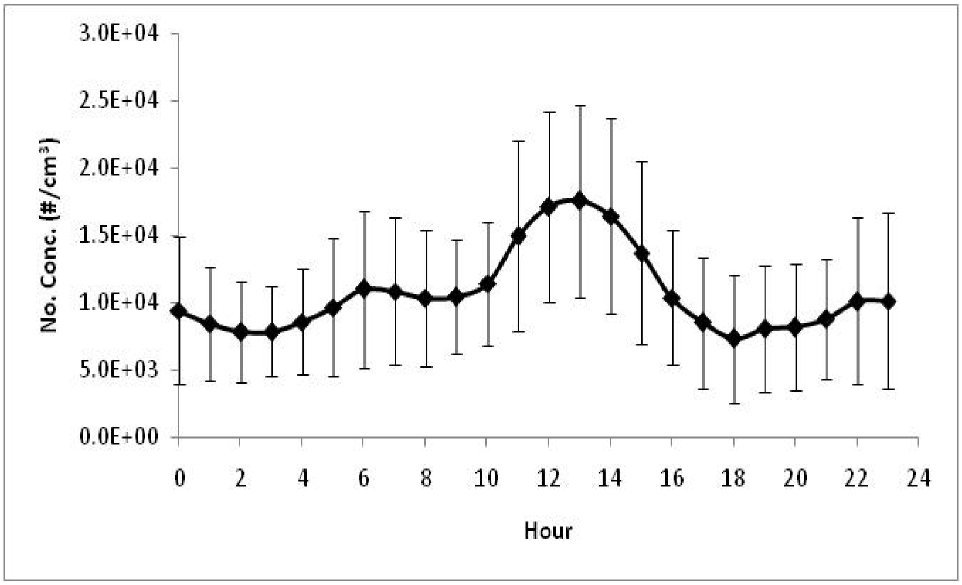

Figure 3.1b

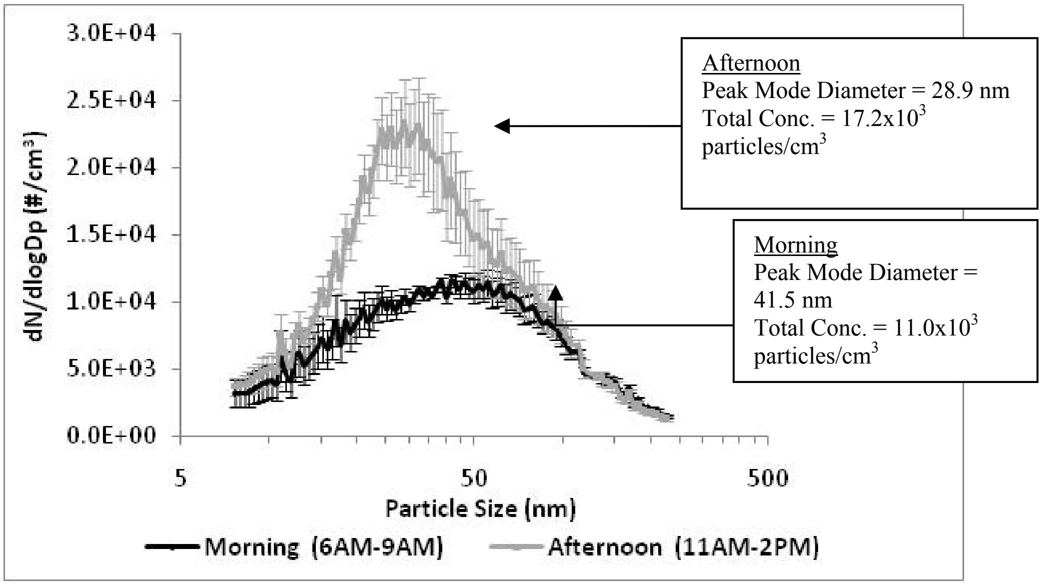

Afternoon
Peak Mode Diameter = 28.9 nm
Total Conc. = 17.2×10^3 particles/cm^3

Morning
Peak Mode Diameter = 41.5 nm
Total Conc. = 11.0×10^3 particles/cm^3

3.1.3.2 Chemical Parameters

Figure 3.2 shows the average mass concentration of major water soluble inorganic ions [sulfate (SO_4^{2-}), ammonium (NH_4^+), and nitrate (NO_3^-)] in quasi-ultrafine particles measured at the sampling site in the morning and afternoon periods.

Figure 3.2: Average concentration of the major inorganic ions in quasi-ultrafine particles collected in the morning and afternoon periods at the USC sampling site.

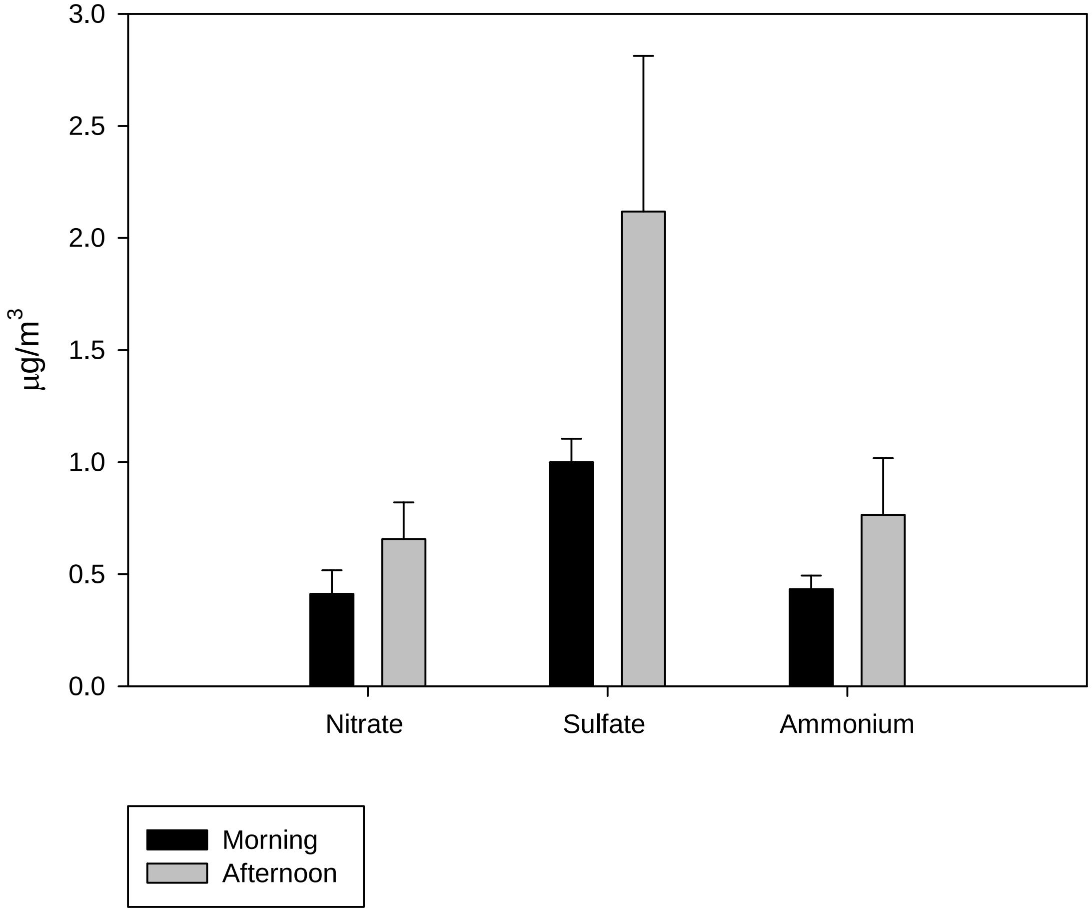

Concentrations of these ionic species are higher in the afternoon period compared to those in the morning, with afternoon-to-morning ratios of 1.76±0.38, 1.60±0.04 and

2.11±0.61 for NH_4^+, NO_3^- and SO_4^{2-}, respectively. This increase in concentrations in the afternoon period may be attributed to the oxidation of precursor gases (e.g. ammonia, sulfur dioxide and nitric oxide) by photo-chemical byproducts [e.g., ozone (O_3), hydroxyl free radical ($HO^\cdot$), hydroperoxyl radical ($HO_2^\cdot$)] followed by nucleation and/or condensation onto pre-existing particles (Ning et al., 2007). Following the approach by Zhang et al., (2004a), particle acidity can be expressed as the ratio of sum of measured ammonium and sodium concentrations to the concentrations needed to fully neutralize the measured sulfate, nitrate and chloride, with a value of unity suggesting the full neutralization and a value close to zero suggesting an acidic aerosol. The ratios measured during the morning and afternoon periods are 0.93±0.03 and 0.82±0.01, respectively, thereby indicating an 11±3 % increase in particle acidity in the afternoon period. This is consistent with the previous studies demonstrating higher acidity of the ultrafine particles [measured to fully neutralizing ammonium ratio of ~0.80; (Zhang et al., 2004a)] in the initial stage of photochemically induced nucleation.

Table 3.1 shows the comparison of the mass concentrations (average and standard deviation) of water-soluble trace elements and metals in the quasi-ultrafine particles in the morning and afternoon. A total of twenty elements have been quantified as shown in the table. Sulfur (S), Aluminum (Al), Calcium (Ca), Iron (Fe) and Sodium (Na) are the dominant species in the ambient atmosphere both in the morning and afternoon periods. The concentration of certain metals [Vanadium (V), Chromium (Cr), Nickel (Ni), Copper (Cu), Arsenic (As), Cadmium (Cd) and Zinc (Zn)] was higher in the morning period.

These heavy metals are known to be emitted from vehicles from both fuel combustion and lube oil emissions (Geller et al., 2006). Cu originates from vehicle brake abrasion (Garg et al., 2000; Sanders et al., 2003; Sternbeck et al., 2002) and Zn is mostly a product of tire attrition (Singh et al., 2002). Elevated levels of these metals in the morning period suggest traffic as the primary source of particles during the morning hours at the sampling site. Other metals such as Na, Magnesium (Mg), Phosphorus (P), Al, Ca, Potassium (K), Titanium (Ti), Manganese (Mn), Fe, Cobalt (Co) and Barium (Ba) displayed a different pattern with higher values in the afternoon period. These metals also exhibited a high degree of correlation amongst themselves ($R>0.70$, not shown) and probably originate from re-suspension of road dust, which is higher in the afternoon due to the higher wind speed (3.5±0.3 m/s compared to 0.9±0.4 m/s in the morning period), lower relative humidity (44±5 % compared to 70±5% in the morning period) and possibly higher vehicle speeds on the nearby streets and freeways, compared to the congested morning traffic hours. Although, the majority of these species are expected to be partitioned in the coarse PM ($PM_{10-2.5}$), there is a significant fraction in the sub-200 nm range, as demonstrated by earlier investigations in urban areas (Garg et al., 2000).

Table 3.1: Average concentrations of water-soluble elements in ambient quasi-ultrafine particles measured by ICP-MS at the USC sampling site during morning and afternoon periods

Metal	Morning		Afternoon		Ratio (Morning/ Afternoon)
	Average Conc., ng/m^3	S.D.	Average Conc., ng/m^3	S.D.	
Na	57.82	24.98	195.59	47.54	0.30
Mg	17.65	8.16	64.36	6.93	0.27
Al	112.55	42.20	311.37	34.95	0.36
P	3.81	6.00	10.44	3.36	0.36
Ca	110.31	127.09	198.15	50.86	0.56
S	472.53	311.01	578.42	130.74	0.82
K	22.39	17.77	82.59	34.39	0.27
Ti	7.02	3.36	24.43	6.77	0.29
V	5.78	4.72	5.50	1.43	1.05
Cr	1.35	1.24	0.55	0.49	2.46
Mn	2.34	1.30	4.73	1.19	0.49
Fe	106.94	62.39	286.21	78.88	0.37
Co	0.09	0.05	0.18	0.03	0.49
Ni	3.09	2.46	2.12	0.75	1.46
Cu	16.26	18.61	10.75	6.13	1.51
Zn	20.26	13.06	14.87	4.42	1.36
As	0.22	0.13	0.19	0.07	1.15
Cd	0.06	0.04	0.05	0.01	1.21
Ba	3.06	1.68	10.49	0.87	0.29
Pb	3.72	2.83	4.38	1.61	0.85

Figure 3.3a shows the average mass concentration of quasi-UFP WSOC and CO in the morning and afternoon periods. CO is an inert gas species often used as a marker of vehicular emissions (Zhu et al., 2002) and atmospheric dilution (Westerdahl et al., 2009), while WSOC consists of a variety of polar organic compounds and is regarded as an indicator of secondary organic aerosols (SOA) (Docherty et al., 2008). As shown in the

figure, the CO concentration decreased by a factor of 2.0±0.1 in the afternoon, as a result of a decrease in vehicular emissions coupled with an increase in the mixing height and atmospheric dilution in the afternoon period. However, despite the 2-fold increase in atmospheric dilution suggested by the CO concentrations, the average concentration of WSOC was elevated by 2.5±0.9 times compared to the morning period. We interpret this to indicate the formation of SOA driven by the oxygenation of particles with aging in the atmosphere during photochemical reactions in the afternoon.

Figure 3.3: Average concentration of the various organic species measured at the USC sampling site during the morning and afternoon periods a) Water Soluble Organic Carbon and Carbon Monoxide, b) Polycyclic Aromatic Hydrocarbons (PAHs), c) Hopanes and Steranes, and d) Alkanes and Organic Acids.

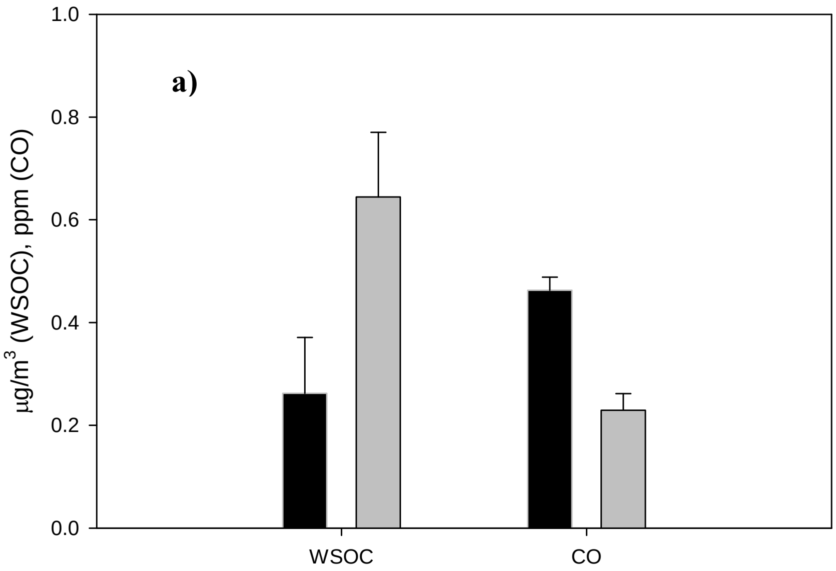

Figure 3.3 (Continued)

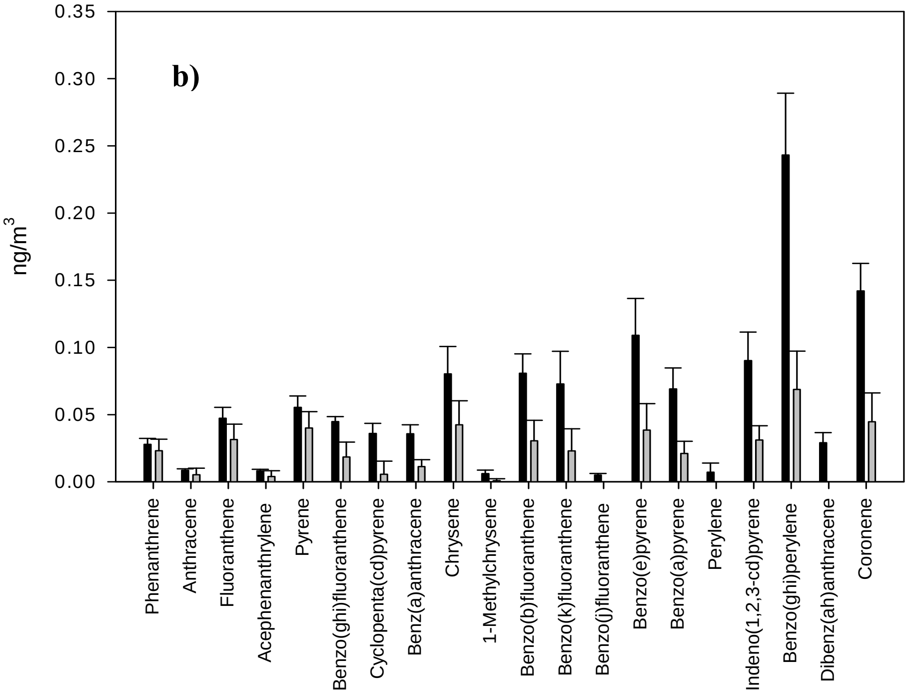

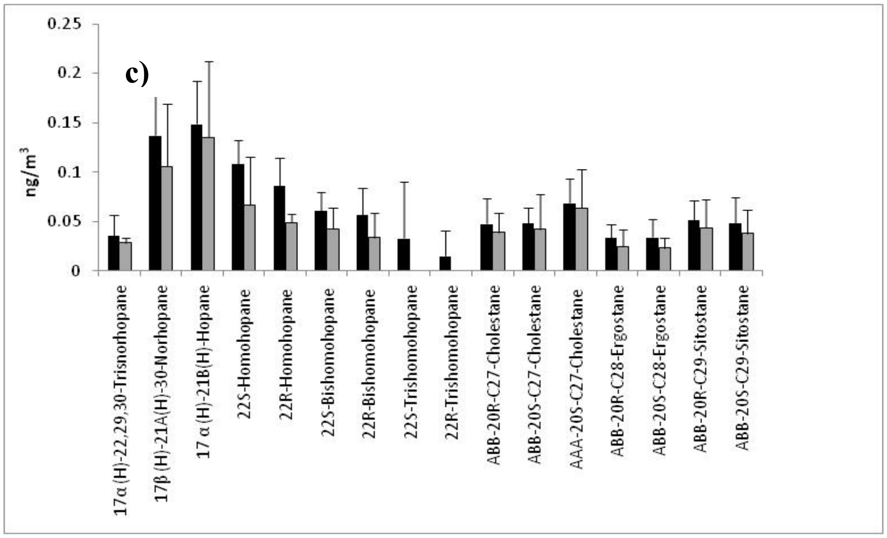

Figure 3.3 (Continued)

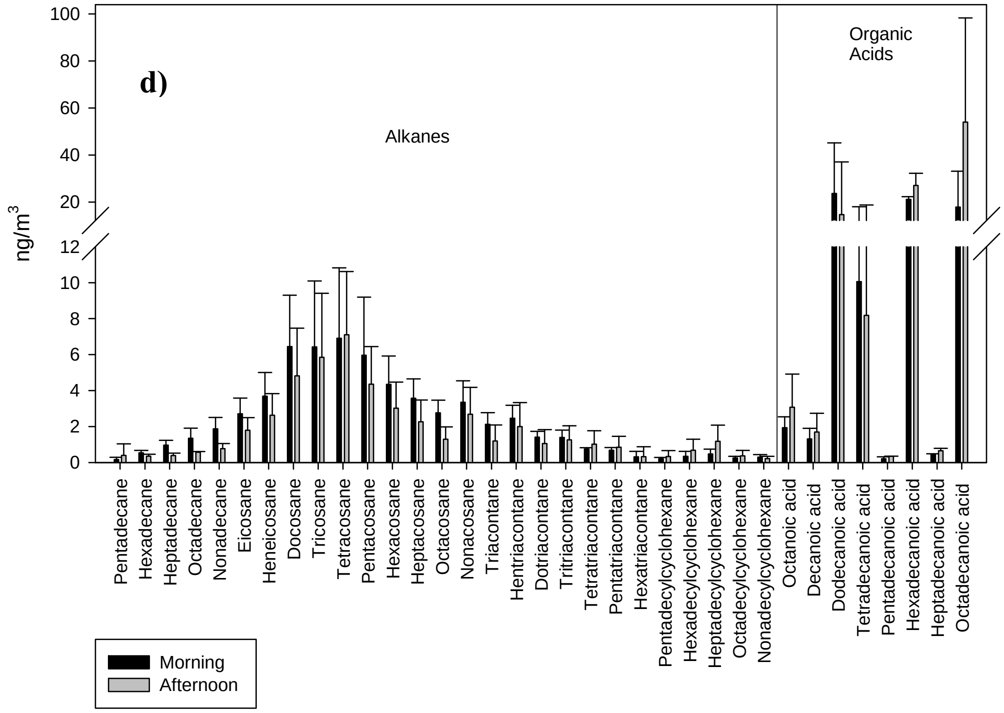

Figure 3.3 also shows the average quasi-UFP mass concentrations of speciated organic compounds [PAHs, (Figure 3.3b); hopanes and steranes, (Figure 3.3c); and alkanes and organic acids, (Figure 3.3d)] in the morning and afternoon periods. Most of the PAHs, hopanes, steranes, and alkanes were higher in the morning period compared to the afternoon period, attributed to their origin from vehicular sources (Ning et al., 2007). However, morning-to-afternoon ratio for certain species (particularly PAHs and alkanes) is relatively higher [up to 3.5±0.9 as for benzo (GHI) perylene], compared to that for CO (morning-to-afternoon ratio = 2.0±0.1; Figure 3a). The relatively larger decrease in the

concentration of PAHs and alkanes compared to CO in the afternoon indicates their possible volatilization and photo-oxidation in addition to dilution. Interestingly, in the fine size range ($PM_{2.5}$), concentrations of these organic species (PAHs and alkanes) were higher in the afternoon than the morning period. We hypothesize that volatilization of these species from the ultrafine particles in afternoon period and subsequent re-condensation onto the larger particles might be responsible for this trend (Venkataraman et al., 1999). Similar observations on the partitioning of PAHs between ultrafine and accumulation PM modes with increasing ambient temperature have also been made in other studies (Miguel and Friedlander, 1978; Pierce and Katz, 1975).

By contrast, concentrations of most of the organic acids were higher in the afternoon period (afternoon-to-morning ratio ranges from 1.2 to 3.0). These acids are probably the products of photo-chemical oxidation of either organic gases or semi-volatile species evaporating from the primary particles (Zhang et al., 2004b). Food cooking and vegetative detritus emissions might be included into other sources of some organic acids, but the sampling site is not substantially impacted by these sources, which supports the notion that atmospheric chemistry is likely responsible for the increased concentrations of these acids in the afternoon. The afternoon-to-morning ratio was higher (up to 3) for high carbon number organic acids (C_{15}-$C_{29,}$ e.g., Octadecanoic Acid, Pentadecanoic Acid) compared to the low carbon number acids (e.g. Octanoic Acid, Decanoic Acid; ratio ~1.5), probably due to the higher volatility of organic species associated with decrease in carbon number (Ning et al., 2007).

3.1.3.3 Oxidative Activity

The oxidative activity of the quasi-ultrafine particles was measured by two different methods as described earlier - the DTT and macrophage ROS assays. Figure 3.4 shows the results of the DTT assay for the three samples sets (S1, S2, and S3) and their average values in the morning and afternoon periods. The results have been expressed as mass (of PM) based activity (Figure 3.4a) in $nmol.min^{-1}.\mu g^{-1}$ and also volume (of air) based activity (Figure 3.4b) in $nmol.min^{-1}.m^{-3}$, respectively. As shown in Figure 3.4a, the mass based DTT activity of the quasi-UFP is consistently higher in the afternoon period for all of the sample sets with an average afternoon-to-morning ratio of 1.8±0.7. The DTT assay measures the capability of particles to generate superoxide radicals (O_2^{*-}) in their interaction with the thiol group compounds, which are the main antioxidants present in endothelial cells (Foresti et al., 1997). Although this assay is insensitive to hydroxyl free radicals ($HO^{\cdot}$), O_2^{*-} produced in the above reaction can play a role in the generation of $HO^{\cdot}$ also, by regenerating the precursors of Fenton's reaction (e.g. Fe^{+2} and H_2O_2) (Schoonen et al., 2006). In a recent experimental study, Li et al., (2009) demonstrated higher oxidative activity measured by the DTT assay of diesel exhaust particles (DEPs) aged with O_3 compared to the freshly emitted diesel PM. Our results showing the increased DTT activity of the quasi-ultrafine particles in afternoon period are very consistent with the work described earlier by Li et al., (2009), and lead to one of the most important findings of this study – compounds associated with secondary aerosols produced by photochemical processes in the afternoon period possess higher oxidative activity, and thus are more capable of generating free radicals and causing cell damage in biological systems.

As shown in Figure 3.4b, the DTT activity per m^3 of air is also consistently higher for the afternoon samples, with an average afternoon-to-morning ratio of 2.8±1.1 (compared to 1.8±0.7 for the mass based activity). The difference between the volume based and mass based DTT activity may have important implications with respect to the assessment of public exposure and the relative PM toxicity. While the mass-based oxidative activity is appropriate for comparing the relative PM toxicity from different sources, the volume-based activities become important in the context of the overall public exposure and the associated risks of individual contributions from various sources to ambient PM concentrations.

Figure 3.4: Oxidative activity (expressed as nmol of DTT/min) of quasi-ultrafine particles collected at the USC sampling site during the morning and afternoon periods; a) per µg of particulate mass and b) per m^3 of volume of air.

Figure 3.4a

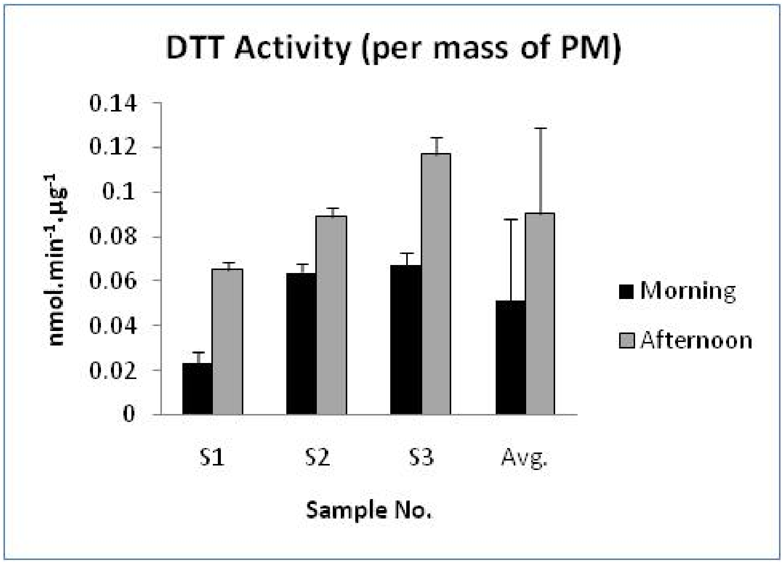

Figure 3.4b

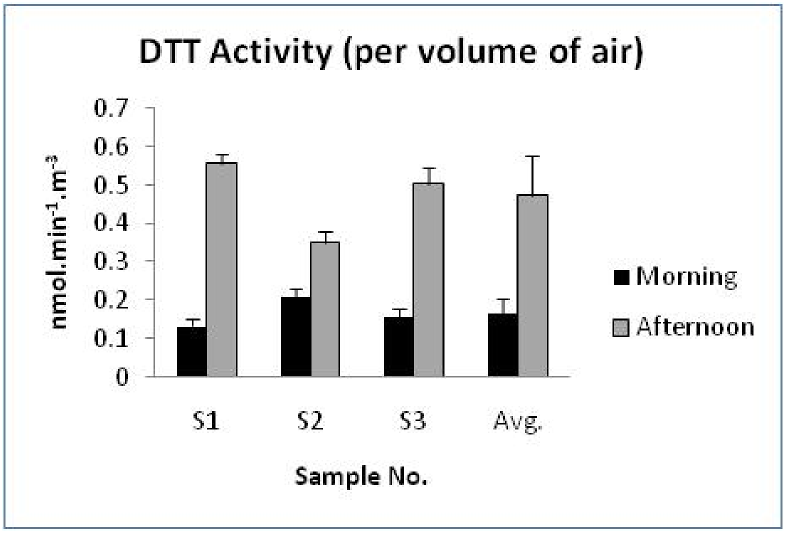

Figure 3.5 shows the results of macrophage ROS assay in the morning and afternoon periods, expressed as µg of Zymosan units per mg of PM mass (a), and per m^3 of air (b) on the collected quasi-UFP. There was significant variation in the ROS activity for the three sample sets (S1, S2 and S3) and the afternoon-to-morning ratio averaged over the three grouped periods was 1.2±1.1. Although the ROS activity of sample sets, S2 and S3 was higher in afternoon period, very high activity was observed for the morning period of sample set S1. The macrophage ROS assay measures the generation of reactive oxygen species by its reaction with DCFH. The ROS probe used in this method is sensitive to a broad spectrum of oxidants including $HO^{\cdot}$, hydrogen peroxide (H_2O_2) and nitric oxides ($NO^{\cdot}$) (Schoonen et al., 2006). The inconsistent trend in ROS activity for the morning and afternoon samples indicates that, although secondary organic compounds formed in afternoon period may contribute to the formation of $HO^{\cdot}$ in biological cells, the overall capability of PM to generate free radicals is also dependent on species emitted from primary sources in the morning period. The following section will further elaborate on the relationship between the PM chemical constituents and free radicals generation.

Figure 3.5: Oxidative activity (expressed as the ROS response, or µg of Zymosan units) of quasi-ultrafine particles collected at the USC sampling site during the morning and afternoon periods; a) per mg of particulate mass and b) per m^3 of volume of air.

Figure 3.5a

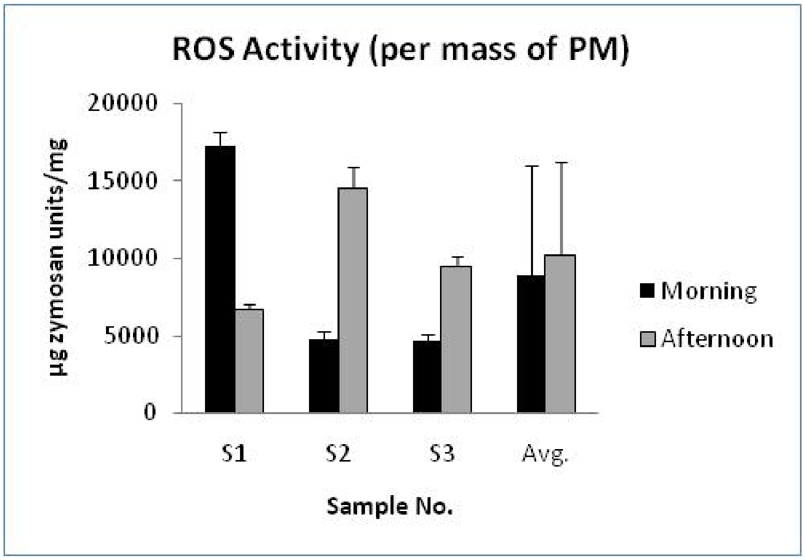

Figure 3.5b

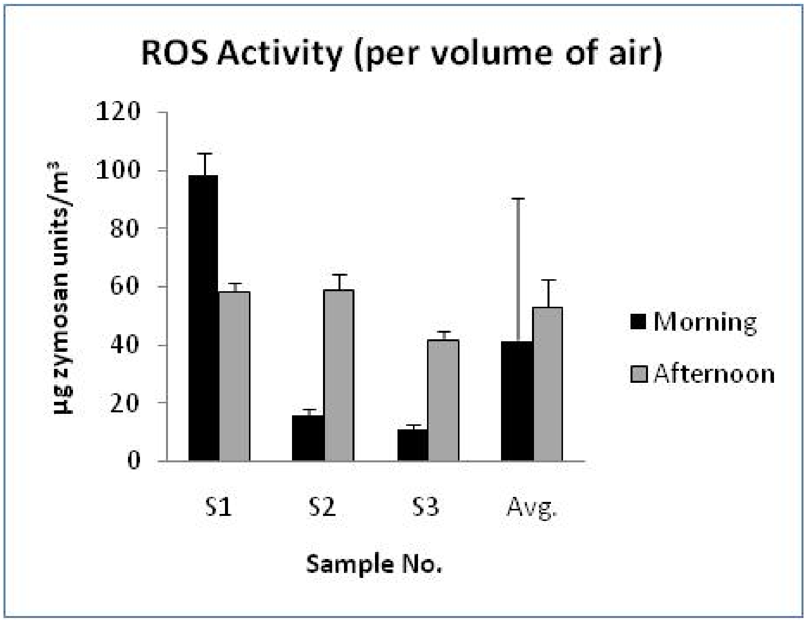

3.1.3.4 Correlation of Oxidative Activity with Chemical Constituents of PM

The DTT and ROS assays measure the PM oxidative activity based on the generation of different reactive oxygen species. The dissimilar diurnal profiles of PM activity obtained by these assays indicate different pathways of redox active chemical PM species in generating cellular oxidative stress. Linear regression analysis was carried out to investigate the association of the DTT and ROS activities with quasi-UFP chemical composition. Table 3.2 shows a summary of the regression analysis [i.e. slope, intercept, correlation coefficients (R^2) and the associated levels of significance (p value)] for select species which were correlated (R^2>0.60) with either the DTT or ROS rates.

As shown in the table, we observed high correlation between WSOC and the DTT activity of quasi-UFP (R^2 = 0.82; p = 0.01), despite the rather limited number of data points. Previous studies have also documented the positive correlation of DTT activity and WSOC content of the PM (Biswas et al., 2009; Hu et al., 2008; Verma et al., 2009). This supports our hypothesis that the increased solubility of organic compounds mediated by photo-chemical oxidants during secondary organic aerosols formation enhances the capability of PM to generate free radicals.

The measured organic compounds were further categorized as per different functional groups (PAHs, hopanes and steranes, alkanes, high and low carbon number organic acids) to investigate their correlation with oxidative activity. As shown in Table 3.2, DTT activity is positively correlated with high carbon number organic acids (C_{15}-C_{29}) (R^2 =

0.71; slope = 0.01). Many of these organic acids are formed by the photo-oxidation of semi-volatile organic species, producing polar oxygenated compounds. Thus their positive correlation with DTT suggests their partial contribution to the association of DTT with WSOC discussed earlier.

Table 3.2: Summary of the regression analysis [slope, intercept, correlation coefficients (R^2) and the associated levels of significance (p value)] for select species with DTT and ROS levels. Species included in this table are correlated (R^2>0.60, shown bolded) with at least one of the assays.

	DTT Activity				**Macrophage ROS**			
Species	**R^2**	**p**	**Slope***	**Intercept$^{\Psi}$**	**R^2**	**p**	**Slope***	**Intercept$^{\Psi}$**
NO_3^-	**0.68**	0.04	0.82	-8.12	0.20	0.37	79.97	4.57
SO_4^{-2}	**0.69**	0.04	0.20	0.01	0.08	0.59	11.88	28.79
NH_4^+	**0.62**	0.07	0.58	-0.03	0.14	0.47	48.41	18.32
WSOC	**0.82**	0.01	0.70	0.00	0.09	0.58	40.11	29.14
Mg	**0.80**	0.02	0.01	0.07	0.15	0.44	0.48	27.75
Al	**0.64**	0.06	1.00E-03	0.05	0.14	0.47	0.10	25.36
Ca	0.17	0.41	0.00	0.20	**0.84**	0.01	0.30	1.45
S	0.04	0.72	0.00	0.24	**0.91**	0.01	0.14	-25.79
K	**0.71**	0.04	3.00E-03	0.12	0.22	0.35	0.37	28.11
Ti	**0.79**	0.02	0.02	0.08	0.15	0.44	1.18	28.72
V	0.01	0.84	-0.01	0.35	**0.91**	0.00	9.83	-8.16
Fe	**0.69**	0.04	1.00E-03	0.07	0.28	0.28	0.15	18.76
Ni	0.13	0.49	-0.04	0.42	**0.73**	0.03	16.12	5.38
As	0.01	0.85	-0.20	0.36	**0.66**	0.05	281.00	-10.08
Cd	0.08	0.60	-1.82	0.42	**0.77**	0.02	1024.00	-9.31
Ba	**0.75**	0.03	0.04	0.07	0.19	0.38	3.35	24.64
PAHs	**0.68**	0.04	-0.33	0.59	0.02	0.79	11.02	38.33
Organic Acids (C_{15}-C_{29})	**0.71**	0.15	0.01	0.07	0.07	0.74	0.45	44.02

Note: Sample size for the regression analysis is N = 6.

*expressed as oxidative activity (nmol/min for DTT and µg Zymosan units for ROS) per µg or ng of species (µg for inorganic ions and WSOC; ng for metals, PAHs and organic acids).

$^{\Psi}$ expressed as nmol/min/m^3 for DTT and µg of Zymosan units/m^3 for macrophage ROS

In the present study, the DTT activity of the ultrafine particles is observed to be negatively correlated with measured PAHs ($R^2 = 0.68$, slope = -0.33) as shown in Table 3.2. This is in contrast to previous studies showing rather modest to strong positive associations between DTT activity and PAHs (Cho et al., 2005; Ntziachristos et al., 2007). Although PAHs themselves do not contain the functional groups capable of catalyzing the oxidation of DTT, their possible photo-oxidation during photochemical episodes in the afternoon period may convert them to oxy-PAHs, quinones and nitro-PAHs, which are all active in DTT assay (Cho et al., 2005). However, we did not quantify these oxygenated products in the present study. Nevertheless, the negative correlation of the measured PAHs with DTT activity may be explained by their lowered concentrations in the afternoon due to possible volatilization. It is important to note that this volatilization may be followed by photo-oxidation to form oxygenated PAHs, which contribute to the increase of DTT activity in the afternoon. The difference in the sampling protocols between our study and previous studies (Cho et al., 2005; Ntziachristos et al., 2007) might explain the contrasting correlations. In the present study, the sampling protocol was intentionally designed to distinguish the impacts of primary and secondary sources on PM toxicity. This differs from the uninterrupted time integrated sampling of previous studies, ranging from several hours to several days, without discriminating the morning and afternoon periods, which would obscure the impact of PAHs chemical transformation on redox properties of PM. Thus, the positive correlation in those studies may be attributed to the confounding relationship between PAHs and oxygenated PAHs. Moreover we did not observe any significant associations between DTT activity and the concentrations of hopanes, steranes and alkanes, which again suggests that organic compounds present in relatively fresh traffic PM emissions are not as redox active as their aged photo-oxidized products.

Inorganic ions such as nitrate (NO_3^-), sulfate (SO_4^{-2}) and ammonium (NH_4^+) and certain water soluble trace elements (Mg, Al, K, Ti, Fe and Ba) are also correlated with DTT activity as shown in Table 3.2, although none of these species is mechanistically active in this assay (Cho et al., 2005). These inorganic species were correlated with WSOC ($R>0.75$), suggesting their co-linearity with the redox active water soluble organic compounds, rather than actual contribution to DTT activity.

Table 3.2 shows that ROS measured PM activity is correlated ($R^2>0.65$; $p<0.05$) with certain water soluble elements such as V, Ni, Cd (transition metals) and As. V and Ni are the metals which participate in Fenton chemistry and are capable of generating hydroxyl radicals once coming in contact with the biological cells (Schoonen et al., 2006). These hydroxyl radicals can effectively oxidize the DCFH probe used in the ROS assay. The ROS activity was significantly correlated with V concentrations ($R^2=0.91$; $p=0.01$), and also Ni ($R^2=0.73$, $p=0.03$). Both of these species are mostly emitted from bunker fuel (heavy fuel oil) combustion, although V is emitted at a proportionally higher rate (Arhami et al., 2009). Hu et al., (2008) also observed an association between V and ROS activity in a comparison of the oxidative activity profiles of PM in the Los Angeles-Long Beach Harbor area and attributed this association to the influence of ship emissions on ambient PM. The significant correlation of V with the ROS activity measured in this study, in agreement with previous studies (Hu et al., 2008; Verma et al., 2009), is of particular note because it confirms the impact of heavy fuel oil combustion on particle oxidative activity. The remaining correlated metals (Cd and As) are associated with primary sources such as vehicular exhaust (Arhami et al., 2009; Thomaidis et al., 2003), and are unaffected by the secondary photo-chemical reactions occurring in afternoon.

We did not observe any significant correlation between WSOC and ROS activity ($R^2=0.09$; $p=0.58$), in contrast to the case of DTT activity. It indicates that despite the possible contribution of secondary organic compounds on $HO^{\cdot}$ production, the cellular generation of oxidants (and thus ROS activity) is predominantly limited by the transition metals, which are the active participants in the ROS assay and are mostly emitted from primary sources. Consequently, the relative fractions of metals and WSOC in PM determine the net change of ROS activity of particles attributable to primary and secondary sources and probably explain its inconsistent trend in the morning and afternoon period, as mentioned in previous section.

There are no studies in recent literature to document the oxidative activity of species such as Ca and S, which are also significantly correlated with the ROS assay results, as shown in the Table 3.2. Their correlation with ROS activity is probably due to their correlation with redox active transition metals.

3.1.4 Conclusions

The ROS measured activity of PM is mostly driven by transition metals and possibly amplified by WSOC, its overall value depends on the relative PM mass properties of both groups of species in the morning and afternoon periods. On the other hand, the DTT activity, determined primarily by WSOC, clearly increases in the afternoon period. Although primary particles have the capability of generating free radicals in cells, their photo-oxidation products - secondary particles appear to be more potent in terms of generating oxidative stress, which underscores the importance of chemical transformations of primary emissions with atmospheric aging on the overall PM toxicity and associated health risks.

3.2 Oxidative Activity Profiles of Ambient Particulate Matter Influenced by Woodsmoke Emissions from Wildfires

3.2.1 Introduction

The semi-arid Mediterranean climate of Southern California, characterized by dry and hot autumns and unusually fast (>85mph) Santa Ana winds, contributes to the occurrence of wildfires in the region, often during the fall period. Ambient levels of air pollutants including carbon monoxide (CO), nitrogen oxides (NOx), volatile organic compounds (VOCs) and particulate matter (PM) increase in the affected areas during these events (Artaxo et al., 1994; Phuleria et al., 2005). Wood smoke generated from wildfires contains a large number of organic/inorganic chemicals such as aldehydes, carboxylic acids, polycyclic aromatic hydrocarbons (PAHs), resin acids, potassium, and magnesium. Many of these chemicals (e.g. PAHs and aldehydes) are toxic and potential human carcinogens (Naeher et al., 2007), while some of these species (e.g. potassium and levoglucosan) are often used as tracers for the presence of wood smoke in the ambient air (Schauer et al., 2001; Simoneit et al., 1999). Several in-vivo studies on laboratory animals found a positive correlation between wood smoke exposure and adverse health effects, such as pulmonary lung cell injury (Thorning et al., 1982), tracheal erosion and oxidative stress (Dubick et al., 2002), and allergic airway inflammation (Barrett et al., 2006).

On October 20, 2007, a series of wildfires began in Southern California, ranging from Santa Barbara County to the U.S.–Mexico border, which burned more than 500,000 acres of land causing the largest mandatory evacuation in the state's history. The counties of San Diego and Los Angeles alone accounted for 91.5% of the total burnt area. Although the last fire was fully contained by November 9, all of the fires in the Los Angeles County were under control by October 30, 2007.

This paper presents measurements of various particulate and gaseous pollutants at a site near the University of Southern California (USC), in downtown Los Angeles, during the October 2007 fire event. Detailed chemical and toxicological characteristics of PM samples collected during the fire episode, including water-soluble organic carbon, inorganic elements, organic compounds and reactive oxygen species, were evaluated and compared to those after the fire event, when outdoor $PM_{2.5}$ levels were mostly impacted by traffic emissions. One of our main goals was to determine the oxidative activity profiles of PM during these two periods and correlate them with source-specific PM constituents, in order to evaluate the potential contributions of the two major PM sources during this campaign (wildfires and vehicular traffic) to the overall PM oxidative properties.

3.2.2 Experimental Methods

3.2.2.1 Sampling Location

Sampling was conducted at the University Park Campus of USC, 2.5 km south of downtown Los Angeles. Further details about the sampling site are provided in section 3.1. Gaseous pollutant data were taken from SCAQMD (South Coast Air Quality

Management District) measurements at North Main Street (Los Angeles), about 2 km northeast from the site.

3.2.2.2 Sampling Protocol

Integrated $PM_{2.5}$ samples were collected using a high volume sampler (HIQ Environmental Products Co., CA; flow rate = 450 l/min) (Misra et al., 2002) on five different days (October 24, October 25, October 27, November 1, November 14). Particles were collected using Teflon coated glass fiber filters (Pallflex, Fiberfilm T60A20 – 8x10 IN, Pall Corp., East Hills, NY) seated in a specially designed 20x25 cm high-volume filter holder. Since the Los Angeles wildfires started on October 20 and continued until October 30, samples collected from October 24 to October 28 represent conditions impacted by both vehicular traffic and wildfire emissions, while the November 1 and 14 samples were considered representative of typical ambient conditions in that area, affected mostly by vehicular traffic emissions.

A Scanning Mobility Particle Sizer (SMPS Model 3080 and DMA Model 3081, TSI Inc., St. Paul., MN) was set up concurrently to measure the particle size distribution. The aerosol sampling flow rate was 0.3 L /min, with a scan up time of 255 s. The minimum and maximum sizes detectable at these settings are 14.1 and 736.5 nm, respectively.

3.2.2.3 Sample Analysis

All Teflon coated glass fiber filter samples were extracted in water and then analyzed for trace elements by Inductively Coupled Plasma-Mass Spectroscopy (ICP-MS) (Lough et al., 2005) and water soluble organic carbon (WSOC) using a Shimadzu TOC-5000A liquid analyzer (Decesari et al., 2001). For quantification of the organic compounds present in the particulate phase during and after the fire event, 3 during-fire samples and 2 post-fire samples were composited, respectively, and analyzed by gas chromatography/mass spectrometry (GC/MS). The oxidative activity of the collected particles was assessed by two different assays: 1) macrophage ROS - in vitro exposure to rat Alveolar Macrophage (AM) cells using Dichlorofluorescin Diacetate (DCFH-DA) as the fluorescent probe (Landreman et al., 2008) and 2) consumption of Dithiothreitol (DTT) in a cell-free system (DTT assay) (Cho et al., 2005).

3.2.3 Results and Discussion

3.2.3.1 Particulate Matter Characteristics

Figure 3.6 shows the evolution of the particle number size distribution from days during wildfires (October 24-25, 26-27, and 27-28) to the post-fire period (November 01-02 and 14-15). All scans were taken from 04:30 pm until 10:30 am of the following day to capture the effects of evening and morning traffic rush hours, which clearly caused an increase in particle number concentration between 07:00 and 11:00 pm, and from 06:00 to 10:00 am. Scans collected between October 24 and 28 are characterized by a higher number of larger particles (mobility diameter ≥ 100 nm). The mode diameter was generally higher for most of the sampling time on days during fire (around 70-110 nm) than that recorded on November 01-02 and 14-15 (peak value at 60 nm). Similar results were observed during the 2003 wildfire event in Southern California (Phuleria et al., 2005), and previous studies also indicated that the particle number size distribution of freshly emitted wood-smoke is unimodal, with average mode diameter around 100 nm (Hays et al., 2002). In addition, the particle number concentration increased during the fire event by an approximate factor of 2 (Figure 3.7) and, although it was also notably high on November 14-15, the mode diameter remained below 60 nm, which is typical of particles emitted mainly from vehicular sources in Los Angeles (Kuhn et al., 2005).

Figure 3.6: Evolution of the particle number size distribution from days characterized by wildfire emissions (October 24-25, 26-27, and 27-28) to periods not directly affected by fire (November 01-02, 14-15). Data were collected using a Scanning Mobility Particle Sizer (SMPS, Classifier Model 3080 and DMA Model 3081, TSI Inc., St. Paul., MN)

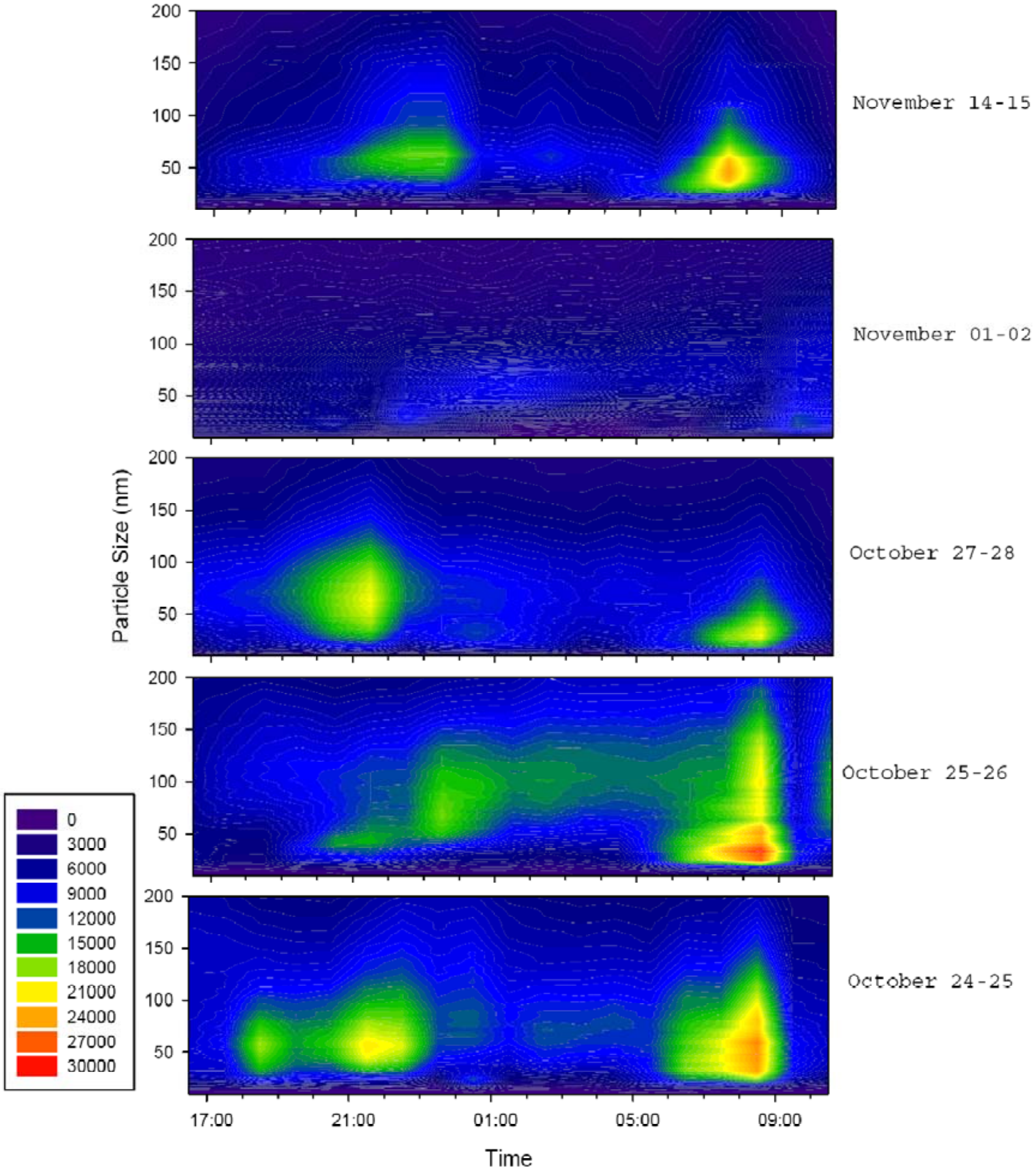

Figure 3.7: 24-hr averaged concentration of NO, NO_2, CO and O_3 at North Main Street (Los Angeles) and Particle Number Concentration at the USC (also 24-hr average) before, during and after the fire period.

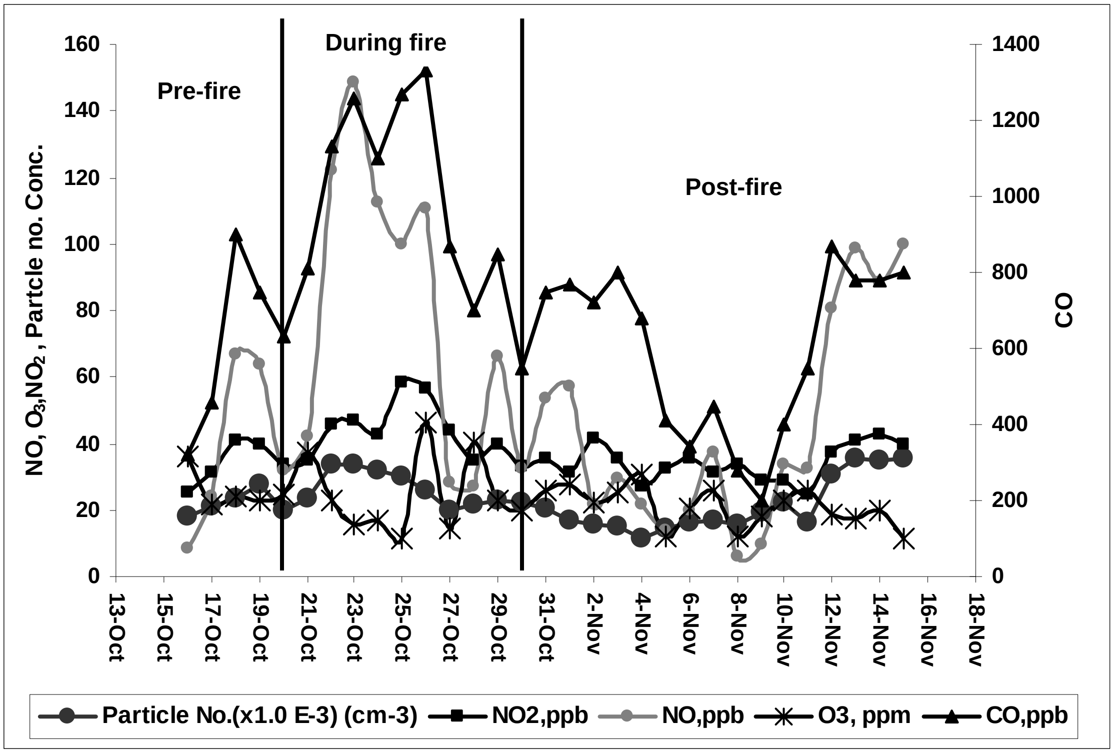

3.2.3.2 Gaseous Pollutants

Figure 3.7 presents 24-hr average concentrations of CO, nitrogen oxide (NO), nitrogen dioxide (NO_2), and Ozone (O_3) in downtown Los Angeles for pre-, during- and post-fire periods. While the concentrations of both CO and NO increased almost 3-fold during the fire event, the O_3 and NO_2 levels were marginally affected by wildfire emissions. Phuleria et al. (2005) observed a similar trend for these gases during the October 2003

Southern California wildfire. Reduced photochemical activity due to the smoke blanket over the region might explain these trends in O_3 and NO_2.

3.2.3.3 Water Soluble Trace Elements

Table 3.3 shows a comparison of the average fractional concentration (expressed in μg/g of PM) of water-soluble elements in ambient particles measured at the USC site during and after the fire event. Ambient levels of these trace elements from a previous study conducted few months before at the same location are also provided (Arhami et al., 2009). It should be noted that the average meteorological conditions during that study were very similar to our post-fire period (temperature ranged from 59 to 63^{o}F, and relative humidity was between 60 and 71%). The fractional concentrations of certain elements increased by a factor of 2 or more between October 24 and 28. The results of one-sample t-test revealed a statistical difference (at the 95% confidence interval, or CI) between the mean fractional concentrations of Mg, P, K and Mn observed during and after the fire event. When a CI of 90% was considered, statistical difference was also observed for Co, Ti, and other less abundant elements (e.g. Ga,Sr, Ru and others, not shown). Potassium, often used as a signature species for biomass combustion and a tracer of forest fires (Artaxo et al., 1994), was one of the elements whose levels were consistently elevated during the fire episode. Interestingly, the fractional concentration of K, even after the fire event, was higher (5447 μg/g) than its typical level (2245 μg/g) at the site, which indicates a likely persistence of residual wood smoke even after the fire was ceased. This may be particularly true for the November 1 sample, whose PM mass may contain a considerable fraction of residual wood smoke constituents, including re-suspended smoke-related particles from the paved roads.

Table 3.3 Average fractional concentration of water soluble elements (ICP-MS) in ambient particles collected at the USC site during (October 24, 26 and 27, 2007) and after (November 1 and 14, 2007) the fire event. Ratios between during- and post-fire concentrations are also reported. Statistically significant levels and ratios (at p=0.10) are shown in bold letters.

Element	**During Fire**		**Post Fire**		**Elevation Ratio (during fire / post fire)**	**Typical ambient levels at the sampling site (µg/g of PM)**	
	Average Value, µg/g of PM	**S.D.**	**Average Value, µg/g of PM**	**S.D.**		**Average Value, µg/g of PM**	**S.D.**
Ti	**7.11**	**0.94**	**2.13**	**1.11**	**3.34**	2.89	0.65
Cu	631.73	546.24	236.10	80.42	2.68	275.23	47.44
Mn	**334.75**	**134.77**	**153.49**	**69.72**	**2.18**	102.52	2.00
Cd	4.00	2.58	1.85	0.71	2.16	3.89	1.45
Mg	**5860.12**	**1328.00**	**2857.33**	**1422.36**	**2.05**	2672.45	982.73
P	**954.06**	**470.36**	**476.40**	**320.41**	**2.00**	178.81	0.18
Al	577.21	464.83	298.70	414.18	1.93	256.40	24.53
K	**9887.85**	**2102.38**	**5446.63**	**2594.56**	**1.82**	2244.88	77.58
Zn	1513.01	1101.37	845.08	462.17	1.79	540.77	69.90
Na	28411.30	18607.50	16205.20	1421.05	1.75	14298.66	2762.341
Co	**3.50**	**0.56**	**2.23**	**0.07**	**1.57**	2.42	0.23
Ca	33829.90	20785.60	26472.00	27208.10	1.28	3228.07	1981.39
Fe	639.61	360.28	524.81	713.10	1.22	590.49	34.45
Cr	7.90	0.42	6.92	0.46	1.14	4.24	2.76
Ni	29.89	17.40	28.04	5.37	1.07	35.48	9.09
Pb	13.81	11.54	13.10	16.16	1.05	21.04	5.24
Ba	968.64	499.50	944.71	1199.34	1.03	404.67	152.45
S	23087.70	9865.16	28102.50	9808.47	0.82	20158.39	4923.36
V	57.08	36.38	77.50	15.20	0.74	105.54	5.86

Several studies have reported increased concentrations of K, P, Cl, Zn, Br, Si, Ca (Echalar et al., 1995) and S (Artaxo et al., 1994) in ambient air affected by biomass combustion or wildfires. These particle-bound elements traversed the Los Angeles basin due to the prevailing westerly wind direction. An analysis of size-segregated biomass burning samples showed that most of these elements dominate the fine PM mode (aerodynamic diameter less than 2.5 µm), which can be transported by winds over hundreds of kilometers (Artaxo et al., 1994). By contrast, the concentrations of other elements (e.g. V, Fe, Ni, Cu, Zn, Ba, Pb) that typically originate from vehicular emissions (Ning et al., 2007) or other combustion sources (residual fuel oil combustion; (Arhami et al., 2009)) and road dust (Wang et al., 2005) were similar between samples collected during and after the fire period.

3.2.3.4 Water Soluble Organic Carbon (WSOC)

The WSOC content of ambient particles was higher during the fire event (170 ± 80 µg/mg of PM) compared to the post-fire period (78±35 µg/mg). A one-sample t-test confirmed a statistically significant difference (95% CI) between the mean WSOC levels observed during and after the fire event. Similar increases in the WSOC concentration were observed by Saarikoski et al. (2007) in ambient particles collected in Helsinki during a major biomass-burning episode in April-May 2006. Wood smoke is rich in organic compounds {56 to 90% by mass, depending on the wood type and combustion conditions (Schauer et al., 2001)}, the majority of which (up to 99%) is oxygenated in the atmosphere and becomes water-soluble (Novakov and Corrigan, 1996).

These studies (including our own) confirm that biomass burning is an important source of water-soluble organic compounds in ambient aerosols. This is of particular note in the context of global climate change, as WSOC plays an important role in the formation of cloud condensation nuclei by modifying the hygroscopicity of atmospheric aerosols (Cruz and Pandis, 1998).

3.2.3.5 Organic Constituents

Figure 3.8 presents the fractional concentrations of the speciated organic compounds in ambient particles collected at USC (expressed as µg/g of PM), during and after the fire period, and also from a previous study conducted at the same site few months before (Arhami et al., 2009).

The concentration of levoglucosan increased by 2-fold during the fire episode compared with the post-fire period (Figure 3.8a). However, post-fire levels of levoglucosan were also significantly higher than those typically present at that site. This may be due to the fact that levoglucosan is an extremely stable compound emitted in large quantities from the pyrolysis of wood cellulose (Jordan et al., 2006), and has a long residence time in the atmosphere. It is also possible that re-suspended smoke-related particles contribute to the elevated levels of levoglucosan in the post fire samples.

The concentrations of most PAHs were not affected by the fire episode, with the exception of retene, which was elevated during the fire event (6.68 µg/g) but was not detected in the post-fire period (Figure 3.8b). Retene is known to be present in wood smoke in relatively higher amounts compared to other PAHs and is commonly used as an indicator of softwood burning (Villalobos-Pietrini et al., 2006).

Figure 3.8: Fractional concentration of the organic constituents in PM samples (expressed in µg/g of PM) collected at the USC site, during and after the fire events: a) Levoglucosan, b) Polycyclic Aromatic Hydrocarbons (PAHs), c) n-Alkanes and Fatty acids

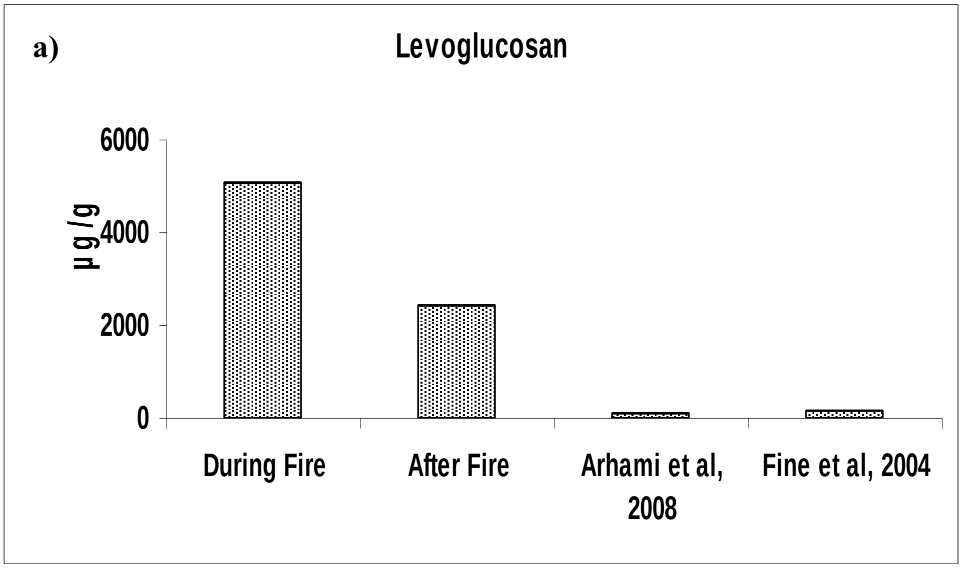

Figure 3.8 (Continued)

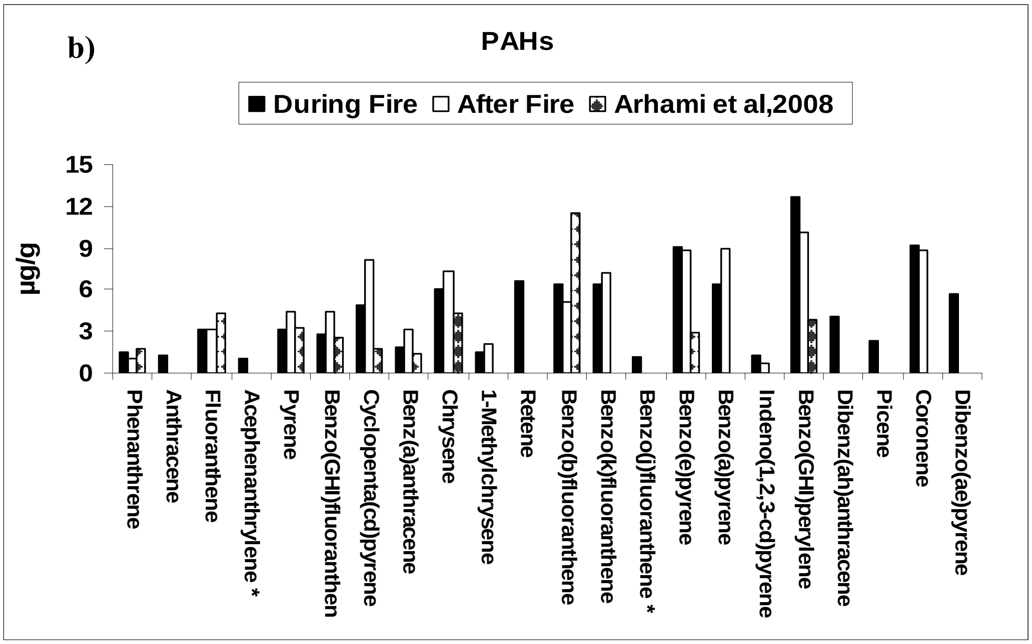

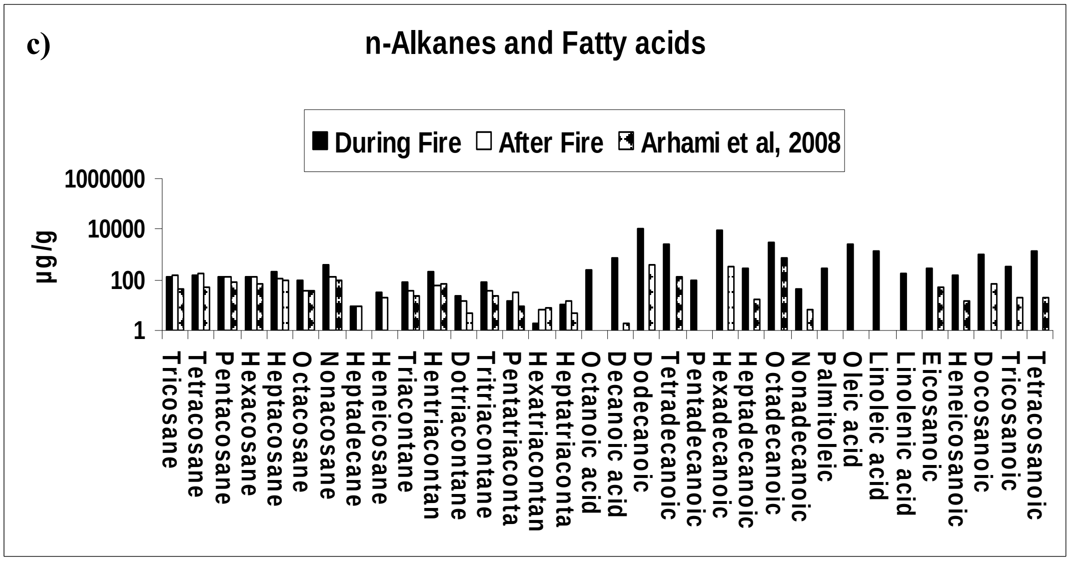

Figure 3.8c shows an increase in some of the n-alkanes concentrations measured in PM samples collected from October 24 to 28. Although this increase was not substantial (up to a factor of 1.4) compared with the corresponding post-fire levels, it was quite marked

(up to a factor of 3.5) with respect to the typical levels reported by Arhami et al., (2009) at the same site. Fatty acids were present in significant amounts in the “during-fire” samples, and were not quantifiable in samples collected on November 01 and November 14 (Figure 3.8c). Arhami et al., (2009) also showed negligible concentrations of fatty acids present in the ambient air at the same site under similar metrological conditions. These hydrocarbons (n-alkanes and fatty acids) are generally emitted by the volatilization of plant waxes from the leaf surface at high temperatures, or from fossil fuel combustion (Yan, 2007).

3.2.3.6 PM Oxidative Activity

Figure 3.9a shows the results of the DTT assay conducted on samples collected during and after the fire event. The outcomes were reported both as nmol of DTT consumption per µg of PM (nmol DTT / min × µg), as well as per m^3 of air (nmol DTT / min ×m^3). Particles collected between October 24 and 28 produced higher DTT activities per unit of PM mass than those collected on November 01 and 14. DTT activity was the highest on October 24 (0.024 nmol DTT / min × µg) and decreased gradually with time to 0.005 nmol DTT / min × µg on November 14. Data by Li et al., (2003) previously obtained at the same site in the absence of wildfire emissions and under similar meteorological conditions (average temperature 55 ± 4^{o}F, relative humidity 61 ± 12 %) is also shown in Figure 3.9 for comparison. Although the DTT activity may vary depending upon a number of factors that influence the PM chemical composition (such as season and traffic intensity), the levels reached at the peak of the fire event on October 24 are remarkably higher than those observed in previous studies at the same site (Cho et al., 2005; Li et al., 2003; Ntziachristos et al., 2007).

Figure 3.9: Oxidative activity of PM samples collected at the USC site during and after the fire period a) expressed as nmol of DTT consumption /min, b) expressed as the ROS response, or µg of Zymosan units

a)

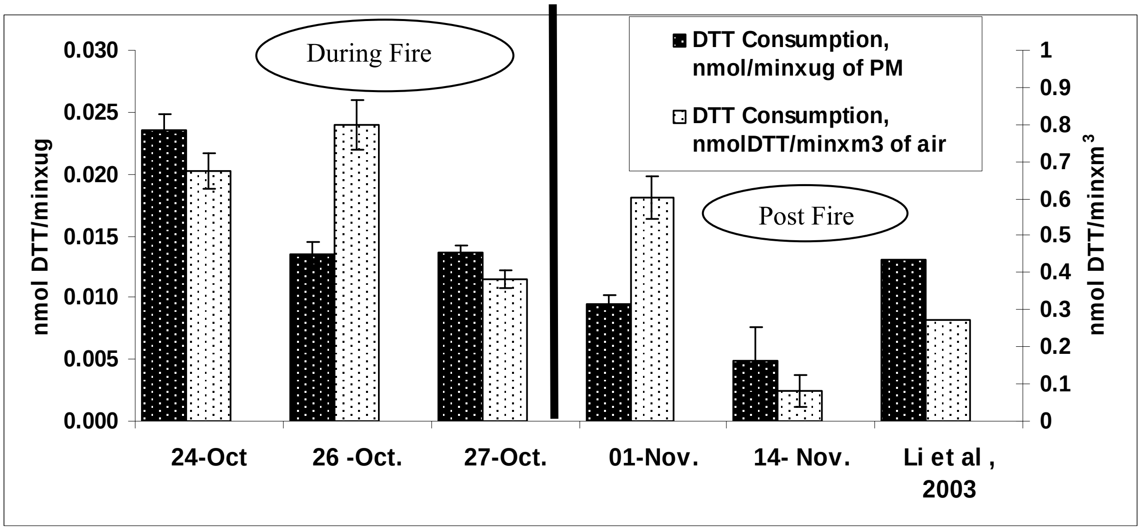

b)

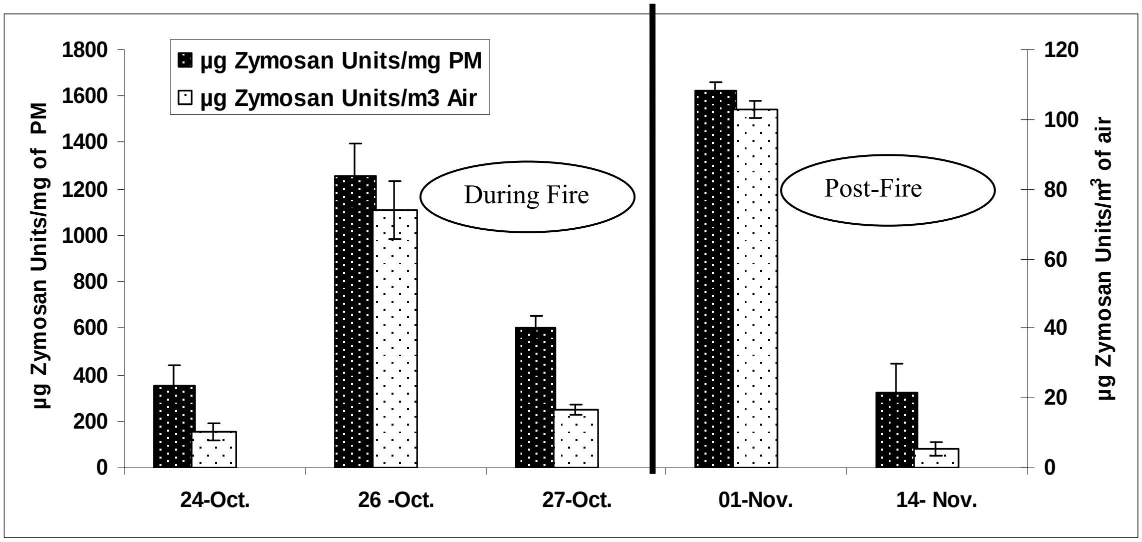

DTT expressed in units of nmol DTT / min × m^3 of air is also important in the context of population exposure to ambient PM. This parameter (DTT activity per m^3 of air) peaked on October 26 (0.80 nmol DTT / min × m^3) because of a very high $PM_{2.5}$ concentration (58.85 μg/m^3; not shown) coupled with an elevated per-mass DTT activity (0.014 nmol DTT / min × μg). Although on November 1, the per-mass activity was quite low (0.009 nmol DTT / min × μg), the high $PM_{2.5}$ concentration (63.47 μg/m^3; not shown) led to a substantial increase in DTT activity per m^3 of air (0.60 nmol DTT / min × m^3). The lower temperature and higher relative humidity on November 1 (the 24-hr average values were 60°F and 80%, respectively, compared to 78°F and 31% on October 24) might have resulted into limited atmospheric mixing and, thus, higher $PM_{2.5}$ concentration. The DTT activity per m^3 of air during the fire event was consistently higher (average, 0.62±0.21 nmol/min x m^3) compared to that reported by Li et al., (2003) (0.27 nmol/min x m^3. This discussion illustrates an important point about the relative oxidative activity of PM emitted from various sources; comparable activity on a per-PM mass basis may not necessarily translate into an equivalent public risk if the overall exposure varies due to changes in total PM concentration.

Figure 3.9b shows the results of the macrophage ROS assays on particles collected during and after the fire period. In contrast to DTT, the highest ROS activity was observed for the November 1 sample, both on per-mass and on per-volume of air basis. Although the per-mass activity was relatively high on October 26, the lower values obtained on October 24 and 27 make it difficult to associate the overall results with the occurrence of wildfires. It should be noted that the DTT and macrophage ROS assays are probably influenced by different PM species. While the former reflects the oxidative potential of a number of polar (water soluble) organic compounds, such as oxygenated PAH, quinones, and nitro-PAHs (Cho et al., 2005), the latter is mostly influenced by water soluble transition metals, such as Fe, Cu, Cr, Ni, and Co (Arredouani et al., 2005). Transition metals, which generate hydroxyl radicals through Fenton chemistry, are not active in the DTT assay. Even PAHs have to be oxidized to water soluble compounds, such as quinones and oxy-PAH before becoming redox active (Ntziachristos et al., 2007) in the DTT assay.

Based on the above discussion, we attempted a correlation of PM oxidative activity with particle constituents such as WSOC and water-soluble elements. We performed a qualitative analysis of the impact of fire emissions on those components that seem to affect the oxidative activity of the collected samples. Table 3.4 shows the coefficients of statistical determination (R^2) and the associated levels of significance (p values) for the correlation of different selected PM species with DTT and ROS. The analysis showed a significant association between DTT and WSOC (R^2 = 0.65, p= 0.102), confirming previous results by Cho et al. (2005), where DTT was well correlated with the organic carbon content of PM (R^2 = 0.53). Although our statistical analysis included only the water-soluble fraction of organic carbon, the majority of organic compounds in wood smoke are oxygenated and polar. The possible oxidation of PAHs during long distance transport might also enhance their solubility in water. Table 3.4 also illustrates that some of the measured elements (e.g. Ti, Mn, K, Mg and Co) are well-correlated with DTT. However, most of these species (in particular Mg, K and Mn) were strongly associated with WSOC, which implies that their relationship with DTT may not reflect their oxidative potential, but rather their common origin with water soluble organic compounds. Similarly, Ntziachristos et al. (2007) attributed the high correlation between DTT and several transition metals (e.g. Mn, Cu, Fe and Zn) to their common source with PAHs (i.e., vehicular emissions).

Table 3.4 Coefficients of statistical determination (R^2) and associated levels of significance (p-value) for the correlations between selected water soluble PM constituents and oxidative activities (as measured by the DTT and ROS assays) for PM samples collected during and after the fire period. Statistically significant correlations ($R^2 \geq 0.60$; $p \leq 0.10$) are shown in bold.

Chemical Constituents	**Correlation with DTT**		**Correlation with ROS**	
	R^2	**p value**	**R^2**	**p value**
WSOC	**0.65**	**0.10**	0.00	0.96
Ti	**0.85**	**0.03**	0.24	0.40
Mn	**0.75**	**0.06**	0.01	0.85
K	**0.73**	**0.06**	0.08	0.61
Mg	**0.71**	**0.07**	0.03	0.75
Co	**0.71**	**0.08**	0.56	0.14
Cr	0.61	0.12	**0.84**	**0.03**
P	0.56	0.15	0.01	0.90
Al	0.43	0.23	**0.71**	**0.07**
Ba	0.43	0.77	**0.95**	**0.04**
Pb	0.40	0.25	**0.94**	**0.00**
Fe	0.39	0.26	**0.96**	**0.00**
Cd	0.39	0.26	0.42	0.23
Ni	0.36	0.28	**0.80**	**0.04**
Zn	0.31	0.32	0.54	0.15
Na	0.29	0.36	0.33	0.31
V	0.25	0.39	**0.79**	**0.04**
S	0.22	0.42	**0.93**	**0.08**
Ca	0.15	0.49	0.21	0.47
Cu	0.08	0.65	0.04	0.75

Conversely, we observed strong associations between macrophage ROS and most of the water soluble transition metals (Cr, V, Fe, Ni, Pb,) (Table 3.4), consistent with earlier studies (Arredouani et al., 2005; Ciapetti et al., 1998) showing the capability of these trace elements to induce oxidative stress in cells through the formation of ROS. The correlation between the ROS assay and elements that are not redox active (e.g., Al, Ba and S) is probably due to their common origin with transition metals. However, no consistent increase in ROS activity was observed for any of these species during the fire episode.

3.2.4 Conclusions

The opportunistic nature of this study constrained our sampling and data collection to a small number of measurement days, which is one of our major limitations. Although results from DTT and ROS assays may not provide definitive answers on the relative health risks associated with PM emitted from motor-vehicles and wildfires (the two main PM sources during the fire episode), the study presents an effective approach to link the chemical composition of ambient PM with their toxicity response and thus to infer their distinct sources. While both assays revealed considerable oxidative activity of PM from traffic sources, which are ubiquitous in the Los Angeles area, the DTT assay showed additional increase in oxidative activity due to the contribution of the wildfires.

Chapter 4: Contribution of Semi-Volatile Organic Compounds and Non-Volatile Transition Metals in the PM Oxidative Activity

This chapter is divided in two sections: section 4.1- evaluating the contribution of semi-volatile organic compounds in the oxidative activity (measured by DTT assay) of ambient particles; and section 4.2 - quantifying the role of transition metals in the ROS activity (measured by macrophage ROS assay) of diesel exhaust particles. The major findings of both studies have been summarized in the respective sections.

4.1 Contribution of Semi-Volatile Organic Compounds in the Oxidative (DTT) Activity of Ambient Particles

4.1.1 Introduction

Atmospheric PM is a complex mixture of semi-volatile and non-volatile species (Seinfeld and Pandis, 2006). Semi-volatile organic compounds (SVOC) exist simultaneously in the gas and particle phases at equilibrium; partitioning between the two phases depends upon their vapor pressure, which is a function of temperature. Since chemical reactions are generally faster in gaseous phase, the oxidation of SVOC vapors yields secondary organic aerosols (SOA), shifting them again into particulate phase (Robinson et al., 2007). Thus, the cycling of SVOC between gas and particle phase ultimately leads to a net increase in the oxygenated organic aerosols (Miracolo et al., 2010) with modified chemical and likely, toxicological, characteristics. Certain SVOC, such as polycyclic aromatic hydrocarbons (PAHs) and their derivatives, are known to be genotoxic and carcinogenic (EPA, 2002). In Chapter 2, we have shown that the semi-volatile fraction of diesel exhaust particles (DEPs), evaluated in chassis dynamometer facilities, is highly redox-active and constitutes a dominant fraction (up to almost 100 % in few vehicles emissions) of the PM oxidative potential. However, freshly emitted PM in the low dilution environment of the dynamometer facilities, in which most of the SVOC are bound to the particle phase, is not directly comparable with the ambient PM. In an ambient urban environment, various atmospheric processes, including dilution and photo-chemical reactions significantly alter the physicochemical and oxidative characteristics of semi-volatile compounds. An improved understanding of these characteristics and the overall contribution of semi-volatile compounds to the atmospheric aerosol toxicity is essential in elucidating the health risks related to PM exposure.

The core objective of this study is to evaluate the contribution of semi-volatile PM constituents in the oxidative potential of ambient quasi-ultrafine particles. A thermodenuder (TD) was used in three temperature configurations - 50, 100 and 200 °C to shift the gas-particle partitioning of semi-volatile components of ambient aerosols sampled at an urban site. The oxidative potential of collected particles is measured by the DTT (dithiothreitol) assay. Detailed chemical analyses of the collected particles, including organic and elemental carbon, water soluble elements, inorganic ions and PAHs, are conducted to quantify the volatility profiles of different PM components, and also to investigate their effect on oxidative potential.

4.1.2 Experimental Methods

4.1.2.1 Sampling Location

The sampling for this study was conducted at the Particle Instrumentation Unit (PIU) of Southern California Particle Center (SCPC) near downtown Los Angeles. Meteorological conditions at the site were mostly consistent during the sampling campaign, with 24-hour average temperature values of 19 ± 2 ^{o}C and relative humidity of 66 ± 7 %. Additional information including the results of earlier PM investigations at the sampling site have been previously reported (Chapter 3).

4.1.2.2 Sampling Protocol

Sampling was conducted in the fall of 2009, over a period of 6 consecutive weeks (excluding weekends), for 5-6 hrs each day. Figure 4.1 shows the schematic of the experimental setup used. The thermodenuder was operated at three different temperatures, i.e. 50, 100 and 200 ^{o}C, and both ambient and denuded particles were collected for each temperature configuration. Thus, three sets of integrated samples, corresponding to the three TD temperature configurations (50, 100 and 200 ^{o}C), each consisting of two samples – ambient and thermodenuded, were collected in succession. The sampling duration of each set of samples varied from 50-80 hrs and was primarily determined by the sufficient mass loading on each filter (~ 600 μg) required to conduct chemical and toxicological analyses. All samples were stored in a freezer at -20 ^{o}C between sampling intervals. A low pressure drop impactor (Misra et al., 2002) was used to select the quasi-ultrafine particles (Dp ≤180 nm in the present study). Particles were concentrated using the versatile aerosol concentration enrichment system (VACES) to enhance the rate of mass collection. Detailed laboratory and field characterization of the VACES are described elsewhere (Khlystov et al., 2005; Kim et al., 2000; Kim et al., 2001a; Kim et al., 2001b; Ning et al., 2006; Zhao et al., 2005), demonstrating its capability to preserve aerosol chemical composition (including semi-volatile species) in both the fine (Khlystov et al., 2005; Kim et al., 2001b; Ning et al., 2006) and the ultrafine (Kim et al., 2000; Kim et al., 2001b; Zhao et al., 2005) PM modes during the concentration enrichment process. In brief, aerosol enrichment is achieved by growing the ambient particles (to 2-3 µm droplets) through a saturation–condensation system and their subsequent concentration by virtual impaction. A diffusion dryer system desiccates the aerosol stream exiting the virtual impactor to relative humidity <50 %. Concentrated particles after VACES were segregated into two airstreams: one stream was fed into the thermodenuder (described below) and the denuded stream was further split for separate collection of particles onto 37 mm quartz (Whatman, QMA, 3.7 cm, 1851-037) and Teflon (PALL Life Sciences, PTFE membrane, 2.0 um, R2PJO37) filters; particles from the stream by-passing the thermodenuder (representing the ambient PM) were similarly collected onto Teflon and quartz filters. The particle size distributions of ambient and denuded aerosols were concurrently measured using two Scanning Mobility Particle Sizers (SMPS Model 3080 and DMA Model 3081, condensation particle counter Model 3022A, TSI Inc., St. Paul., MN) set up at inlet and exit of the thermodenuder, throughout the sampling period. The particle size range detectable by SMPS is 14.6-685.4 nm at an aerosol flow rate of 0.3 lpm and with a scan time of 300 s. Within the context of this study, ultrafine particles <50 nm in diameter are designated as the ‘‘nucleation’’ mode, whereas those in the 50–180 nm range are called the ‘‘Aitken’’ mode (Hinds, 1999). This terminology helps to a better description of the size-segregated particle losses described later in the chapter.

Figure 4.1: Experimental setup

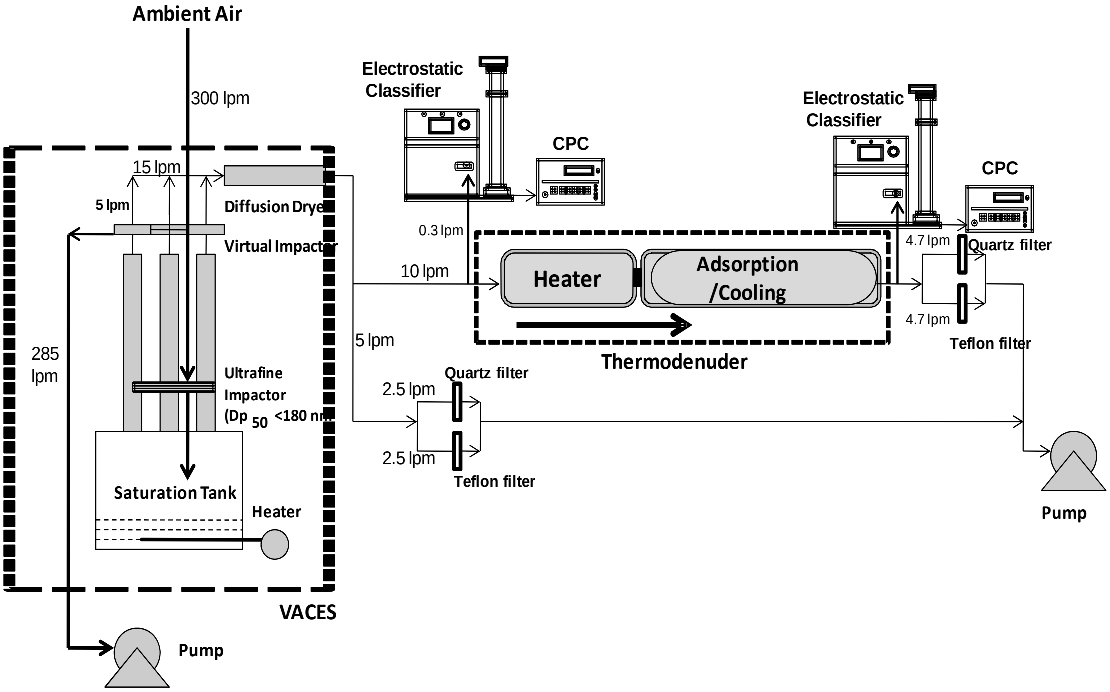

The thermodenuder (TD; Model ELA-230, Dekati Ltd. Osuusmyllynkatu 13, FIN-33700 Tampere, Finland) consists of a heating section, followed by an adsorption tube, which is actively cooled. As the ambient aerosol is drawn and passed through the heating section, part of its volatile/semi-volatile component is evaporated. The aerosol then enters the adsorption/cooling tube, where the evaporated compounds are adsorbed onto activated charcoal placed on the walls of this section. The remaining PM (not volatilized) is collected onto the filters placed downstream of TD. The Dekati thermodenuder used in this study allows a relatively small residence time of 0.7s in the heating section at 10 lpm. The aerosol mass fraction remaining (MFR) after heating is quite sensitive to TD residence time. Recent studies have shown that thermal equilibration time scales of ambient particles vary over several orders of magnitude (from less than a second to hours), depending on the factors including vaporization enthalpies and mass accommodation coefficients of the evaporating species (An et al., 2007; Riipinen et al., 2010). Although the condition of equilibrium is necessary to calculate thermodynamic properties of aerosol species (e.g. enthalpy and vapor pressure) based on the TD data, our goal was not to investigate these relationships. Instead, we successively removed semi-volatile inorganic and organic species at different temperatures and determined the degree to which their removal affects PM oxidative potential. In that respect, deviation from the thermal equilibrium of aerosols should not pose a serious limitation in the present case.

4.1.2.3 Sample Analysis

Sections of all PM samples were extracted in high purity deionized (18 mega-ohm) water at ambient temperature. The water extracts from the Teflon filters were analyzed for trace elements and major ions. Trace elements in the 0.45 μm filtered water extracts were analyzed using a magnetic-sector (high resolution) Inductively Coupled Plasma-Mass Spectroscopy (SF-ICP-MS) following the approach of Zhang et al. (2008). Ion Chromatography (IC) was used to analyze the water soluble ions (Zhang et al., 2008). The elemental and organic carbon (EC and OC) contents of deposited PM on the quartz filters were analyzed by the ACE (aerosol characterization experiments)-Asia Method (Schauer et al., 2003). A separate section of the quartz filters was analyzed for PAHs by TD-GCMS (Thermal Desorption- Gas chromatography/mass spectrometry) method (Sheesley et al., 2009) using Markes International Thermal Desorption Unit (model M-10140; Foster City, CA, USA) coupled with an Agilent Technologies GCMS system (a 6890 GC interfaced with a 5973 MSD). Several field blanks and laboratory blanks collected during the sampling were similarly processed and all analytical results were blank corrected. The oxidative potential of PM collected on the Teflon filters was quantified by consumption of dithiothreitol (DTT) in a chemical system (DTT assay).

4.1.3. Results and Discussion

4.1.3.1 Physical Parameters

Particle losses in the thermodenuder were evaluated with ambient and ammonium sulfate [$(NH_4)_2SO_4$] particles without heating the aerosols. Penetration efficiency was determined by concurrent measurements of the particle size distributions at inlet and exit of the thermodenuder. For 20 nm size and at a flow-rate of 10 lpm, the particle number losses were less than 9 % for both ambient and $(NH_4)_2SO_4$ aerosols, with even lower losses for larger particles (~2 % for 30 nm). This is consistent with theoretical diffusional loss calculations for laminar flow (Reynolds number <1200) at 25 ^{o}C (Baron and Willeke, 2001). Although diffusional loss increases with a rise in temperature, it does not substantially affect the denuder's penetration efficiency in our experimental range (25-200 ^{o}C). Theoretical calculations showed a slight (<3 %) increase in diffusional loss for 20 nm particles on increasing the temperature from 25 to 200 ^{o}C. The size-segregated particle diffusion losses were used to correct the size distributions of denuded aerosols.

Figure 4.2 shows the number and volume size distributions of ambient as well as thermodenuded aerosols. In general, these measurements show that heating the aerosols causes substantial particle shrinkage due to the evaporation of semi-volatile components. However, a small amount of water associated with the particles also evaporates on heating, leading to a slight overestimation of the measured loss of semi-volatile species. The relative magnitude of total number and volume losses provides an approximate indication of the differential evaporation profiles of nucleation (<50 nm) and Aitken mode (50 - 180 nm) particles. While number loss is mostly governed by the loss of nucleation mode particles, shrinkage of Aitken mode particles is reflected in the volume reduction. It should be noted that particle loss might imply shrinkage below the detection limit of SMPS, i.e. 14.6 nm in our case. Thus, the substantial loss of nucleation mode particles at 50 ^{o}C, as evident from Figure 4.2 is pronounced in the higher number loss (47±2 %) compared to the corresponding volume loss (41±7 %). Due to the Kelvin effect (Hinds, 1999), nucleation mode particles tend to be more volatile at a given temperature than larger particles. Earlier observations at the sampling site have shown that organic carbon dominates (>40 %) the mass fraction of particles below 50 nm (Sardar et al., 2005). Although size-segregated PM chemical speciation was not conducted in the present study, bulk loss of the nucleation mode at 50 ^{o}C is most likely attributed to the evaporation of organic compounds.

Figure 4.2: Particle size distributions (number and volume based) of the concentrated ambient and thermodenuded particles at 50, 100 and 200 °C.
Note: Error bars show the standard deviation of multiple scans.

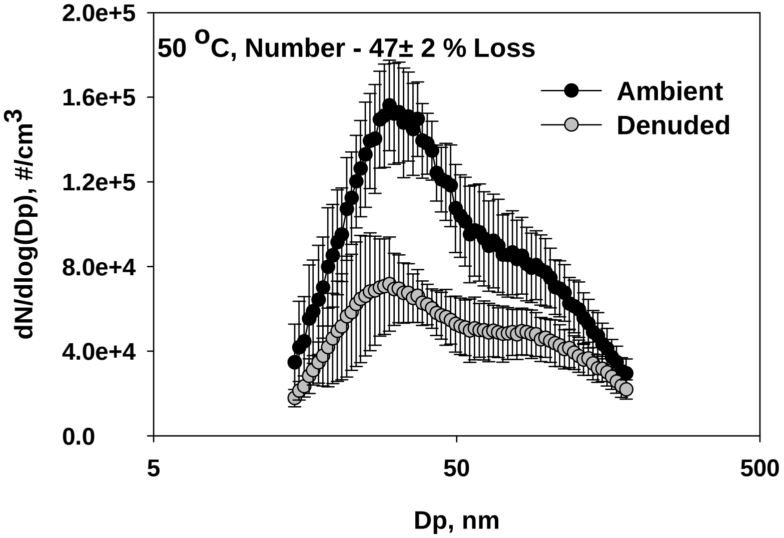

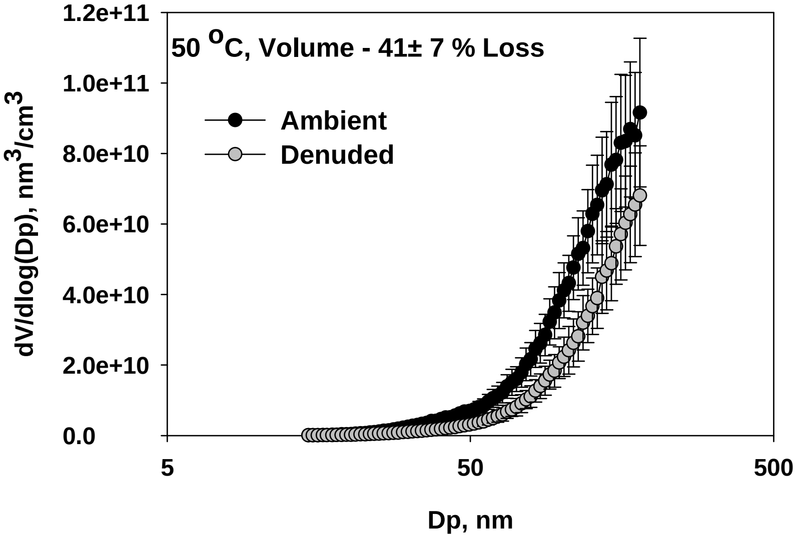

Figure 4.2 (Continued)

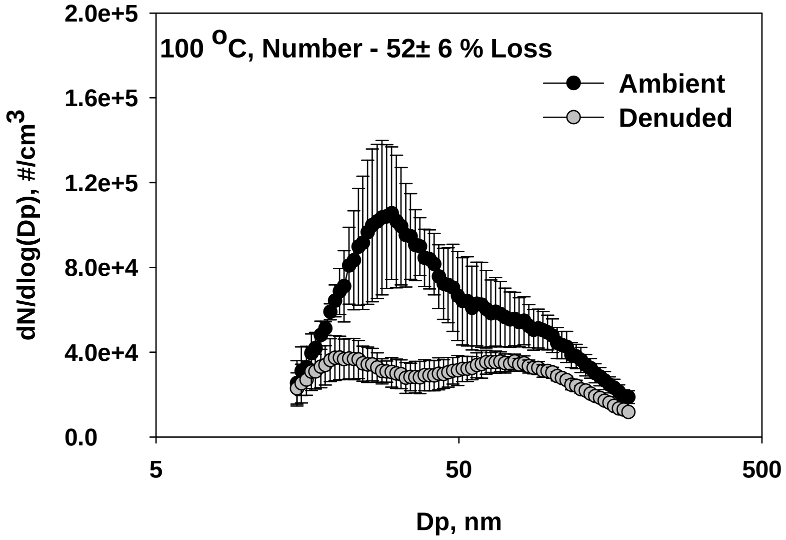

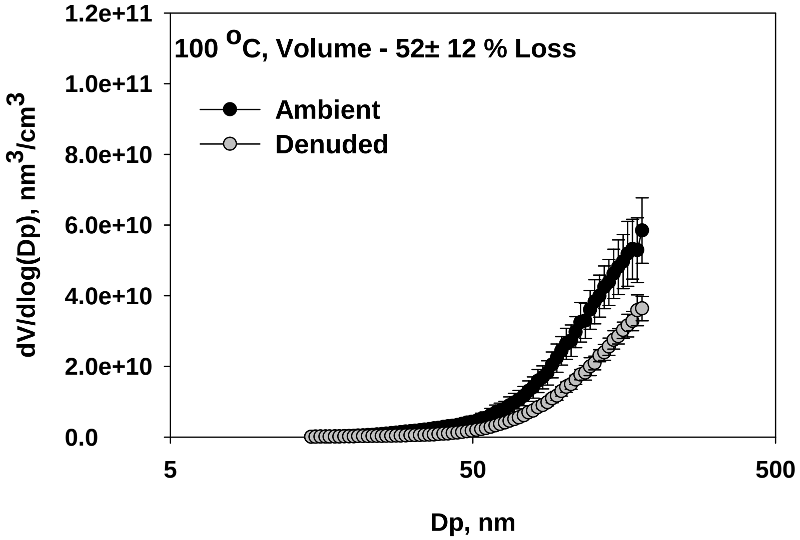

Figure 4.2 (Continued)

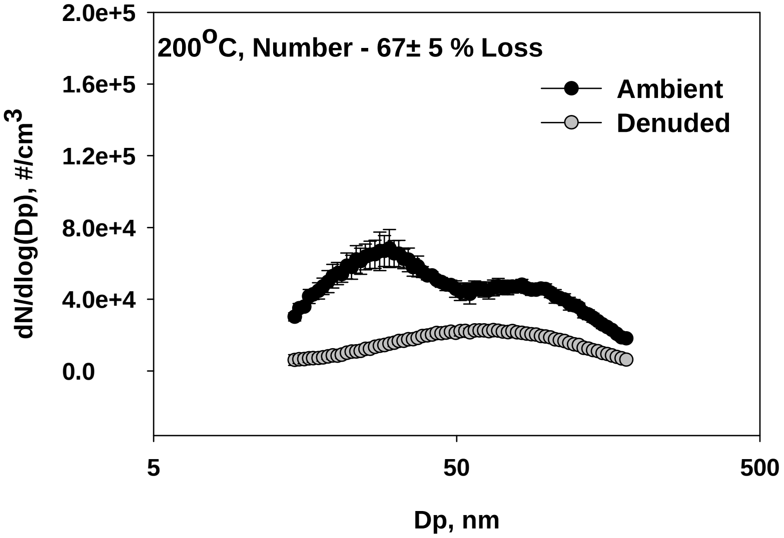

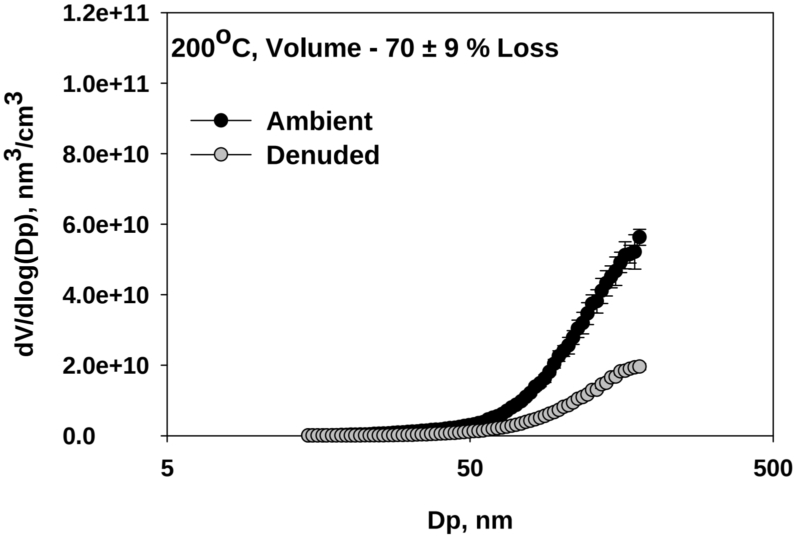

As the temperature is increased, shrinkage of the Aitken mode particles also becomes prominent, leading to an equivalent loss in both number and volume concentration at 100 ^{o}C (~52 %). The particle size distribution of thermodenuded aerosols remains bimodal at 100 ^{o}C, with a slight shift in mode diameter of the first peak (~32 nm in ambient particle size distribution) towards lower size (~20 nm) due to particle shrinkage. Further increase in temperature to 200 ^{o}C causes loss of smaller particles to the extent that nucleation mode is almost eliminated, resulting in a unimodal size distribution. These observations are consistent with previous findings showing that the fraction of ambient particles below 50 nm is internally mixed, consisting mostly of volatile materials, while particles in the Aitken mode are externally mixed (Moore et al., 2007). These externally mixed particles shrink upon heating by evaporation of semi-volatile material from the surface, leaving behind the solid core, with a mode at around 80 nm. The fractional losses in volume concentration of the denuded aerosols at 50, 100 and 200 ^{o}C are consistent with the gravimetrically measured mass reduction ratios at these temperatures (42 %, 52 % and 67 %, respectively).

4.1.3.2 Chemical Parameters

Water Soluble Ions

Figure 4.3 shows the concentrations of major water soluble inorganic ions in concentrated ambient and denuded particles at three TD temperatures: 50, 100 and 200 ^{o}C. Significant loss of all of these inorganic ions occurs with heating. At 50 ^{o}C, a higher loss was observed for nitrate (NO_3^-; 49±7 %) and ammonium (NH_4^+; 44±5 %), than sulfate (SO_4^{-2}; 33±4 %). The general trends in the loss of these ions are consistent with their predominant molecular speciation [ammonium nitrate (NH_4NO_3), $(NH_4)_2SO_4$, and sulfuric acid (H_2SO_4)] in an urban atmosphere (Sardar et al., 2005). However, the small fraction remaining at 200 ^oC is likely explained by the presence of refractory species, such as $NaNO_3$ and Na_2SO_4, which are probably formed by the heterogeneous chemical reactions of sea-salt with nitric and sulfuric acid (Engler et al., 2007).

Elemental and Organic Carbon (EC-OC)

Figure 4.4 shows the comparison of elemental (EC) and organic carbon (OC) in concentrated ambient and denuded particles collected at different TD temperature settings, i.e. 50, 100 and 200 ^oC. These two species dominate the quasi-ultrafine particulate mass, accounting for up to 70 % at the sampling site (Sardar et al., 2005). EC is often considered as an indicator of diesel vehicular emissions, which is one of the predominant sources of carbonaceous compounds in the Los Angeles atmosphere (Schauer, 2003). In addition to traffic sources, OC is also contributed by photo-chemical processes producing secondary organic compounds (Ning et al., 2007). Despite the divergence in individual levels of both of these species, apparent in Figure 4.4, which is attributed to the daily variations in emission source strengths, the ratio [$(OC/EC)_{ambient}$] is relatively stable, with an average value of 3.4±0.5 (not shown). This consistency primarily reflects the similarity in meteorological conditions prevailing throughout the study period, which also strengthens our comparison of the various parameters at different TD temperature configurations, as discussed in the paper.

Figure 4.3: Concentration of water soluble inorganic ions (NH_4^+; Figure 4.3a, NO_3^- ; Figure 4.3b and SO_4^{-2}; Figure 4.3c) in the concentrated ambient and thermodenuded particles at different TD temperature configurations – 50, 100, 200 °C.

Note:

1. Error bars show analytical uncertainties in the chemical analysis.
2. Percentages on top of the bars show loss in concentration on heating the aerosols.

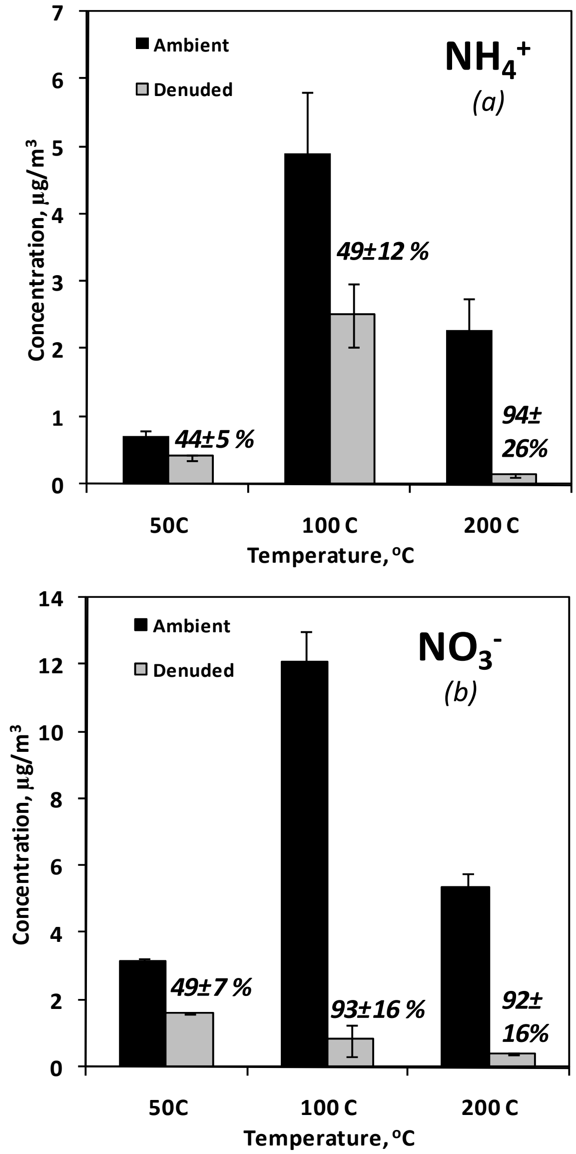

Figure 4.3 (Continued)

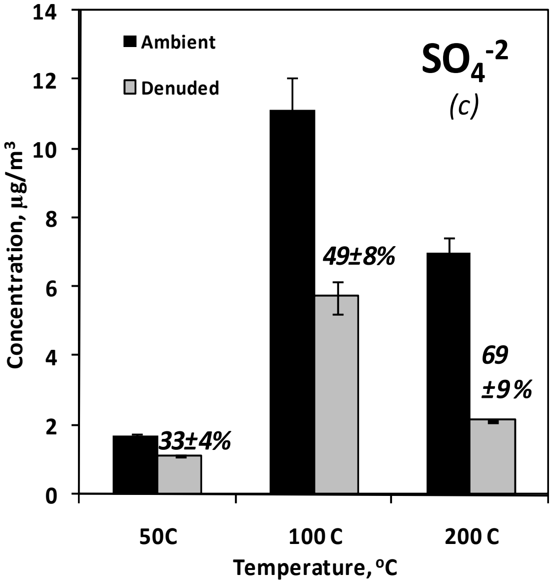

Figure 4.4: Concentration of elemental (Figure 4.4a) and organic (Figure 4.4b) carbon in the concentrated ambient and thermodenuded particles collected at three TD temperature configurations (50, 100 and 200 ^{o}C).

Note:

1. Error bars show analytical uncertainties in the chemical analysis.
2. Percentages on top of the bars show loss in concentration on heating the aerosols.

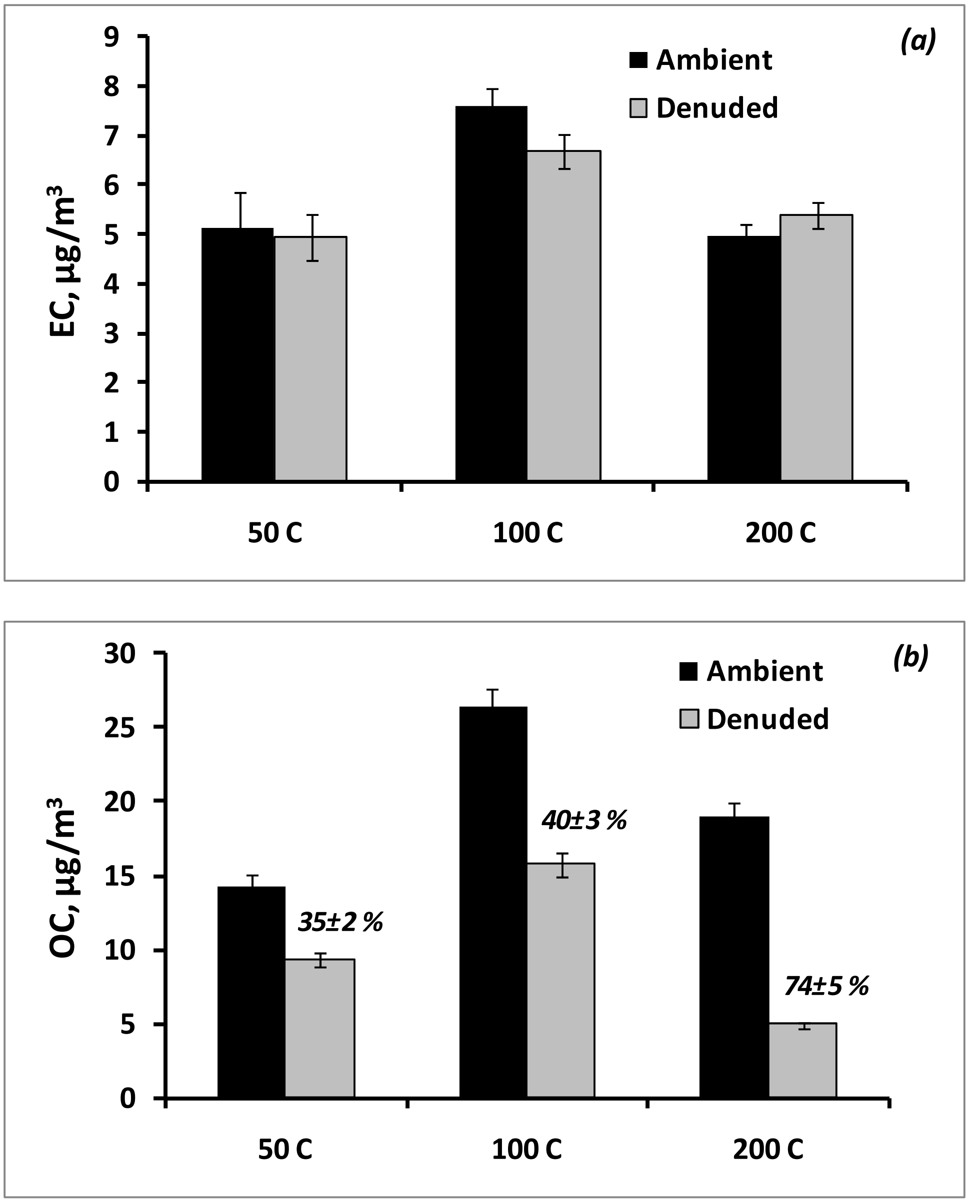

As defined by the measurement methodology (ACE-Asia method), EC is considered refractory even up to a temperature of 870 ^{o}C (Schauer et al., 2003). As expected, this species is only marginally affected [(within the measurement uncertainty (±5-13 %)] by heating. In contrast, OC is progressively decreased with an increase in TD temperature (35±2 %, 40±3 % and 74±5 % loss at 50, 100 and 200 oC, respectively). OC consists of a variety of organic compounds such as PAHs, hopanes, steranes, alkanes and organic acids. Most of these compounds are semi-volatile at ambient temperatures (Subramanyam et al., 1994), which explains the substantial loss of OC with heating.

Polycyclic Aromatic Hydrocarbons (PAHs)

The concentration of PAHs in concentrated ambient and denuded aerosols as a function of TD temperature is shown in Figure 4.5. In general, a substantial evaporative loss (up to 80 %) upon heating is evident. PAHs are semi-volatile organic compounds and traffic emissions from the nearby freeway (I-110) is their most obvious source at our sampling site (Ning et al., 2007). Twenty-one PAHs were quantified and for a more illustrative interpretation of the loss profiles, these are divided into two groups, based on their molecular weights, i.e. low molecular weight (LMW- Phenanthrene, Anthracene, Fluoranthene, Pyrene, Benzo[ghi]fluoranthene, Cyclopenta[cd]pyrene, Benzo[a]anthracene, Chrysene, Retene,; <252 g/mol), and high molecular weight (HMW-Benzo[b]fluoranthene, Benzo[k]fluoranthene, Benzo[j]fluoranthene, Benzo[e]pyrene, Benzo[a]pyrene, Perylene, Indeno[1,2,3-cd]pyrene, Benzo[ghi]perylene, Dibenzo[ah]anthracene, Picene, Coronene, Dibenzo[ae]pyrene; ≥252 g/mol). The fractions of LMW PAHs lost are 31±6 %, 66±7 % and 78±21 % at 50, 100 and 200 ^{o}C, respectively (Figure 4.5a). Recent studies have indicated that more than 80% of the PAH mass in an urban atmosphere may be adsorbed onto the surface of soot particles rather than absorbed into the organic matter (Dachs and Eisenreich, 2000; Perraudin et al., 2005; Tran-Duc et al., 2010). The relatively lower enthalpy of adsorption compared to that of absorption might further facilitate the volatilization of these compounds from the particle surface. The loss in concentration of HMW PAHs is smaller at 50 and 100 ^{o}C (14±2% and 53±4%, respectively; Figure 4.5b), compared to the LMW PAHs. This is consistent with the decreasing volatility of PAHs with an increase in number of carbon atoms (Zheng and Fang, 2000). However, a difference in the evaporation profiles is not apparent at 200 ^{o}C, when most of the PAH mass is volatilized (~80%), leading to a similar loss for both LMW and HMW PAHs.

Figure 4.5: Concentration of PAHs [categorized based on their molecular weights, i.e. low molecular weight (LMW; Figure 4.5a) and high molecular weight (HMW; Figure 4.5b)], in concentrated ambient and thermodenuded aerosols collected at three TD temperature configurations – 50, 100 and 200 °C.

Note:

1. Error bars show analytical uncertainties in the chemical analysis.
2. Percentages on top of the bars show loss in concentration on heating the aerosols.

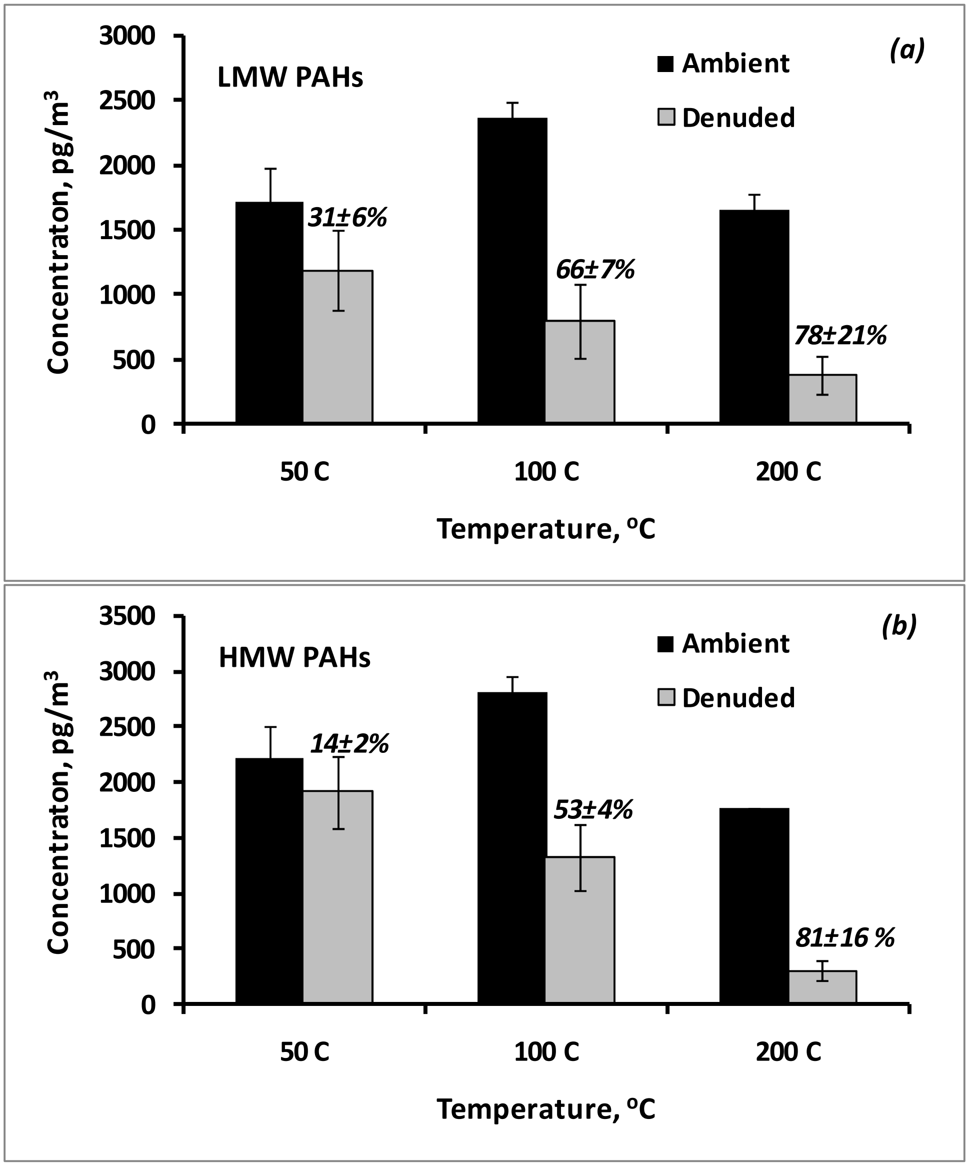

4.1.3.3 Oxidative Potential

Figure 4.6 shows the oxidative potential of concentrated ambient and thermodenuded particles at three TD temperatures (50, 100 and 200 °C), measured by the DTT assay. The oxidative potential is decreased by 42±5 %, 47±8 % and 66±6 % as the particles are heated at 50, 100 and 200 °C, respectively. The marked decline in DTT activity as the aerosols are denuded of their semi-volatile components highlights the significant contribution of semi-volatile compounds to the oxidative load of ambient quasi-ultrafine particles in an urban atmosphere.

Figure 4.6: Percentage loss in oxidative potential, measured by DTT activity on heating the ambient aerosols at 50, 100 and 200 °C. The DTT activity of the concentrated ambient (undenuded) PM, corresponding to different temperature settings of the thermodenuder is also shown on secondary Y-axis as a reference.
Note: Error bars in DTT activity represent 95 % confidence intervals.

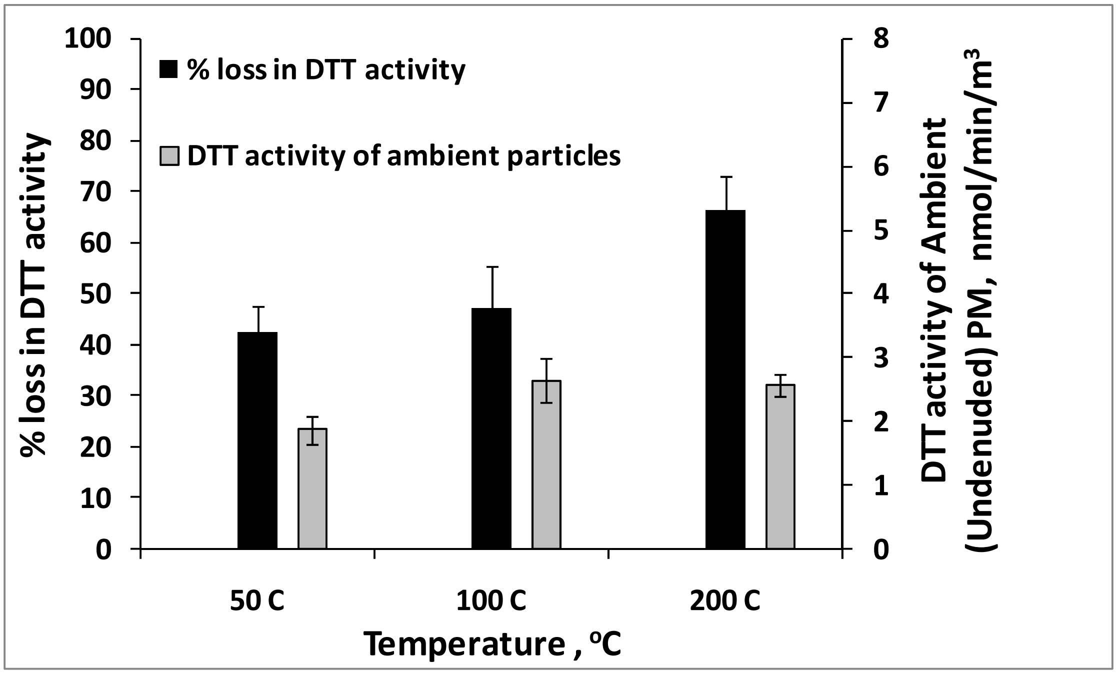

The sizable decrease in DTT activity at 50 °C (42 %) implies that a large fraction of oxidative activity may be associated with constituents that are volatile at 50 °C. Similarly, compounds volatilizing in the temperature window of 100-200 °C also appear to be fairly redox active, resulting in an additional 19 % loss of DTT activity in this temperature range. The relationship between volatility temperature and decrease in oxidative potential may provide some insights in identifying the PM-bound chemical species with considerable oxidative activity. For example, the loss profile of DTT activity with temperature closely follows the thermal desorption profile of OC, with substantial loss in the ambient-50 °C (42 % and 35 % for DTT and OC, respectively) and 100-200 °C (19 % and 34 % for DTT and OC, respectively) compared to 50-100 °C (5 % for both DTT and OC). The temperature window of 50-100 °C, although associated with a major loss of inorganic ions [(NO_3^- (44 %), SO_4^{-2} (16%))], does not impact the DTT activity significantly. The association of oxidative potential with various chemical constituents is further investigated by regression analysis in the following section.

The overall decrease in oxidative potential with heating the ambient PM is relatively lower compared to that of DEPs evaluated in the dynamometer study (Chapter 2). That study showed a roughly 70-100 % decrease at 220 °C depending on the vehicle type, after-treatment technology used and the driving cycle. However, the dilution ratio of the vehicular exhaust in that study was much lower (i.e. ~ 6-80) compared to the atmospheric dilution (on the order of thousands) in the present case. The increase in dilution ratio shifts the gas-to-particle phase equilibrium, with a lower fraction of semi-volatile species in the particulate phase under high dilution conditions. Other physicochemical processes, including photo-chemical reactions, might also modify the net content of SVOC and their contribution to the oxidative potential of ambient particles. These differences in the loss profiles of DTT activity between freshly emitted PM and aged ambient PM underline the importance of atmospheric processes, in characterizing the overall toxicity of inhaled aerosols and assessing their health impacts.

4.1.3.4 Association of Oxidative Potential with PM Chemical Composition

To further examine the linkage between oxidative potential and chemical PM species, linear regression between the DTT activity and PM constituents was performed. Both ambient and denuded samples were included in regression and the results are summarized in Table 4.1. The analysis shows a strong association between DTT activity and OC concentration ($R = 0.92$; $p = 0.01$), which is consistent with earlier investigations demonstrating the capability of organic compounds to catalyze the oxidation of DTT (Cho et al., 2005; Obrien, 1991). In the context of present study, the excellent correlation of DTT activity with OC concentration further emphasizes the significant role of semi-volatile organic compounds in the PM oxidative potential.

Table 4.1: Summary of the regression analysis [slope, intercept, Pearson coefficient (R) and the associated level of significance (p value)] between major PM chemical constituents and DTT activity.

	DTT Activity					
			Slope*		**Intercept**$^{\Psi}$	
Species	**R**	**p**	**Value**	**Unc.**	**Value**	**Unc.**
NO_3^-	0.85	0.03	0.15	0.04	1.16	0.25
SO_4^{-2}	0.79	0.06	0.15	0.06	1.01	0.36
NH_4^+	0.77	0.08	0.32	0.13	1.15	0.33
OC	0.92	0.01	0.09	0.02	0.35	0.34
EC	0.35	0.49	0.24	0.32	0.32	1.89
LMW PAHs	0.88	0.02	937.84	250.43	0.47	0.38
HMW PAHs	0.80	0.05	645.04	305.34	0.63	0.58

Note: Sample size for the regression analysis is N = 6.
*expressed as DTT activity (nmol/min) per µg of species.
$^{\Psi}$ expressed as nmol of DTT/min/m^3.

The DTT activity is also well correlated with both groups of PAHs, i.e. LMW (R = 0.88, p = 0.02) and HMW PAHs (R = 0.80, p = 0.05). PAHs themselves do not contain functional groups capable of catalyzing the oxidation of DTT. However, atmospheric chemistry e.g. photo-oxidation, may transform PAHs to quinones and nitro-PAHs (Ntziachristos et al., 2007), both of which are major classes of redox cycling agents. Thus, the positive correlation of PAHs with DTT activity is probably due to their correlation with quinones and nitro-PAHs, which have been shown to be active in the DTT assay (Cho et al., 2005). In addition to the cellular oxidation of thiols, some quinones (e.g. 1, 4-benzoquinone) have been shown to also inactivate the antioxidants such as glyceraldehyde-3-phosphate dehydrogenase (GAPDH) (Rodrigueza et al., 2005). Although quinones are not analyzed in our study, the correlation with DTT underscores the importance of PAHs as possible surrogates or precursors of redox active organic species that augments the PM oxidative potential.

Some inorganic ions, such as SO_4^{-2}, NO_3^- and NH_4^+ are also correlated with DTT activity as shown in Table 4.1. To the best of our knowledge, there is no evidence in literature that these species are redox active in the aerobic environment. Their association with DTT may be due to co-linearity with redox active organic compounds, instead of actual contribution to the PM oxidative potential. Species, minimally affected by heating (EC and water soluble trace elements) were not correlated with the DTT activity.

4.1.4 Summary and Conclusions

We assessed the role of semi-volatile compounds in the oxidative potential of ambient quasi-ultrafine particles at an urban site. The investigation follows the dynamometer study (Chapter 2), which demonstrated a dominant contribution of semi-volatile components in the DTT activity of PM emitted from heavy-duty diesel vehicles in a dynamometer facility. Compared to that study, a lower, although still considerable fraction (42-66 %) of the oxidative potential of ambient PM, is contributed by its semi-volatile compounds. The difference in DTT activity profiles between the two studies is attributed to the lower content of semi-volatile species in ambient PM, as a result of the much higher atmospheric dilution, compared to the freshly emitted DEPs in dynamometer studies. Species that are volatile at ~ 50 ^{o}C and between 100 and 200 ^{o}C (e.g. OC) appear to be strongly associated with the DTT activity.

4.2 Contribution of Transition Metals in the Reactive Oxygen Species Activity of PM Emissions from Retrofitted Heavy-Duty Vehicles

4.2.1 Introduction

Recent toxicological studies indicate that PM-associated reactive oxygen species (ROS; particle-bound and/or their cellular generation upon PM exposure) and the resulting oxidative stress may be responsible for the initiation of inflammatory cascades in biological systems (Donaldson et al., 1996; Donaldson et al., 2005; Kunzli et al., 2006). The macrophage ROS assay is a fluorogenic cellular method to measure the generation of reactive oxygen species in alveolar macrophages on exposure to aqueous suspensions of PM. Due to the location of alveolar macrophages on inner epithelial surface of the lung, this assay represents an excellent model of pulmonary inflammation in response to PM exposure (Landreman et al., 2008). Recent investigations have also indicated that ROS activity measured by this assay is highly associated with the transition metal content of PM samples [Fe, V, Ni, Cr; (Hu et al., 2008; Verma et al., 2009)]. However, most of these associations have been inferred based on statistical analysis - either simple or multiple linear regressions between PM chemical constituents and ROS activity. While these statistical tools can provide valuable insights, the inherent limitations of any regression technique, i.e. lack of an explicit causal relationship irrespective of the strength of correlation, and multi-colinearity among independent variables, pose challenges to comprehend the underlying mechanisms linking particle composition to toxicity. For an improved understanding of these associations, mechanistic studies must be conducted, which include successive removal of various PM components from the exposure samples to analyze their individual impacts on the measured activity. One of such approaches could be the use of a chelation technique for segregating the contribution of metals to ROS activity of PM as demonstrated by Shafer et al. (2010).

The objective of this study is to assess the role of water-soluble metals in ROS activity of DEPs. Particles were collected from heavy-duty vehicles with and without retrofits (e.g. DPF, SCR, etc.) in a dynamometer set-up. The contribution of water-soluble transition metals in the measured activity was quantified by their complexation and subsequent removal using chelation method. The significant variations in metal composition of PM collected from different vehicle-configurations provided insights on the effect of emission control technologies on exhaust PM toxicity as well as demonstrated the robustness of the analytical approach. Observations are further supported by uni- and multi-variate regression analyses between ROS activity and the water-soluble metal content of PM.

4.2.2 Experimental Methods

4.2.2.1 Sampling Protocol

DEPs were collected from heavy-duty vehicles tested on a chassis dynamometer at the California Air Resources Board’s laboratory in Los Angeles. The details of the test vehicle-configurations including their efficiency to control mass and number based PM emissions have been reported previously (Chapter 2).

All vehicles were tested under three standard simulated driving conditions, i.e. steady state cruise (80 km/h), transient [EPA urban dynamometer driving schedule (UDDS) (Ayala et al., 2002)] and idling. Vehicle exhaust was transported by a stainless steel hose pipe and was mixed with filtered (high efficiency particulate air filter) air in a constant volume sampler (CVS) for primary dilution. Integrated PM samples from the CVS were collected using a high volume sampler [HI-Q Environmental Products Co., San Diego, CA; flow rate = 450 l/min; (Misra et al., 2002)] on Teflon coated glass fiber filters (Pallflex, Fiberfilm T60A20 – 8x10 inch, Pall Corp., East Hills, NY). Both tunnel (from CVS dilution tunnel) and field blanks (from high volume sampler) were similarly collected during sampling.

4.2.2.2 Sample Analysis

Sub-sections of the filter-collected PM were extracted with 15 mL of high purity (18 mega-ohm) water. Extractions were performed in 20 mL acid-leached, capped, polypropylene tubes, with continuous agitation for 16 hours at room temperature in the dark. Extracts were filtered through acid-leached 0.22 µm polypropylene syringe filters prior to analysis by magnetic sector inductively-coupled plasma mass spectrometry (SF-ICPMS). Numerous field/tunnel filter blanks and laboratory method blanks were similarly processed (Zhang et al., 2008). Estimates of uncertainty for each measurement were derived by propagating the uncertainty (1 standard deviation, stdev) components from the SF-ICPMS analysis (3-analytical replicates) and blank subtraction (1 stdev of multiple blanks).

The ROS-activity of the PM extracts was measured by in vitro exposure to rat alveolar macrophage (NR8383, ATCC# CRL-2192) cells using 2',7'-dichlorofluorescin diacetate (DCFH-DA) as the fluorescent probe. All samples, as well as positive and negative controls were analyzed in triplicate (3-wells). A minimum of six dilutions (each of them in triplicate) of every sample extract was run to ensure that a linear dose-response region could be identified. Uncertainty in ROS method was estimated by propagating the standard deviation of triplicate ROS measurements with standard deviation of the applied method blank. These values ranged from 5 to 78% (median = 20%, n=24).

Sub-samples of the primary water extracts (samples and controls) were further processed by chelation with the immobilized ligand iminodiacetate (Chelex chromatography) to remove the metal ions. For the Chelex treatment, mini-columns (1 mL polypropylene with Teflon frits) of Chelex were prepared with 0.2 g of 18 mega-ohm water-slurried Na-Chelex. Columns were rinsed with high purity water and buffered with 0.1 M sodium acetate. PM extracts (~1.75 mL) were processed through the columns, under gravity flow, in a solid phase extraction manifold, at a flow rate of ~1.0 mL/min. The Chelex-processed extract was collected and immediately assayed for ROS-activity and subsequent elemental analysis by SF-ICPMS. Control samples were processed through the Chelex columns to ensure that the treatment did not produce ROS active species or inhibit the activity of Zymosan (a β-1,3 polysaccharide of D-glucose). Zymosan was used as a positive control as it is recognized by TLR-2 (Toll-like receptors) on macrophage cells, activating a strong immuno-chemical and ROS response (Ciapetti et al., 1998).

Blank-corrected ROS fluorescence data were normalized to the response of a standardized unit of Zymosan to correct for minor variations in method sensitivity between assay batches. ROS activity is therefore reported in terms of Zymosan units to facilitate the comparison of various data sets. None of the Chelex method blanks exhibited detectable ROS activity, and Chelex column blanks (high-purity water eluants) produced no measurable (<5%) suppression of ROS activity in Zymosan positive controls.

4.2.3 Results and Discussion

4.2.3.1 Water Soluble Metals

Figure 4.7 shows the distribution of metals in the exhaust PM collected from various vehicle-configurations, under three driving cycles, i.e. cruise, UDDS and idle. For a more illustrative interpretation, these metals are categorized into different groups based on their periodic properties.

Figure 4.7: Distribution of water-soluble metals, categorized into different groups based on their periodic properties, in the exhaust PM from various vehicle-configurations, under three driving cycles, i.e. cruise, UDDS and idle.

Redox Active Transition metals: Mn, V, Ni, Cu, Fe, Cr; Divalent Transition metals: Zn, Cd, Co: Heavy metals: Tl, Pb, U, Th, W; Alkaline Earth Metals: Sr, Mg, Ba, Ca; PGE: Rh, Pt, Pd; Rare Earth: Eu, Pr, Ce, Nd, La, Sm, Y, Dy, Ho, Yb, Lu; Semi Metals: As, Sb; Higher valent/hydrolyzed metals: Ti, Sc, Al

Notes: NA implies “not available”.

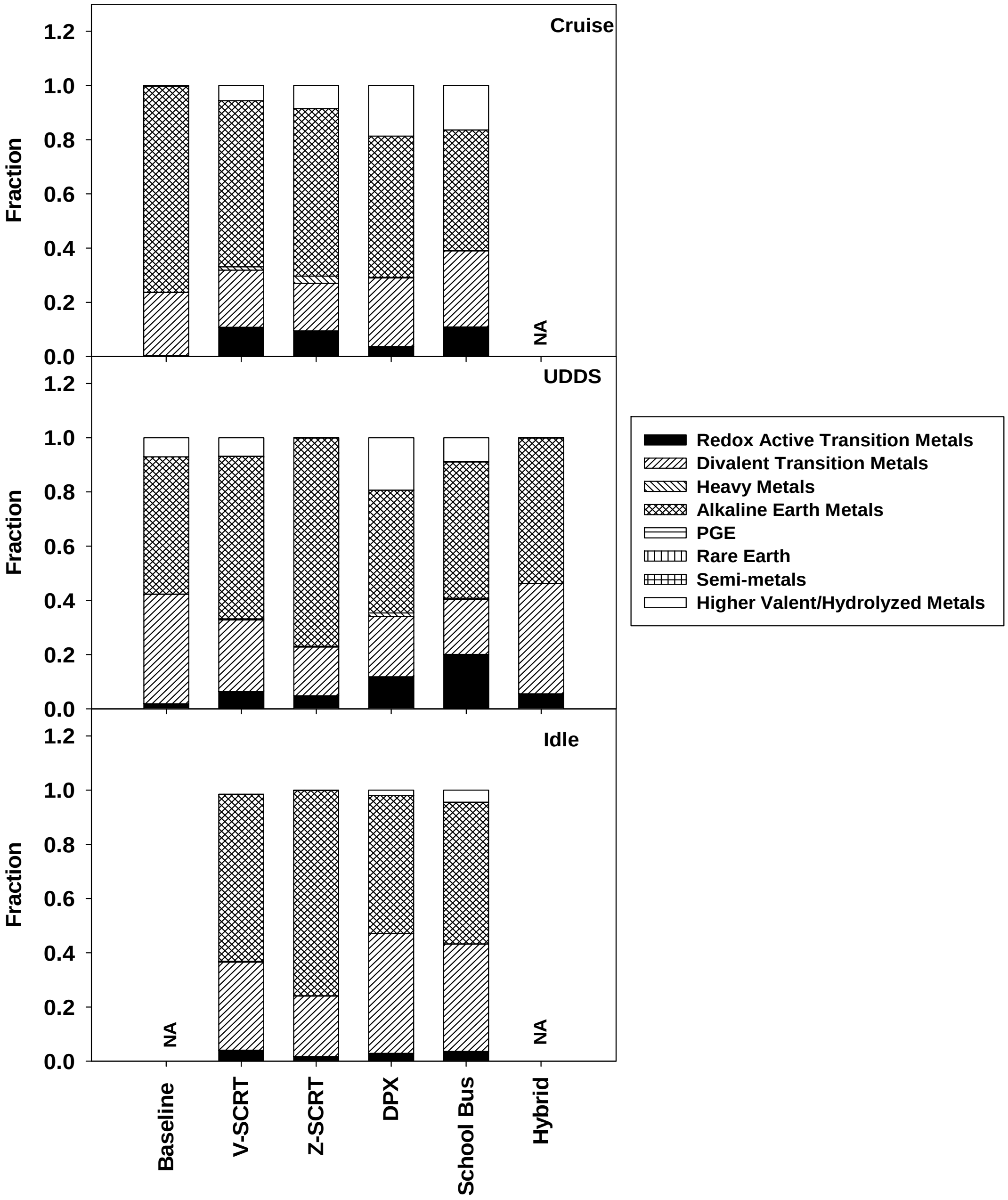

As shown, the differential removal of these metals by control technologies and also their probable release in some systems [e.g. V, Ni and Cr in SCRTs (Hu et al., 2009)] lead to significant changes in the emitted PM elemental composition. In the cruise cycle, baseline vehicle elemental matrix is composed largely of alkaline earth metals (Sr, Mg, Ba and Ca; 75%) and divalent transition metals (Zn, Cd and Co; 23 %). Most of these metals primarily originate from the lube oil and its additives (Liu et al., 2008; McGeehan et al., 2005). A reduction in the fraction of alkaline earth metals is observed in the PM downstream of all retrofits, along with a corresponding increase in other metal fractions, such as transition metals and hydrolyzed metals (mostly Al, not shown). The most notable increase is in the relative abundance of redox active transition metals (Mn, V, Ni, Cu, Fe and Cr), which are negligible in baseline vehicle (0.4 %), but constitute a significant fraction in almost all of the retrofitted vehicles, with V-SCRT and school bus among the highest (9.4 %, both), followed by Z-SCRT (8.6 %). The other groups of metals such as heavy metals (Tl, Pb, U, Th, W), platinum group elements (Rh, Pt, Pd; PGE), rare earth metals (Eu, Pr, Ce, Nd, La, Sm, Y, Dy, Ho, Yb, Lu) and semi-metals (As, Sb) account for less than 3 % of the total metals emissions.

The PM metals distribution in UDDS cycle of the baseline vehicle is similar to that of the cruise cycle, with a comparable fraction of both alkaline earth and divalent transition metals. Although the fraction of divalent transition metals is decreased by retrofits in UDDS cycle, an increase in the fraction of redox active metals is evident here as well. PM samples from the baseline truck in the idle cycle were not available for assessing the impact of retrofits on metals distribution during idling. However, a comparison with cruise and UDDS cycles of the same vehicle-configuration shows a significantly smaller fraction of redox active transition metals, as well as lower contribution from higher valent metals in the idle cycle.

The increase in the fraction of redox active metals by retrofitted vehicles is of particular interest and is better elucidated by plotting these species in terms of their individual contents (µg/g of exhaust PM) as shown in Figure 4.8. The highest content of V in PM samples from V-SCRT (both cruise and UDDS cycles) can be attributed to the possible leaching of wash-coat catalyst from SCR system at high temperatures (Hu et al., 2009). The most prominent increase is in the content of Fe by retrofitted configurations, i.e. several (2-4) orders of magnitude difference, compared to the baseline vehicle. The Fe content is the highest in school bus PM both in cruise and UDDS cycles. Remaining metals (Cr, Ni, Mn and Cu) were also generally escalated (elevation factor reaching up to ~80 for Cr in VSCRT-cruise) in the PM samples from retrofitted vehicles, compared to the baseline truck.

Figure 4.8: Water-soluble content (μg/g) of major redox active metals in the exhaust PM from various vehicle-configurations, under (a) cruise, and (b) UDDS driving cycles
Note: BDL indicates "below detection levels" [of Ni (baseline-both cruise and UDDS), V (baseline-UDDS) and Cu (school bus-cruise)].

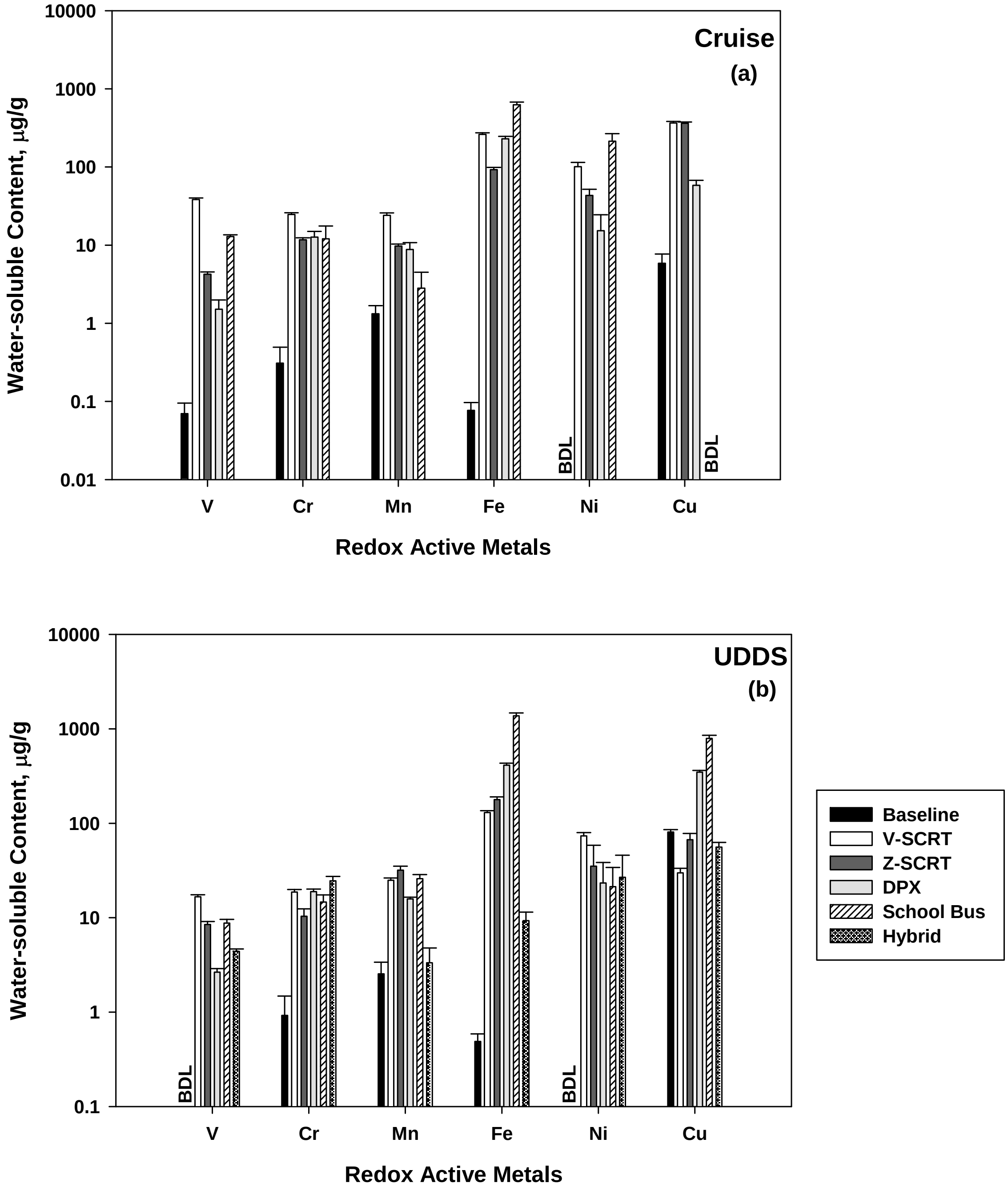

4.2.3.2 Macrophage ROS Activity

Figure 4.9 shows the results of macrophage ROS assay conducted on the water extracts of exhaust PM samples from all test vehicles. The results have been expressed both on a per mass of PM emitted basis (µg ROS activity/mg of PM) (Figure 4.9a) as well as ROS activity per km (or per hr for idle) of vehicle driven (Figure 4.9b). To place our results in a broader perspective, ROS activity measurements from other studies, both for ambient aerosols in central Los Angeles at USC as well as engine exhaust PM (Cheung et al., 2010), have also been presented as an insert in Figure 4.9a. As shown, a large variation in intrinsic ROS activity of PM from various vehicle-configurations – over 100 fold - was observed, although, excluding the very high activity for the school bus, measurements are in the range of typical levels observed for ambient and diesel exhaust particles.

Figure 4.9: Reactive Oxygen Species (ROS) activity of PM from the tested vehicles, expressed as (a) per mass of PM, and (b) per km (or hr for idle) of vehicle driven

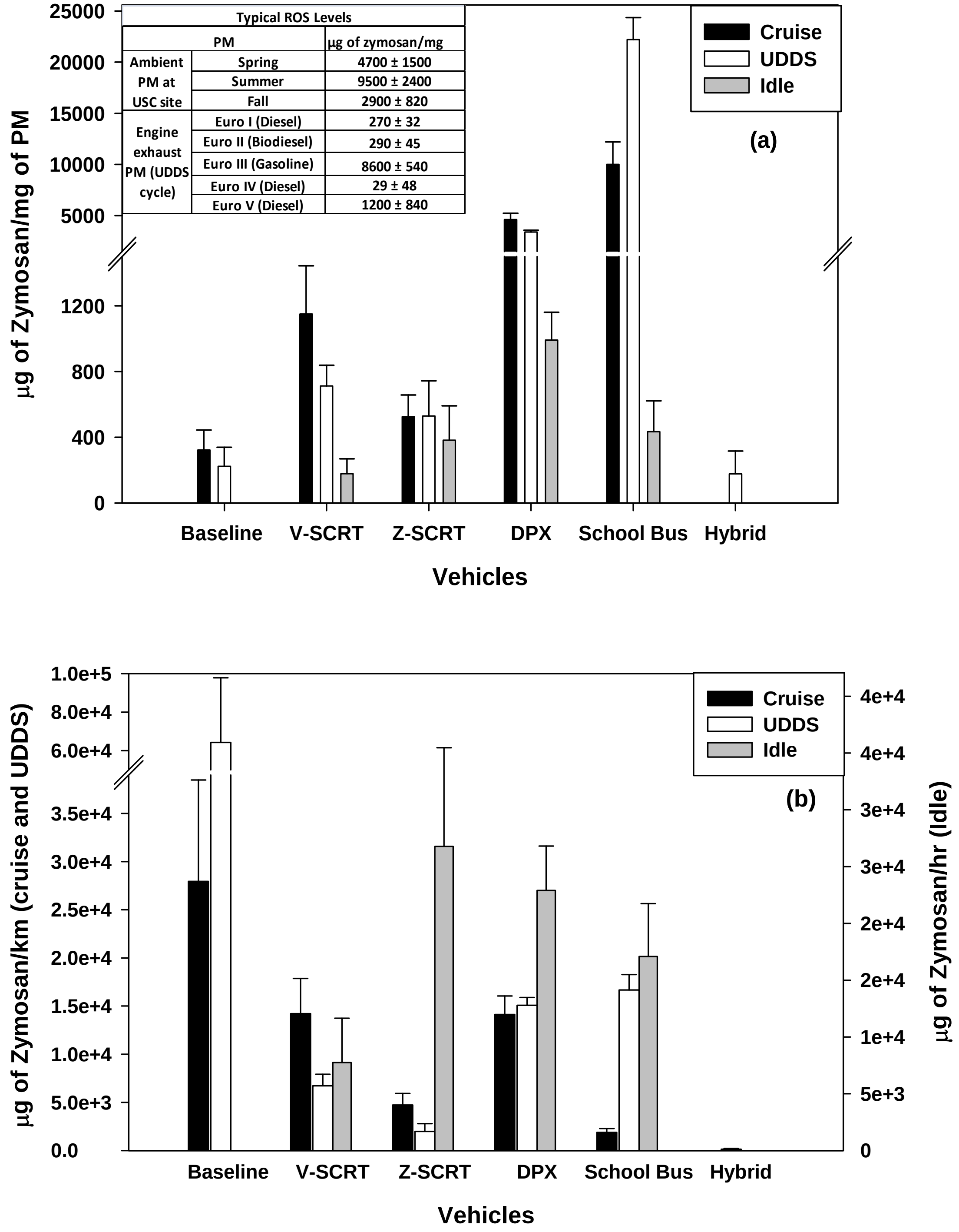

Typical ROS Levels

PM		µg of zymosan/mg
Ambient PM at USC site	Spring	4700 ± 1500
	Summer	9500 ± 2400
	Fall	2900 ± 820
Engine exhaust PM (UDDS cycle)	Euro I (Diesel)	270 ± 32
	Euro II (Biodiesel)	290 ± 45
	Euro III (Gasoline)	8600 ± 540
	Euro IV (Diesel)	29 ± 48
	Euro V (Diesel)	1200 ± 840

The ROS activity per mass of particles emitted from all retrofitted configurations is higher than the baseline truck, with a sole exception of the hybrid vehicle. The highest activity is observed for the school bus, which has been shown to be one of the most efficient vehicles in controlling both mass and number emissions (>99 %; Chapter 2). It is interesting to note that the hybrid vehicle, with similar particle mass and number emissions as that of the school bus (Chapter 2), yields the lowest ROS activity. The DPX vehicle, which is also quite efficient in reducing PM mass emissions (up to 95 %; Chapter 2), generates particles with high ROS activity (up to ~ 4600 µg of Zymosan units/mg of PM). Of particular note are also the elevated ROS levels observed for both vanadium and Zeolite based SCRTs compared to the baseline vehicle. Thus, although SCRTs effectively remove the targeted pollutants for which they were designed (i.e, hydrocarbons and NOx) in the exhaust emissions (Herner et al., 2009; Pakbin et al., 2009), their in-built catalysts appear to increase the fraction of certain redox active species in DEPs.

The ROS results expressed on per km (or per hr for idle) basis (Figure 4.9b) provide an overall assessment of the effectiveness of control technologies on total oxidative load imparted by the exhaust PM. It is of particular note that, although per PM mass activity is increased by most of the control technologies, all of the retrofitted configurations are efficient in reducing the per km (or per hr) ROS activity, compared to the baseline vehicle. This reduction is a result of the lower particulate mass emissions (by more than one order of magnitude) from retrofitted configurations compared to the baseline truck

(Chapter 2). The decrease in ROS activity is, however, not linear with the overall PM mass reduction in retrofitted vehicles. For example, an approximate 10-times reduction in PM mass emission achieved by Z-SCRT (cruise) lowers the ROS activity (per km) by only 5 times. The contrast between distance and mass based activity is consistent with the measurements using DTT assay on the same suite of vehicles (Chapter 2). These findings have potential implications from the perspective of human exposure and risk assessment, and underscore the importance of both the intrinsic toxicity of PM, and its mass emission rate, while evaluating the net environmental impacts of an after-treatment technology.

4.2.3.3 Chelex Treatment

Figure 4.10 shows the percent removal (average of all vehicle-configurations) of major water-soluble elements from the exhaust PM extracts after Chelex treatment. The figure illustrates that chelation is highly efficient in removing most cationic di- and tri-valent metals from the DEP extracts. Except for Cr and V (which exhibited removal percentages of 57 % and 26 %, respectively), the removal efficiency for most of the transition metals was greater than 70 %. The extent of metal chelation from the water extracts depends on a number of factors including their oxidation states and aqueous complexation (Haas and Northup, 2004; Thompson et al., 2002). The high removal efficiency for most of the transition metals indicate minimal complexation of these species in solution, making them biochemically available. Of the redox-active metals, Mn was most effectively removed (93%) on Chelex, followed by Cu (79%), Fe and Ni (73%). The tendency of Cr ions to form hydrates (octahedral coordination with water molecules), probably impedes its attachment and removal with the iminodiacetate ligands (Fackler and Holah, 1965). Further, the soluble Cr likely has a significant Cr (VI) component, which is an oxyanion and is not effectively removed on Chelex (Gad, 1989). The formation of oxyanions by vanadium (vanadate ion; VO_4^{-3}) might be responsible for its poor removal efficiency (Tischer et al., 2004). Other metals exhibiting very high removal efficiency include Mg, Al, Ca, Ba, Cd and Pb. The non-metals (S and P) and semi-metals (As), mostly present as oxyanions (Shafer et al., 2010) exhibit low removal efficiency.

Figure 4.10: Percent removal (average of all vehicle-configurations) of major water-soluble elements using Chelex treatment of the exhaust PM samples

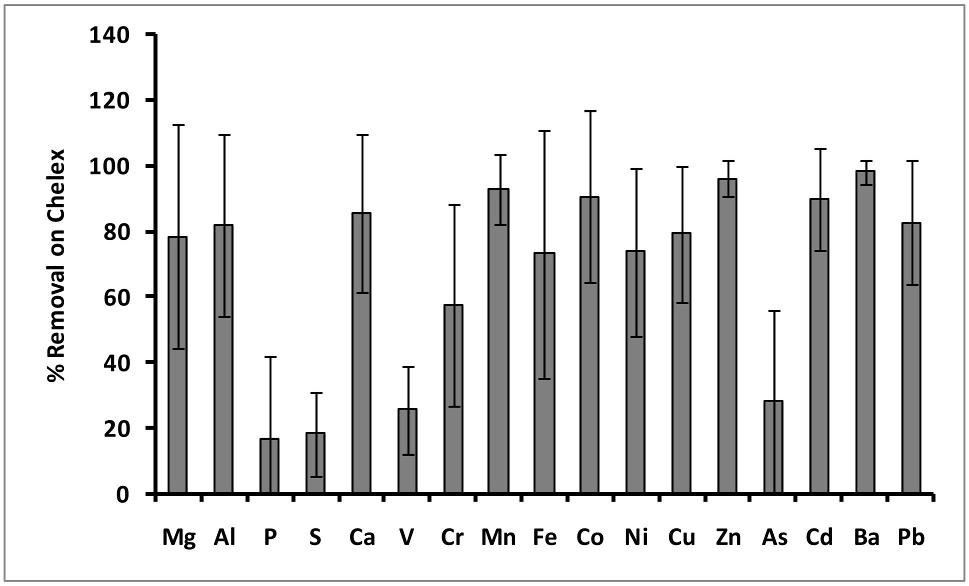

Figure 4.11 shows the percent removal of ROS activity after Chelex treatment of the exhaust PM extracts from all test vehicles under different driving cycles. To emphasize the correspondence between water-soluble metals and ROS activity, the percent removal

of the sum of major metals from respective PM samples is also shown (Figure 4.11). Chelex treatment of DEPs water extracts removed a very large and fairly consistent fraction of ROS activity across most of the vehicles. The reduction in ROS activity averages at 77 (±20) % (range: 36% for DPX-idle to 100 % for baseline-UDDS and hybrid vehicles). The substantial reduction in ROS activity after metals chelation and removal highlights the dominant contribution of water soluble metals to redox properties of PM and is one of the important findings of this study.

Figure 4.11: Percent removal of ROS activity in relation to that of aggregate water soluble metals after Chelex treatment of the exhaust PM samples from test vehicle-configurations under different driving cycles.

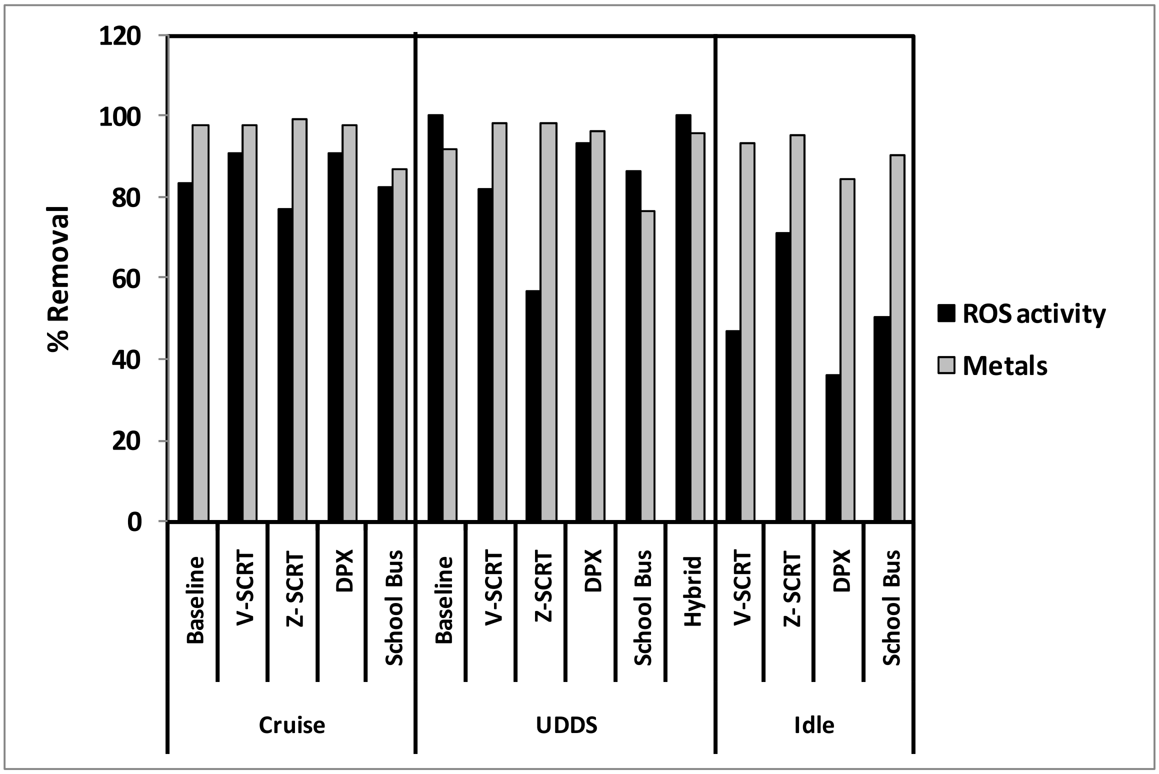

Under idling conditions, the V-SCRT, DPX and school bus show significantly lower ROS removal (<50 %), despite comparable reductions in the aggregate metals content of their PM samples. The results of one-sample t-test revealed that the mean fractional removal of ROS in idle cycle is statistically different from that in cruise (p=0.002) and UDDS (p=0.001) cycles. A vehicle-specific analysis of the percent removal of individual metals illustrated minimal chelation (<40 %) of transition metals for these vehicles [V, Cr, Fe for VSCRT and V, Cr, Fe and Cu for DPX and school bus] in idle cycle. Thus, it is likely that the chemical speciation of many relevant metals is substantially different in the PM emitted under idling conditions, which is reflected in both Chelex and ROS removal efficiencies. In addition, these data imply that not all measured elements are capable of generating PM related oxidative stress and only a few species – mostly redox active transition metals appear to play a central role. The identification of major contributors to PM toxicity is further investigated in the regression section discussed below.

4.2.3.4 Statistical Association between ROS Activity and Metals

Univariate Regression

To further support our observations and provide indications on the specific metals driving ROS activity, a regression analysis was conducted investigating the associations between ROS activity and major water-soluble elements in PM. As a preliminary step, univariate linear regression was performed to screen the elements that are significantly correlated with ROS activity. This selection process was conducted in three steps: 1) including only untreated (i.e. not Chelexed) samples; 2) including only Chelexed samples; and 3) using untreated minus Chelexed levels (designated as “delta” hereafter), in the regression analysis. Table 4.2 summarizes all of these correlations along with the associated levels of significance.

Table 4.2: Pearson correlation coefficients and associated levels of significance for the univariate regression between ROS activity and major water-soluble metals of PM

	Untreated samples		**Chelexed Samples**		**Untreated-Chelexed (delta)**	
Elements	***R***	***p***	***R***	***p***	***R***	***p***
Mg	-0.19	0.36	0.26	0.22	-0.18	0.39
Al	0.38	0.07	0.13	0.56	0.39	0.06
P	0.27	0.21	**0.66**	0.00	0.12	0.56
S	0.13	0.53	-0.32	0.12	0.22	0.30
Ca	-0.01	0.95	0.36	0.09	-0.02	0.94
V	-0.02	0.92	0.03	0.88	0.16	0.47
Cr	**0.67**	0.00	0.30	0.15	**0.65**	0.00
Mn	**0.62**	0.01	0.33	0.11	**0.61**	0.01
Fe	**0.93**	0.00	0.58	0.00	**0.91**	0.00
Co	**0.61**	0.04	-0.08	0.70	**0.63**	0.04
Ni	0.22	0.31	0.20	0.36	0.21	0.32
Cu	0.47	0.02	0.17	0.43	0.48	0.02
Zn	0.46	0.02	0.12	0.56	0.47	0.02
As	0.03	0.89	0.42	0.04	-0.29	0.17
Cd	0.50	0.01	0.59	0.00	0.47	0.02
Ba	0.31	0.15	0.09	0.67	0.27	0.20
Pb	0.47	0.02	0.11	0.59	0.47	0.02

As shown in Table 4.2, for the untreated sample set, ROS activity is reasonably correlated with several transition metals such as Fe, Cr, Mn and Co ($R>0.60$; $p<0.05$). The highest correlation was observed for Fe ($R=0.93$; $p=0.00$), followed by Cr ($R=0.67$; $p=0.00$), Mn ($R=0.62$, $p=0.01$) and Co ($R=0.61$; $p=0.04$). By contrast, none of the transition metals are significantly correlated with ROS activity in the Chelexed sample set, which is not surprising, given the very low levels of these species (most of which were not significantly different than zero) remaining after chelation. Thus, regression analysis on Chelexed sample set was deemed inappropriate. Interestingly, the correlation coefficients obtained for delta levels are very similar to that for the untreated samples, which is again due to the near complete removal of most metals and ROS after chelation. Other metals (Mg, Al, Ca, V, Ni and Ba), semi-metals (As) and non-metals (P and S) are not significantly correlated with ROS activity in either untreated or delta set.

Multivariate Regression

The univariate regression employed in previous section may not allow us to discriminate and quantify the impact of individual elements on PM toxicity. We therefore applied multivariate regressions in order to better understand the variance of ROS activity as a function of transition metals content. The metals exhibiting highest correlations with ROS activity in the untreated dataset (Fe, Cr, Mn, Co, Cd, Cu, Pb and Zn) were selected and stepped through one-by-one to generate multiple linear models (Sigma Plot 11.0, Systat Software Inc).

As a first step, the regression model included only Fe as the independent variable. The predicted ROS activity based on this model is plotted as a function of the measured ROS activity in Figure 4.12a. The regression analysis yielded a high coefficient of determination ($R^2 = 0.84$) with a slope and intercept of 0.84 and 992.4 μg of Zymosan units/mg of PM, respectively, which is a very satisfactory prediction of the ROS activity. The dominant influence of Fe on ROS activity has been reported in earlier investigations also, evaluating the toxicity of ambient particles (Hu et al., 2008; Shafer et al., 2010; Verma et al., 2009; Zhang et al., 2008). These statistical findings support our chemical fractionation measurements and suggest that the soluble Fe content of the PM is a very robust indicator of its ROS activity.

Figure 4.12: Correlation of measured and reconstructed ROS activity with successive inclusions of different species in the multivariate regression model: a) only Fe; b) Fe and Co; c) Fe, Co and Cr.

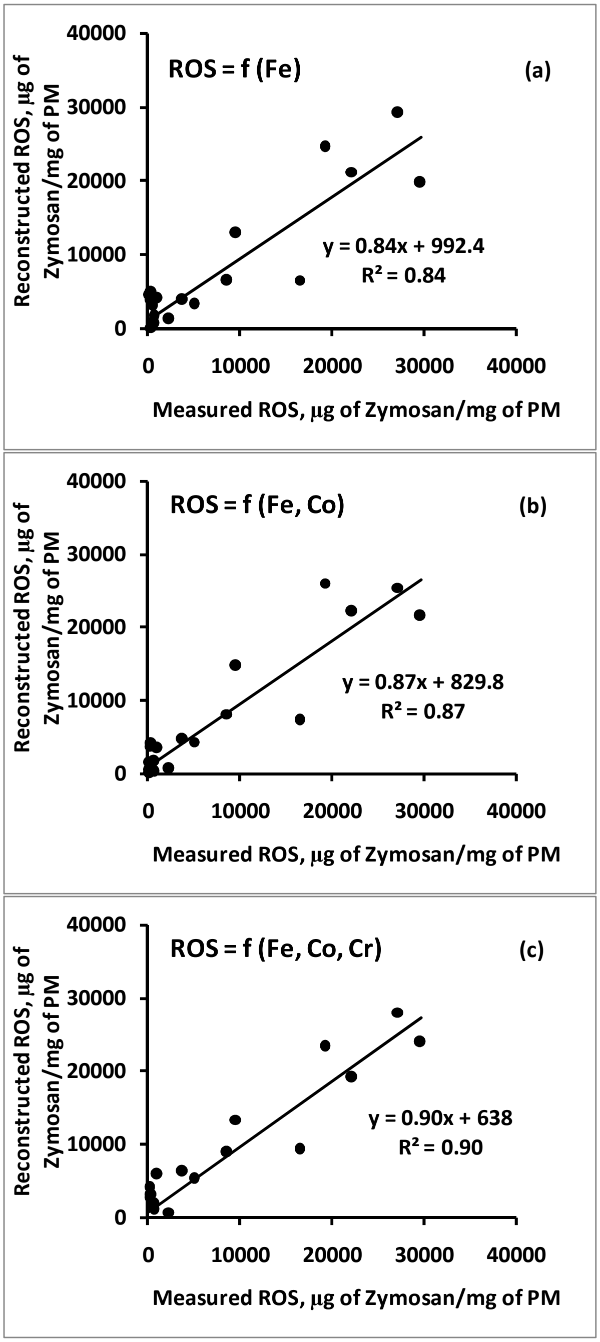

Fe is among the most abundant transition metals in DEPs and is generally present in two oxidation states, Fe (II) and Fe (III). The solubility of Fe (II) is much higher than that of Fe (III); aqueous equilibrium concentrations of amorphous ferrous and ferric hydroxide [am-$Fe(OH)_2$ and am-$Fe(OH)_3$] are nearly 10^{-5} M and 10^{-10} M, respectively (Nico et al., 2009). The redox cycling of Fe, generating an array of free radicals (e.g. OH^*, O_2^{*-}, and HO_2^*) through Fenton reaction, is well documented (Chen and Lippmann, 2009; Rose and Waite, 2005; Valko et al., 2005; Welch et al., 2002). Although, the exact mechanism of the reaction is still a matter of debate, Fe (II) catalyzed reduction of molecular oxygen to release hydroxyl radicals [Haber Weiss reaction; (Winterbourn, 1987)] is considered to be largely responsible in Fe mediated toxicity. The comparatively higher water solubility of Fe (II) further makes it more bioavailable to probably participate in the reactions yielding ROS activity of DEP extracts.

The next step in the multivariate regression modeling involved iterative inclusions of each of the additional correlated metals (Cr, Mn, Co, Cd, Cu, Pb and Zn), and examination of their impacts on the model's ability to predict ROS levels. The comparison of reconstructed and measured ROS activity, considering both Fe and Co into the model, is shown in Figure 4.12b. Both correlation coefficient and slope of the regression equation increased to 0.87, while the intercept decreased to 829.8 µg of Zymosan units/mg of PM. Similarly, inclusion of Cr further improved the model by increasing the correlation coefficient and slope to 0.90, and decreasing the intercept to 638 µg of Zymosan units/mg of PM (Figure 4.12c). The multivariate regression was concluded at this final step as no additional species significantly contributed to improve the correlation.

The parameters for the final regression equation are summarized in Table 4.3. As evident, all metals included into the model contributed independently [variance inflation factor (VIF) < 4] and significantly ($p<0.05$) to account for 90 % of the variance ($R^2=0.90$) in ROS activity. The standardized coefficients listed in the table may be used to quantify an approximate contribution of the individual species in measured ROS activity. The highest coefficient of Fe (0.94) implies that ROS activity is most sensitive to the changes in Fe content of PM; a unit standard deviation change in Fe content would change the ROS activity by 0.94 standard deviations, which is about 3 times higher compared to that by an equivalent change in Cr content (standardized coefficient = 0.28).

Table 4.3: Parameters of the multivariate regression analysis between ROS activity and water-soluble metals of PM

Species	**Unstandardized Coefficient** (µg of Zymosan /ng of metal)		**Standardized Coefficient**	**p**	**VIF**
	Value	**error**			
Constant	-539.24	985.84			
Fe	17.77	1.84	0.94	0.00	1.86
Co	-2468.18	766.22	-0.34	0.00	2.20
Cr	226.94	92.54	0.28	0.02	2.45

Interestingly, despite the positive correlation of Co as shown in Table 4.2, its coefficient becomes negative after Fe is included into the model (Table 4.3). Perhaps the negative association of Co in ROS predicting equation is a statistical artifact driven by the large positive coefficient of Fe. Similar anomalies were observed in previous explorations (Ntziachristos et al., 2007; Zhang et al., 2008), and illustrate one of the limitations of any study attempting to link toxicological PM properties to their chemical constituents strictly based on regression analysis. Accordingly, the apparent associations of different metals with ROS activity as implied from their coefficients might not be representative of their independent toxic potency, but rather in relation to other included redox species, and is thus highly subjective to the variables selection in multiple regressions.

4.2.4 Summary and Conclusions

This investigation explores the linkage between the ROS activity of DEPs and their water-soluble metals content. A macrophage-based in vitro ROS assay was coupled with the elemental fractionation of exhaust PM from various heavy-duty diesel vehicles. The test fleet included a baseline (without any control technology), two SCRTs (vanadium and Zeolite based), a DPX (DPF), a school bus (EPF) and a hybrid (CCRT) vehicle. The fleet was tested under three driving cycles: cruise, UDDS and idle. The study demonstrates that despite generally similar reductions in PM mass emissions from diesel vehicles by various control technologies, the intrinsic ROS activity of the emitted particles may vary dramatically with retrofit types. Although, mass based ROS levels (µg/mg of PM) increased with the application of after-treatment devices, a significant reduction was observed in the overall ROS activity (per km for cruise and UDDS and per hr for idle) for retrofitted configurations, compared to the baseline vehicle.

A substantial fraction of ROS activity of DEPs was associated with the water-soluble metals as evident from the near complete attenuation of activity after chelation of PM sample extracts. However, relatively lower removal of the activity in few vehicle-configurations (V-SCRT, DPX and school bus -idle), despite a large aggregate metals removal, indicated that the generation of ROS was driven by a select group of metal species. A univariate regression analysis further supported that ROS activity is associated with only few transition metals such as Fe, Cr, Co and Mn. Multivariate regressions conducted on the selected transition metals and oxidative activity of PM revealed that Fe accounts for most of the variability in ROS levels.

Chapter 5: Conclusions and Future Research Directions

5.1 Summary and Conclusions

Several recent toxicological studies have confirmed the oxidative properties of particulate matter and their capability to generate reactive oxygen species in biological systems (Donaldson et al., 2002; Xia et al., 2004). The production of these pro-oxidant species and their subsequent damage to important macromolecules (e.g. DNA, proteins, lipids) are thought to be implicated in numerous diseases including respiratory (Gauderman et al., 2007; Stayner et al., 1998), cardiovascular (Delfino et al., 2005) and neurodegenerative disorders (Peters et al., 2006). Diesel exhaust particles represent an important component of fine and ultrafine PM in urban areas (Steerenberg et al., 1998). The newer diesel engines with emission control devices are very efficient in reducing the mass emissions of particulate matter. The emissions of major chemical constituents (e.g. elemental and organic carbon) are also substantially reduced by these late model vehicles. However, the enhanced formation of nucleation mode particles is observed in the exhausts of some retrofitted configurations. Much of the mass of these nucleation mode particles is semi-volatile in nature (e. g. sulfuric acid). Although, the retrofitted vehicles emit less WSOC (per mile of vehicle driven), water soluble fraction of the organic carbon (WSOC/OC) is increased for most of the configurations.

Despite an increase in the intrinsic oxidative activity (per mass basis) of exhaust PM with the use of most control technologies, the overall activity (expressed per km or per hr) was substantially reduced for retrofitted configurations compared to the uncontrolled vehicle. The responses of two toxicity assays – DTT, and macrophage ROS assay, used in our investigation to measure the oxidative activity of the particles, appear to be driven by different PM components. The DTT activity was found to be correlated mostly with the polar organic compounds. Secondary organic aerosol (SOA) formed by the photo-chemical reactions during afternoon period and woodsmoke particles emitted during the wildfire events, both are enriched in water soluble organic compounds, and show increased DTT activity compared to the primary particles generated from vehicular emissions. The dominant contribution of organic compounds in the DTT assay was further confirmed by a mechanistic analysis using thermodenuder; in which, the successive removal of semi-volatile organic compounds (SVOC) progressively declined the DTT activity of the particles. These SVOC are found to be highly redox-active and constitute a dominant fraction (up to almost 100 %) of PM oxidative potential for the DEPs evaluated in chassis dynamometer facilities. Compared to that, in ambient PM, a lower but still significant fraction (42-66 %) of the oxidative potential is contributed by its semi-volatile compounds. The difference in DTT activity profiles between DEPs and ambient PM is attributed to the lower content of semi-volatile species in ambient PM, as a result of the much higher atmospheric dilution, compared to the freshly emitted DEPs in dynamometer facilities, in which most of the SVOC are bound to the particle phase.

However, another important metric of oxidative activity – macrophage ROS assay, doesn't appear to be much affected by organic compounds, but was found to be correlated mostly with the transition metals (Fe, V, Cr, Ni, Co, Cd, Cu and Zn). These metals participate in the Fenton chemistry to generate hydroxyl radicals, which can effectively oxidize the DCFH probe used in this assay. The key role of the transition metals in ROS activity of PM was further quantified by their removal using a Chelex® complexation method; by which, chelation of the DEPs samples removed a substantial (≥70 %) fraction of the ROS activity. Identification of the major drivers of ROS activity by means of a multivariate regression analysis revealed Fe as the most important metal, accounting for the highest (84%) fraction of variability in the ROS levels.

The DTT and ROS assays used in this study are two independent and intrinsically different types of analyses, likely driven by different particle components, and in that respect, they should be considered complementary to each other. Collectively, these two assays provide an important framework for designing an effective methodology to understand the mechanism of PM toxicity and to infer the subsequent health risks. The variation in the oxidative activity profiles of PM originating from different sources measured by these assays is helpful in linking the PM toxicity to its source specific composition.

5.2 Recommendations

This study offers an important perspective in analyzing and comparing the toxicological characteristics of PM from different sources, which can be directly/indirectly useful in formulating the policies for human health prevention from PM exposure. However, considering the complexity of atmospheric reactions and their impacts on the PM physicochemical properties, further investigations are required which should focus on developing the appropriate sampling and measurement strategies to capture these variations affecting the PM toxic potency. We will discuss some of these aspects in this section with our recommendations to address these concerns.

Recent studies have indicated that the mechanisms by which transition metals cause cellular oxidative stress are largely governed by the oxidation state of the metal, which determines its bio-availability and thus subsequent toxicity (Shafer et al., 2010; Verma et al., 2010). For example, two most common oxidation states of iron under environmentally relevant conditions are: Fe (II) and Fe (III). Cr, like Fe, also has two major oxidation states, Cr (III) and Cr (VI). Cr (III) compounds are generally insoluble and non-toxic, whereas Cr (VI) is highly soluble, and potentially toxic (Gad, 1989). Manganese has three readily available oxidation states: Mn (II), Mn (III), and Mn (IV). Manganese appears to exert its toxic effects through a variety of pathways including ROS formation by Mn (II) and direct oxidation of biological molecules by Mn (III). While Mn (II) salts are more bioavailable (soluble), the cytotoxicity of Mn (III) compounds appears to be significantly greater than those of Mn (II) (Aschner et al., 2005; Dorman et al., 2001; Reaney and Smith, 2005). The oxidation state of these metals within a particle at the time of inhalation is a function of the emission source and changes occurred during atmospheric aging. Studies have indicated that photochemistry plays a major role in determining the pertinent oxidation state of a metal by inducing either oxidation or reduction of metals in the ambient atmosphere (Hoffmann et al., 1997; Siefert et al., 1996). For example, particulate iron has been shown to undergo both atmospheric oxidation and/or reduction depending on the factors such as presence of electron donors (oxalate, formate, acetate) and pH (Siefert et al., 1994). Most of the previous investigations studying the redox reactions of particulate metals are based on a simulated atmosphere in laboratory, without sampling the real world aerosols. As ambient aerosols are generally complex mixture of a variety of organic and inorganic species, it is extremely difficult to predict how the redox active transition metals will behave in atmospheric PM. The mechanisms of redox reactions involving transition metals are also a function of size of the particles. It has been hypothesized that in ultrafine particles, Fe (II) oxidation might be the dominating mechanism, while photo-reduction dominates in larger particles (Majestic et al., 2007). Thus, an analysis of the diurnal variations in oxidation states of major transition metals should be very useful in providing the insights on bio-availability of these metals from the perspectives of ambient PM toxicity. In addition, this analysis would help to assess the role of photo-chemistry and infer the net mechanisms (among various oxidative and reductive reactions occurring simultaneously) governing the changes in oxidation states of transition metals in a real world atmosphere.

In the present study, DTT activity of the particles (both ambient and DEPs) is found to be strongly correlated with their WSOC content. However, WOSC itself is a complex mixture of diverse group of species, including dicarboxylic acids, poly acidic compounds, polyethers etc (Decesari et al., 2000). Our investigation measured only a few organic acids, constituting a very small fraction (2-5% in most cases) of WSOC. Thus, it is difficult to conclude what specific species contribute to the observed relationship between WSOC and the DTT activity of PM. We believe that more research is needed to identify the organic compounds present in water soluble components of the particles and to quantify their individual contribution in the overall PM oxidative potential.

There have been issues also about the changes in chemical characteristics of organic compounds by using thermodenuder for sampling the semi-volatile species. A detailed discussion of these heating effects on the particle composition can be found in Denkenberger et al., (2007). In general, accelerated kinetics at high temperatures may lead to the formation of oligomers inside thermodenuder. This would mean that thermodenuders might introduce an artifact by altering the chemical characteristics of the organic compounds in addition to thermal stripping. Considering these issues, we recommend to develop a vacuum based denuder for stripping the semi-volatile compounds from PM matrix, such that the chemical characteristics of both volatile and non-volatile species remain preserved.

Lastly, we recommend that in addition to the *in-vitro* evaluations as conducted in our investigation, *in-vivo* studies will also be useful in addressing the importance of semi-volatile and non-volatile PM fractions from the perspectives of their distinct toxicity profiles. As previously mentioned, DTT assay measures the oxidative potential of organic compounds by their capability to generate superoxide radicals in a reaction between DTT and oxygen. Although attenuation of DTT activity with aerosol heating demonstrates the significant contribution of semi-volatile organic compounds to the PM oxidative potential; superoxide radicals formed in the oxidation reaction can interact with transition metals, also present in PM, to generate hydroxyl radicals. Thus, for a comprehensive assessment of the relative toxicity profiles of semi-volatile and non-volatile components and their overall contributions to the PM toxicity, further mechanistic research is needed, including *in-vivo* exposure studies focusing on these two categories of PM.

Bibliography

An, W.J., Pathak, R.K., Lee, B.H., Pandis, S.N., 2007. Aerosol volatility measurement using an improved thermodenuder: application to secondary organic aerosol. Journal of Aerosol Science 38 (3), 305-314.

Arhami, M., Sillanpaa, M., Hu, S.H., Olson, M.R., Schauer, J.J., Sioutas, C., 2009. Size-Segregated Inorganic and Organic Components of PM in the Communities of the Los Angeles Harbor. Aerosol Science and Technology 43 (2), 145-160.

Arredouani, M.S., Palecanda, A., Koziel, H., Huang, Y.C., Imrich, A., Sulahian, T.H., Ning, Y.Y., Yang, Z.P., Pikkarainen, T., Sankala, M., Vargas, S.O., Takeya, M., Tryggvason, K., Kobzik, L., 2005. MARCO is the major binding receptor for unopsonized particles and bacteria on human alveolar macrophages. Journal of Immunology 175 (9), 6058-6064.

Artaxo, P., Gerab, F., Yamasoe, M.A., Martins, J.V., 1994. Fine Mode Aerosol Composition at 3 Long-Term Atmospheric Monitoring Sites in the Amazon Basin. Journal of Geophysical Research-Atmospheres 99 (D11), 22857-22868.

Aschner, M., Erikson, K.M., Dorman, D.C., 2005. Manganese dosimetry: Species differences and implications for neurotoxicity. Critical Reviews in Toxicology 35 (1), 1-32.

Ayala, A., Kado, N.Y., Okamoto, R.A., Holmen, B.A., Kuzmicky, P.A., Kobayashi, R., Stiglitz, K.E., 2002. Diesel and heavy-duty transit bus emissions over multiple driving schedules: regulated pollutants and project overview. Society of Automotive Engineers Technical Paper Series No. 2002-01-1722.

Ayala, A.K.N., Okamoto, R.A., Holmen, B.A., Kuzmicky, P.A., Kobayashi, R., Stiglitz, K.E., 2002. Diesel and CNG heavy-duty transit bus emissions over multiple driving schedules: regulated pollutants and project overview. SAE Technical Paper No. 2002-01-1722.

Baltensperger, U., Dommen, J., Alfarra, R., Duplissy, J., Gaeggeler, K., Metzger, A., Facchini, M.C., Decesari, S., Finessi, E., Reinnig, C., Schott, M., Warnke, J., Hoffmann, T., Klatzer, B., Puxbaum, H., Geiser, M., Savi, M., Lang, D., Kalberer, M., Geiser, T., 2008. Combined determination of the chemical composition and of health effects of secondary organic aerosols: The POLYSOA project. Journal of Aerosol Medicine and Pulmonary Drug Delivery 21 (1), 145-154.

Baron, P.A., Willeke, K., 2001. Aerosol measurement; principles, techniques, and application. NewYork: Wiley Interscience Publication.
Barrett, E.G., Henson, R.D., Seilkop, S.K., McDonald, J.D., Reed, M.D., 2006. Effects of hardwood smoke exposure on allergic airway inflammation in mice. Inhalation Toxicology 18 (1), 33-43.

Bayona, J.M., Markides, K.E., Lee, M.L., 1988. Characterization of Polar Polycyclic Aromatic-Compounds in a Heavy-Duty Diesel Exhaust Particulate by Capillary Column Gas-Chromatography and High-Resolution Mass-Spectrometry. Environmental Science & Technology 22 (12), 1440-1447.

Becker, S., Dailey, L.A., Soukup, J.M., Grambow, S.C., Devlin, R.B., Huang, Y.C.T., 2005. Seasonal variations in air pollution particle-induced inflammatory mediator release and oxidative stress. Environmental Health Perspectives 113 (8), 1032-1038.

Biswas, S., Verma, V., Schauer, J.J., Cassee, F.R., Cho, A.K., Sioutas, C., 2009. Oxidative potential of semi-volatile and non-volatile particulate matter (PM) from heavy-duty vehicles retrofitted with emission control technologies. Environmental Science & Technology 43 (10), 3905-3912.

Castranova, V., Ma, J.Y.C., Yang, H.M., Antonini, J.M., Butterworth, L., Barger, M.W., Roberts, J., Ma, J.K.H., 2001. Effect of exposure to diesel exhaust particles on the susceptibility of the lung to infection. Environmental Health Perspectives 109 609-612.

Chen, L.C., Lippmann, M., 2009. Effects of metals within ambient air particulate matter (PM) on human health. Inhalation Toxicology 21 (1), 1-31.

Cheung, K.L., Ntziachristos, L., Tzamkiozis, T., Schauer, J.J., Samaras, Z., Moore, K.F., Sioutas, C., 2010. Emissions of particulate trace elements, metals and organic species from gasoline, diesel, and biodiesel passenger vehicles and their relation to oxidative potential. Aerosol Science and Technology 44 (7), 500-513.

Cho, A.K., Sioutas, C., Miguel, A.H., Kumagai, Y., Schmitz, D.A., Singh, M., Eiguren-Fernandez, A., Froines, J.R., 2005. Redox activity of airborne particulate matter at different sites in the Los Angeles Basin. Environmental Research 99 (1), 40-47.

Ciapetti, G., Granchi, D., Verri, E., Savarino, L., Cenni, E., Savioli, F., Pizzoferrato, A., 1998. Fluorescent microplate assay for respiratory burst of PMNs challenged in vitro with orthopedic metals. Journal of Biomedical Materials Research 41 (3), 455-460.

Cruts, B., van Etten, L., Toernqvist, H., Blomberg, A., Sandstrom, T., Mills, N.L., Borm, P.J.A., 2008. Exposure to diesel exhaust induces changes in EEG in human volunteers. Particle and Fibre Toxicology 5 (4), doi:10.1186/1743-8977-1185-1184.

Cruz, C.N., Pandis, S.N., 1998. The effect of organic coatings on the cloud condensation nuclei activation of inorganic atmospheric aerosol. Journal of Geophysical Research-Atmospheres 103 (D11), 13111-13123.

Dachs, J., Eisenreich, S.J., 2000. Adsorption onto aerosol soot carbon dominates gas-particle partitioning of polycyclic aromatic hydrocarbons. Environmental Science & Technology 34 (17), 3690-3697.

Decesari, S., Facchini, M.C., Fuzzi, S., Tagliavini, E., 2000. Characterization of water-soluble organic compounds in atmospheric aerosol: A new approach. J. Geophys. Res-Atmos. 105 (D1), 1481-1489.

Decesari, S., Facchini, M.C., Matta, E., Lettini, F., Mircea, M., Fuzzi, S., Tagliavini, E., Putaud, J.P., 2001. Chemical features and seasonal variation of fine aerosol water-soluble organic compounds in the Po Valley, Italy. Atmospheric Environment 35 (21), 3691-3699.

Delfino, R.J., Sioutas, C., Shaista, M., 2005. Potential Role of Ultrafine Particles in Associations between Airborne Particle Mass and Cardiovascular Health. Environmental Health Perspectives 113 (8), 934–946.

Delfino, R.J., Staimer, N., Tjoa, T., Gillen, D.L., Polidori, A., Arhami, M., Kleinman, M.T., Vaziri, N.D., Longhurst, J., Sioutas, C., 2009. Air Pollution Exposures and Circulating Biomarkers of Effect in a Susceptible Population: Clues to Potential Causal Component Mixtures and Mechanisms. Environmental Health Perspectives 117 (8), 1232-1238.

Denkenberger, K.A., Moffet, R.C., Holecek, J.C., Rebotier, T.P., Prather, K.A., 2007. Real-time, single-particle measurements of oligomers in aged ambient aerosol particles. Environmental Science & Technology 41 (15), 5439-5446.

DiStefano, E., Eiguren-Fernandez, A., Delfino, R.J., Sioutas, C., Froines, J.R., Cho, A.K., 2009. Determination of metal-based hydroxyl radical generating capacity of ambient and diesel exhaust particles. Inhalation Toxicology 21 (9), 731-738.

Docherty, K.S., Stone, E.A., Ulbrich, I.M., DeCarlo, P.F., Snyder, D.C., Schauer, J.J., Peltier, R.E., Weber, R.J., Murphy, S.M., Seinfeld, J.H., Grover, B.D., Eatough, D.J., Jiimenez, J.L., 2008. Apportionment of Primary and Secondary Organic Aerosols in Southern California during the 2005 Study of Organic Aerosols in Riverside (SOAR-1). Environmental Science & Technology 42 (20), 7655-7662.

Donaldson, K., Beswick, P.H., Gilmour, P.S., 1996. Free radical activity associated with the surface of particles: a unifying factor in determining biological activity? Toxicology Letters 88 (1-3), 293-298.

Donaldson, K., Brown, D., Clouter, A., Duffin, R., MacNee, W., Renwick, L., Tran, L., Stone, V., 2002. The pulmonary toxicology of ultrafine particles. Journal of Aerosol Medicine-Deposition Clearance and Effects in the Lung 15 (2), 213-220.

Donaldson, K., Stone, V., Borm, P.J.A., Jimenez, L.A., Gilmour, P.S., Schins, R.P.F., Knaapen, A.M., Rahman, I., Faux, S.P., Brown, D.M., MacNee, W., 2003. Oxidative stress and calcium signaling in the adverse effects of environmental particles (PM10). Free Radical Bio Med 34 (11), 1369-1382.

Donaldson, K., Tran, L., Jimenez, L.A., Duffin, R., Newby, D.E., Mills, N., MacNee, W., Stone, V., 2005. Combustion-derived nanoparticles: a review of their toxicology following inhalation exposure. Particle and Fibre Toxicology 2 (10), doi:10.1186/1743-8977-2-10.

Dorman, D.C., Struve, M.F., James, R.A., Marshall, M.W., Parkinson, C.U., Wong, B.A., 2001. Influence of particle solubility on the delivery of inhaled manganese to the rat brain: Manganese sulfate and manganese tetroxide pharmacokinetics following repeated (14-day) exposure. Toxicology and Applied Pharmacology 170 (2), 79-87.

Dubick, M.A., Carden, S.C., Jordan, B.S., Langlinais, P.C., Mozingo, D.W., 2002. Indices of antioxidant status in rats subjected to wood smoke inhalation and/or thermal injury. Toxicology 176 (1-2), 145-157.

Echalar, F., Gaudichet, A., Cachier, H., Artaxo, P., 1995. Aerosol Emissions by Tropical Forest and Savanna Biomass Burning - Characteristic Trace-Elements and Fluxes. Geophysical Research Letters 22 (22), 3039-3042.

Engler, C., Rose, D., Wehner, B., Wiedensohler, A., Bruggemann, E., Gnauk, T., Spindler, G., Tuch, T., Birmili, W., 2007. Size distributions of non-volatile particle residuals (Dp < 800 nm) at a rural site in Germany and relation to air mass origin. Atmospheric Chemistry and Physics 7 (22), 5785-5802.

EPA, 2002. Health assessment document for diesel engine exhaust. EPA/600/8-90/057F; U.S. Environmental Protection Agency: Washington, DC.

Fackler, J.P., Holah, D.G., 1965. Properties of chromium (II) complexes. I. electronic spectra of simple salt hydrates. Inorganic Chemistry 4 (7), 954-958.

Fine, P.M., Chakrabarti, B., Krudysz, M., Schauer, J.J., Sioutas, C., 2004. Diurnal variations of individual organic compound constituents of ultrafine and accumulation mode particulate matter in the Los Angeles basin. Environ Sci Technol 38 (5), 1296-1304.

Folkmann, J.K., Risom, L., Hansen, C.S., Loft, S., Moller, P., 2007. Oxidatively damaged DNA and inflammation in the liver of dyslipidemic ApoE(-/-) mice exposed to diesel exhaust particles. Toxicology 237 (1-3), 134-144.

Foresti, R., Clark, J.E., Green, C.J., Motterlini, R., 1997. Thiol compounds interact with nitric oxide in regulating heme oxygenase-1 induction in endothelial cells - Involvement of superoxide and peroxynitrite anions. Journal of Biological Chemistry 272 (29), 18411-18417.

Gad, S.C., 1989. Acute and chronic systemic chromium toxicity. Science of the Total Environment 86 (1-2), 149-157.

Garg, B.D., Cadle, S.H., Mulawa, P.A., Groblicki, P.J., Laroo, C., Parr, G.A., 2000. Brake wear particulate matter emissions. Environmental Science & Technology 34 (21), 4463-4469.

Garshick, E., Laden, F., Hart, J.E., Rosner, B., Smith, T.J., Dockery, D.W., Speizer, F.E., 2004. Lung cancer in railroad workers exposed to diesel exhaust. Environmental Health Perspectives 112 (15), 1539-1543.

Gauderman, W.J., Vora, H., McConnell, R., Berhane, K., Gilliland, F., Thomas, D., Lurmann, F., Avoli, E., Kunzli, N., Jerrett, M., Peters, J., 2007. Effect of exposure to traffic on lung development from 10 to 18 years of age: a cohort study. Lancet 369 (9561), 571-577.

Geller, M., Biswas, S., Sioutas, C., 2006. Determination of particle effective density in urban environments with a differential mobility analyzer and aerosol particle mass analyzer. Aerosol Science and Technology 40 (9), 709-723.

Grose, M., Sakurai, H., Savstrom, J., Stolzenburg, M.R., Watts, W.F., Morgan, C.G., Murray, I.P., Twigg, M.V., Kittelson, D.B., Mcmurry, P.H., 2006. Chemical and physical properties of ultrafine diesel exhaust particles sampled downstream of a catalytic trap. Environmental Science & Technology 40 (17), 5502-5507.

Haas, J.R., Northup, A., 2004. Effects of aqueous complexation on reductive precipitation of uranium by Shewanella putrefaciens. Geochemical Transactions 5 (3), 41-48.

Halliwell, B., Cross, C.E., 1994. Oxygen-derived species - their relation to human-disease and environmental stress. Environmental Health Perspectives 102, 5-12.

Hameri, K., Vakeva, M., Aalto, P.P., Kulmala, M., Swietlicki, E., Zhou, J., Seidl, W., Becker, E., O'Dowd, C.D., 2001. Hygroscopic and CCN properties of aerosol particles in boreal forests. Tellus Series B-Chemical and Physical Meteorology 53 (4), 359-379.

Hansen, K.F., Jensen, M.G., Ezerman, N., 2001. Measurement of the ‘‘true’’ efficiency of a CRT filter. Report to Danish Road Safety and Transport Agency /http://www.fstyr.dk/sw24048.aspS.

Hays, M.D., Geron, C.D., Linna, K.J., Smith, N.D., Schauer, J.J., 2002. Speciation of gas-phase and fine particle emissions from burning of foliar fuels. Environmental Science & Technology 36 (11), 2281-2295.

Herner, J.H., Hu, S., Robertson, W.H., Huai, T., Collins, J.F., Dwyer, H., Ayala, A., 2009. Effect of advanced aftertreatment for PM and NOx control on heavy-duty diesel truck emissions. Environmental Science & Technology 43 (15), 5928–5933.

Herner, J.H., Robertson, W.H., Ayala, A., 2007a. Investigation of ultrafine particle number measurements from a clean diesel truck using the European PMP protocol. Society of Automotive Engineers Technical Paper Series No. 2007-01-1114.

Herner, J.H., Robertson, W.H., Ayala, A., Chang, O., Biswas, S., Sioutas, C., 2007b. Nucleation mode particle emissions from in-use heavy duty vehicles equipped with DPF and SCR retrofits. American Association for Aerosol Research. 26th Annual Aerosol Conference, September 24–18, 2007 Reno, NV.

Hinds, W.C., 1999. Aerosol technology: properties, behavior, and measurement of airborne particles New York: Wiley Interscience Publication.

Hiura, T.S., Kaszubowski, M.P., Li, N., Nel, A.E., 1999. Chemicals in diesel exhaust particles generate reactive oxygen radicals and induce apoptosis in macrophages. J Immunol 163 (10), 5582-5591.

Hoek, G., Brunekreef, B., Goldbohm, S., Fischer, P., van den Brandt, P.A., 2002. Association between mortality and indicators of traffic-related air pollution in the Netherlands: a cohort study. Lancet 360 (9341), 1203-1209.

Hoffmann, M.R., Webb, S.M., Siefert, R.S., 1997. Determination of photochemically available iron in ambient aerosols. Abstracts of Papers of the American Chemical Society 213 115-GEOC.

Hu, S., Polidori, A., Arhami, M., Shafer, M.M., Schauer, J.J., Cho, A., Sioutas, C., 2008. Redox activity and chemical speciation of size fractioned PM in the communities of the Los Angeles-Long Beach harbor. Atmospheric Chemistry and Physics 8 (21), 6439-6451.

Hu, S.H., Herner, J.D., Shafer, M., Robertson, W., Schauer, J.J., Dwyer, H., Collins, J., Huai, T., Ayala, A., 2009. Metals emitted from heavy-duty diesel vehicles equipped with advanced PM and NOx emission controls. Atmospheric Environment 43 (18), 2950-2959.

Hughes, L.S., Cass, G.R., Gone, J., Ames, M., Olmez, I., 1998. Physical and chemical characterization of atmospheric ultrafine particles in the Los Angeles area. Environmental Science & Technology 32 (9), 1153-1161.

Jordan, T.B., Seen, A.J., Jacobsen, G.E., 2006. Levoglucosan as an atmospheric tracer for woodsmoke. Atmospheric Environment 40 (27), 5316-5321.

Khlystov, A., Zhang, Q., Jimenez, J.L., Stanier, C., Pandis, S.N., Canagaratna, M.R., Fine, P., Misra, C., Sioutas, C., 2005. In situ concentration of semi-volatile aerosol using water-condensation technology. Journal of Aerosol Science 36 (7), 866-880.

Kim, S., Chang, M.C., Kim, D., Sioutas, C., 2000. A new generation of portable coarse, fine, and ultrafine particle concentrators for use in inhalation toxicology. Inhalation Toxicology 12, 121-137.

Kim, S., Jaques, P.A., Chang, M.C., Barone, T., Xiong, C., Friedlander, S.K., Sioutas, C., 2001b. Versatile aerosol concentration enrichment system (VACES) for simultaneous in vivo and in vitro evaluation of toxic effects of ultrafine, fine and coarse ambient particles - part II: field evaluation. Journal of Aerosol Science 32 (11), 1299-1314.

Kim, S., Jaques, P.A., Chang, M.C., Froines, J.R., Sioutas, C., 2001a. Versatile aerosol concentration enrichment system (VACES) for simultaneous in vivo and in vitro evaluation of toxic effects of ultrafine, fine and coarse ambient particles - part I: development and laboratory characterization. Journal of Aerosol Science 32 (11), 1281-1297.

Kittelson, D.B., 1998. Engines and nanoparticles: A review. Journal of Aerosol Science 29 (5-6), 575-588.

Kittelson, D.B., Watts, W.F., Johnson, J.P., Rowntree, C., Payne, M., Goodier, S., Warrens, C., Preston, H., Zink, U., Ortiz, M., Goersmann, C., Twigg, M.V., Walker, A.P., Caldow, R., 2006. On-road evaluation of two Diesel exhaust aftertreatment devices. Journal of Aerosol Science 37 (9), 1140-1151.

Kleeman, M.J., Schauer, J.J., Cass, G.R., 1999. Size and composition distribution of fine particulate matter emitted from wood burning, meat charbroiling, and cigarettes. Environmental Science & Technology 33 (20), 3516-3523.

Koike, E., Hirano, S., Shimojo, N., Kobayashi, T., 2002. cDNA microarray analysis of gene expression in rat alveolar macrophages in response to organic extract of diesel exhaust particles. Toxicological Sciences 67 (2), 241-246.

Kuhn, T., Biswas, S., Fine, P.M., Geller, M., Sioutas, C., 2005. Physical and chemical characteristics and volatility of PM in the proximity of a light-duty vehicle freeway. Aerosol Science and Technology 39 (4), 347-357.

Kumagai, Y., Arimoto, T., Shinyashiki, M., Shimojo, N., Nakai, Y., Yoshikawa, T., Sagai, M., 1997. Generation of reactive oxygen species during interaction of diesel exhaust particle components with NADPH-cytochrome P450 reductase and involvement of the bioactivation in the DNA damage. Free Radical Biology and Medicine 22 (3), 479-487.

Kunzli, N., Mudway, I.S., Gotschi, T., Shi, T.M., Kelly, F.J., Cook, S., Burney, P., Forsberg, B., Gauderman, J.W., Hazenkamp, M.E., Heinrich, J., Jarvis, D., Norback, D., Payo-Losa, F., Poli, A., Sunyer, J., Borm, P.J.A., 2006. Comparison of oxidative properties, light absorbance, and total and elemental mass concentration of ambient PM2.5 collected at 20 European sites. Environmental Health Perspectives 114 (5), 684-690.

Landreman, A.P., Shafer, M.M., Hemming, J.C., Hannigan, M.P., Schauer, J.J., 2008. A macrophage-based method for the assessment of the reactive oxygen species (ROS) activity of atmospheric particulate matter (PM) and application to routine (daily-24 h) aerosol monitoring studies. Aerosol Science and Technology 42 (11), 946-957.

Li, N., Sioutas, C., Cho, A., Schmitz, D., Misra, C., Sempf, J., Wang, M.Y., Oberley, T., Froines, J., Nel, A., 2003. Ultrafine particulate pollutants induce oxidative stress and mitochondrial damage. Environmental Health Perspectives 111 (4), 455-460.

Li, N., Wang, M.Y., Oberley, T.D., Sempf, J.M., Nel, A.E., 2002. Comparison of the pro-oxidative and proinflammatory effects of organic diesel exhaust particle chemicals in bronchial epithelial cells and macrophages. J Immunol 169 (8), 4531-4541.

Li, Q.F., Wyatt, A., Kamens, R.M., 2009. Oxidant generation and toxicity enhancement of aged-diesel exhaust. Atmospheric Environment 43 (5), 1037-1042.

Liu, Z.G., Berg, D.R., Swor, T.A., Schauer, J.J., 2008. Comparative analysis on the effects of diesel particulate filter and selective catalytic reduction systems on a wide spectrum of chemical species emissions. Environmental Science & Technology 42 (16), 6080-6085.

Liu, Z.G., Victoria, N.V., Swor, T., Kittelson, D.B., 2007. Significance of fuel sulfur content and dilution conditions on particle emissions from a heavily-used diesel engine during transient operation. Society of Automotive Engineers Technical Paper Series No. 2007-01-0319.

Lough, G.C., Schauer, J.J., Park, J.S., Shafer, M.M., Deminter, J.T., Weinstein, J.P., 2005. Emissions of metals associated with motor vehicle roadways. Environmental Science & Technology 39 (3), 826-836.

Majestic, B.J., Schauer, J.J., Shafer, M.M., 2007. Application of synchrotron radiation for measurement of iron red-ox speciation in atmospherically processed aerosols. Atmospheric Chemistry and Physics 7 (10), 2475-2487.

Matter, U., Siegmann, H.C., Burtscher, H., 1999. Dynamic field measurements of submicron particles from diesel engines. Environmental Science & Technology 33 (11), 1946-1952.

McGeehan, J.A., Yeh, S., Couch, M., Hinz, A., Otterholm, B., Walker, A.P., Blakeman, P., 2005. On the road to 2010 emissions: field test results and analysis with DPF–SCR system and ultra-low-sulfur diesel fuel. SAE Technical Paper 2005-01-3716.

Merrion, D., 2003. Heavy duty diesel emission regulations—past, present, and future. Society of Automotive Engineers Technical Paper Series No. 2003-01-0040.

Miguel, A.H., Friedlander, S.K., 1978. Distribution of benzo[a]pyrene and coronene with respect to particle size in Pasadena aerosols in the submicron range. Atmospheric Environment 12 2407-2413.

Miracolo, M.A., Presto, A.A., Lambe, A.T., Hennigan, C.J., Donahue, N.M., Kroll, J.H., Worsnop, D.R., Robinson, A.L., 2010. Photo-oxidation of low-volatility organics found in motor vehicle emissions: production and chemical evolution of organic aerosol mass. Environmental Science and Technology 44 (5), 1638-1643.

Misra, C., Kim, S., Shen, S., Sioutas, C., 2002. A high flow rate, very low pressure drop impactor for inertial separation of ultrafine from accumulation mode particles. Journal of Aerosol Science 33 (5), 735-752.

Moore, K.F., Ning, Z., Ntziachristos, L., Schauer, J.J., Sioutas, C., 2007. Daily variation in the properties of urban ultrafine aerosol - part I: physical characterization and volatility. Atmospheric Environment 41 (38), 8633-8646.

Naeher, L.P., Brauer, M., Lipsett, M., Zelikoff, J.T., Simpson, C.D., Koenig, J.Q., Smith, K.R., 2007. Woodsmoke health effects: A review. Inhalation Toxicology 19 (1), 67-106.

Nico, P.S., Kumfer, B.M., Kennedy, I.M., Anastasio, C., 2009. Redox dynamics of mixed metal (Mn, Cr, and Fe) ultrafine particles. Aerosol Science and Technology 43 (1), 60-70.

Ning, Z., Geller, M.D., Moore, K.F., Sheesley, R., Schauer, J.J., Sioutas, C., 2007. Daily variation in chemical characteristics of urban ultrafine aerosols and inference of their sources. Environmental Science & Technology 41 (17), 6000-6006.

Ning, Z., Moore, K.F., Polidori, A., Sioutas, C., 2006. Field validation of the new miniature Versatile Aerosol Concentration Enrichment System (mVACES). Aerosol Science and Technology 40 (12), 1098-1110.

Novakov, T., Corrigan, C.E., 1996. Cloud condensation nucleus activity of the organic component of biomass smoke particles. Geophysical Research Letters 23 (16), 2141-2144.

Ntziachristos, L., Froines, J.R., Cho, A.K., Sioutas, C., 2007. Relationship between redox activity and chemical speciation of size-fractionated particulate matter. Particle and Fibre Toxicology 4 (5), doi:10.1186/1743-8977-4-5.

Obrien, P.J., 1991. Molecular mechanisms of quinone cytotoxicity. Chemico-Biological Interactions 80 (1), 1-41.

Pakbin, P., Ning, Z., Schauer, J.J., Sioutas, C., 2009. Characterization of particle bound organic carbon from diesel vehicles equipped with advanced emission control technologies. Environmental Science & Technology 43 (13), 4679-4686.

Perraudin, E., Budzinski, H., Villenave, E., 2005. Analysis of polycyclic aromatic hydrocarbons adsorbed on particles of atmospheric interest using pressurised fluid extraction. Analytical and Bioanalytical Chemistry 383 (1), 122-131.

Peters, A., Veronesi, B., Calderón-Garcidueñas, L., Gehr, P., Chen, L.C., Geiser, M., Reed, W., Rothen-Rutishauser, B., Schürch, S., Schulz, H., 2006. Translocation and potential neurological effects of fine and ultrafine particles a critical update. Particle and Fibre Toxicology 3 (13), doi:10.1186/1743-8977-3-13.

Phuleria, H.C., Fine, P.M., Zhu, Y.F., Sioutas, C., 2005. Air quality impacts of the October 2003 Southern California wildfires. Journal of Geophysical Research-Atmospheres 110 (D7), D07S20, doi:10.1029/2004JD004626.

Pierce, R.C., Katz, M., 1975. Dependency of Polynuclear Aromatic Hydrocarbon Content on Size Distribution of Atmospheric Aerosols. Environ. Sci. Technol. 9 (4), 347-353.

Polidori, A., Hu, S., Biswas, S., Delfino, R.J., Sioutas, C., 2008. Real-time characterization of particle-bound polycyclic aromatic hydrocarbons in ambient aerosols and from motor-vehicle exhaust. Atmospheric Chemistry and Physics 8 (5), 1277-1291.

Reaney, S.H., Smith, D.R., 2005. Manganese oxidation state mediates toxicity in PC12 cells. Toxicology and Applied Pharmacology 205 (3), 271-281.

Riediker, M., Cascio, W.E., Griggs, T.R., Herbst, M.C., Bromberg, P.A., Neas, L., Williams, R.W., Devlin, R.B., 2004. Particulate matter exposure in cars is associated with cardiovascular effects in healthy young men. American Journal of Respiratory and Critical Care Medicine 169 (8), 934-940.

Riipinen, I., Pierce, J.R., Donahue, N.M., Pandis, S.N., 2010. Equilibration time scales of organic aerosol inside thermodenuders: evaporation kinetics versus thermodynamics. Atmospheric Environment 44, 597- 607.

Robinson, A.L., Donahue, N.M., Shrivastava, M.K., Weitkamp, E.A., Sage, A.M., Grieshop, A.P., Lane, T.E., Pierce, J.R., Pandis, S.N., 2007. Rethinking organic aerosols: semivolatile emissions and photochemical aging. Science 315 (5816), 1259-1262.

Rodrigueza, C.E., Fukutoa, J.M., Taguchic, K., Froines, J., Cho, A.K., 2005. The interactions of 9,10-phenanthrenequinone with glyceraldehyde-3-phosphate dehydrogenase (GAPDH), a potential site for toxic actions. Chemico-Biological Interactions 155, 97-110.

Rose, A.L., Waite, T.D., 2005. Reduction of organically complexed ferric iron by superoxide in a simulated natural water. Environmental Science & Technology 39 (8), 2645-2650.

Rusznak, C., Devalia, J.L., Davies, R.J., 1994. The Impact of Pollution on Allergic Disease. Allergy 49 (18), 21-27.

Saarikoski, S., Sillanpaa, M., Sofiev, M., Timonen, H., Saarnio, K., Teinela, K., Karppinen, A., Kukkonen, J., Hillamo, R., 2007. Chemical composition of aerosols during a major biomass burning episode over northern Europe in spring 2006: Experimental and modelling assessments. Atmospheric Environment 41 (17), 3577-3589.

Saldiva, P.H.N., Clarke, R.W., Coull, B.A., Stearns, R.C., Lawrence, J., Murthy, G.G.K., Diaz, E., Koutrakis, P., Suh, H., Tsuda, A., Godleski, J.J., 2002. Lung inflammation induced by concentrated ambient air particles is related to particle composition. American Journal of Respiratory and Critical Care Medicine 165 (12), 1610-1617.

Samet, J.M., Dominici, F., Curriero, F.C., Coursac, I., Zeger, S.L., 2000. Fine particulate air pollution and mortality in 20 US Cities, 1987-1994. New England Journal of Medicine 343 (24), 1742-1749.

Sanders, P.G., Xu, N., Dalka, T.M., Maricq, M.M., 2003. Airborne brake wear debris: Size distributions, composition, and a comparison of dynamometer and vehicle tests. Environmental Science & Technology 37 (18), 4060-4069.

Sardar, S.B., Fine, P.M., Mayo, P.R., Sioutas, C., 2005. Size-fractionated measurements of ambient ultrafine particle chemical composition in Los Angeles using the NanoMOUDI. Environmental Science & Technology 39 (4), 932-944.

Schauer, J.J., 2003. Evaluation of elemental carbon as a marker for diesel particulate matter. Journal of Exposure Analysis and Environmental Epidemiology 13 (6), 443-453.

Schauer, J.J., Kleeman, M.J., Cass, G.R., Simoneit, B.R.T., 2001. Measurement of emissions from air pollution sources. 3. C-1-C-29 organic compounds from fireplace combustion of wood. Environmental Science & Technology 35 (9), 1716-1728.

Schauer, J.J., Mader, B.T., Deminter, J.T., Heidemann, G., Bae, M.S., Seinfeld, J.H., Flagan, R.C., Cary, R.A., Smith, D., Huebert, B.J., Bertram, T., Howell, S., Kline, J.T., Quinn, P., Bates, T., Turpin, B., Lim, H.J., Yu, J.Z., Yang, H., Keywood, M.D., 2003. ACE-Asia intercomparison of a thermal-optical method for the determination of particle-phase organic and elemental carbon. Environmental Science & Technology 37 (5), 993-1001.

Schoonen, M.A.A., Cohn, C.A., Roemer, E., Laffers, R., Simon, S.R., O'Riordan, T., 2006. Mineral-induced formation of reactive oxygen species. Medical Mineraology and Geochemistry 64 179-221.

Seinfeld, J.H., Pandis, S.N., 2006. Atmospheric chemistry and physics: from air pollution to climate change. New Jersey: John Wiley and Sons, Inc.

Shafer, M.M., Perkins, D.A., Antkiewicz, D.S., Stone, E.A., Quraishi, T.A., Schauer, J.J., 2010. Reactive oxygen species activity and chemical speciation of size-fractionated atmospheric particulate matter from Lahore, Pakistan: an important role for transition metals. Journal of Environmental Monitoring 12 (3), 704-715.

Sheesley, R.J., Schauer, J.J., Garshick, E., Laden, F., Smith, T.J., Blicharz, A.P., Deminter, J.T., 2009. Tracking personal exposure to particulate diesel exhaust in a diesel freight terminal using organic tracer analysis. Journal of Exposure Science and Environmental Epidemiology 19 (2), 172-186.

Shinyashiki, M., Eiguren-Fernandez, A., Schmitz, D.A., Di Stefano, E., Li, N., Linak, W.P., Cho, S.H., Froines, J.R., Cho, A.K., 2009. Electrophilic and redox properties of diesel exhaust particles. Environmental Research 109 (3), 239-244.

Siefert, R.L., Pehkonen, S.O., Erel, Y., Hoffmann, M.R., 1994. Iron Photochemistry of Aqueous Suspensions of Ambient Aerosol with Added Organic-Acids. Geochimica Et Cosmochimica Acta 58 (15), 3271-3279.

Siefert, R.L., Webb, S.M., Hoffmann, M.R., 1996. Determination of photochemically available iron in ambient aerosols. Journal of Geophysical Research-Atmospheres 101 (D9), 14441-14449.

Simoneit, B.R.T., Schauer, J.J., Nolte, C.G., Oros, D.R., Elias, V.O., Fraser, M.P., Rogge, W.F., Cass, G.R., 1999. Levoglucosan, a tracer for cellulose in biomass burning and atmospheric particles. Atmospheric Environment 33 (2), 173-182.

Singh, M., Jaques, P.A., Sioutas, C., 2002. Size distribution and diurnal characteristics of particle-bound metals in source and receptor sites of the Los Angeles Basin. Atmospheric Environment 36 (10), 1675-1689.

Stayner, L., Dankovic, D., Smith, R., Steenland, K., 1998. Predicted lung cancer risk among miners exposed to diesel exhaust particles. American Journal of Industrial Medicine 34 (3), 207-219.

Steerenberg, P.A., Zonnenberg, J.A.J., Dormans, J.A.M.A., Joon, P.N.T., Wouters, I.M., van Bree, L., Scheepers, P.T.J., Van Loveren, H., 1998. Diesel exhaust particles induced release of interleukin 6 and 8 by (primed) human bronchial epithelial cells (BEAS 2B) in vitro. Experimental Lung Research 24 (1), 85-100.

Sternbeck, J., Sjodin, A., Andreasson, K., 2002. Metal emissions from road traffic and the influence of resuspension - results from two tunnel studies. Atmospheric Environment 36 (30), 4735-4744.

Stone, E.A., Snyder, D.C., Sheesley, R.J., Sullivan, A.P., Weber, R.J., Schauer, J.J., 2008. Source apportionment of fine organic aerosol in Mexico City during the MILAGRO experiment 2006. Atmospheric Chemistry and Physics 8 (5), 1249-1259.

Subramanyam, V., Valsaraj, K.T., Thibodeaux, L.J., Reible, D.D., 1994. Gas-to-particle partitioning of polycyclic aromatic hydrocarbons in an urban atmosphere. Atmospheric Environment 28 (19), 3083-3091.

Thomaidis, N.S., Bakeasa, E.B., Siskos, P.A., 2003. Characterization of lead, cadmium, arsenic and nickel in PM2.5 particles in the Athens atmosphere, Greece. Chemosphere 52 (6), 959-966.

Thompson, K.H., Tsukada, Y., Xu, Z.M., Battell, M., McNeill, J.H., Orvig, C., 2002. Influence of chelation and oxidation state on vanadium bioavailability, and their effects on tissue concentrations of zinc, copper, and iron. Biological Trace Element Research 86 (1), 31-44.

Thorning, D.R., Howard, M.L., Hudson, L.D., Schumacher, R.L., 1982. Pulmonary Responses to Smoke Inhalation - Morphologic Changes in Rabbits Exposed to Pine Wood Smoke. Human Pathology 13 (4), 355-364.

Tischer, C.A., Oliveira, M.B.M., Reicher, F., Iacomini, M., Petkowicz, C.L.O., Duarte, M.E.R., Noseda, M.D., Gorin, P.A.J., 2004. Complexation of vanadium (V) oxyanions with hexopyranose- and mannopyranoseuronic acid-containing polysaccharides: stereochemical considerations. Carbohydrate Research 339 (4), 771-775.

Tran-Duc, T., Thamwattana, N., Cox, B.J., Hill, J.M., 2010. Adsorption of polycyclic aromatic hydrocarbons on graphite surfaces. Computational Materials Science 49 (4), S307-S312.

Vaaraslahti, K., Virtanen, A., Ristimaki, J., Keskinen, J., 2004. Nucleation mode formation in heavy-duty diesel exhaust with and without a particulate filter. Environ Sci Technol 38 (18), 4884-4890.

Valko, M., Morris, H., Cronin, M.T.D., 2005. Metals, toxicity and oxidative stress. Current Medicinal Chemistry 12 (10), 1161-1208.

Venkataraman, C., Thomas, S., Kulkarni, P., 1999. Size distributions of polycyclic aromatic hydrocarbons - Gas/particle partitioning to urban aerosols. Journal of Aerosol Science 30 (6), 759-770.

Verma, V., Polidori, A., Schauer, J.J., Shafer, M.M., Cassee, F.R., Sioutas, C., 2009. Physicochemical and toxicological profiles of particulate matter in Los Angeles during the October 2007 Southern California wildfires. Environmental Science & Technology 43 (3), 954-960.

Verma, V., Shafer, M.M., Schauer, J.J., Sioutas, C., 2010. Contribution of transition metals in the reactive oxygen species activity of PM emissions from retrofitted heavy-duty vehicles. Atmospheric Environment 44 (39), 5165-5173.

Villalobos-Pietrini, R., Amador-Munoz, O., Waliszewski, S., Hernandez-Mena, L., Munive-Colin, Z., Gomez-Arroyo, S., Bravo-Cabrera, J.L., Frias-Villegas, A., 2006. Mutagenicity and polycyclic aromatic hydrocarbons associated with extractable organic matter from airborne particles <= 10 mu m in southwest Mexico City. Atmospheric Environment 40 (30), 5845-5857.

Wang, C.F., Chang, C.Y., Tsai, S.F., Chiang, H.L., 2005. Characteristics of road dust from different sampling sites in northern Taiwan. Journal of the Air & Waste Management Association 55 (8), 1236-1244.

Watanabe, N., Oonuki, Y., 1999. Inhalation of diesel engine exhaust affects spermatogenesis in growing male rats. Environmental Health Perspectives 107 (7), 539-544.

Welch, K.D., Davis, T.Z., Van Eden, M.E., Aust, S.D., 2002. Deleterious iron-mediated oxidation of biomolecules. Free Radical Biology and Medicine 32 (7), 577-583.

Westerdahl, D., Wang, X., Pan, X.C., Zhang, K.M., 2009. Characterization of on-road vehicle emission factors and microenvironmental air quality in Beijing, China. Atmospheric Environment 43 (3), 697-705.

Winterbourn, C.C., 1987. The ability of scavengers to distinguish OH. production in the iron-catalyzed Haber-Weiss reaction - comparison of 4 assays for OH. Free Radical Biology and Medicine 3 (1), 33-39.

Xia, T., Korge, P., Weiss, J.N., Li, N., Venkatesen, M.I., Sioutas, C., Nel, A., 2004. Quinones and aromatic chemical compounds in particulate matter induce mitochondrial dysfunction: Implications for ultrafine particle toxicity. Environmental Health Perspectives 112 (14), 1347-1358.

Yan, B.Z., M.; Hu,Y. T.; Lee,S.; Kim,H. K.; Russell, A. G.; , 2007. Organic composition of carbonaceous aerosols in an aged prescribed fire plume Atmos. Chem. Phys. Discuss. 7 18015–18042, 12007.

Yin, X.J.J., Dong, C.C., Ma, J.Y.C., Roberts, J.R., Antonini, J.M., Ma, J.K.H., 2007. Suppression of phagocytic and bactericidal functions of rat alveolar macrophages by the organic component of diesel exhaust particles. Journal of Toxicology and Environmental Health-Part a-Current Issues 70 (9-10), 820-828.

Zhang, Q., Stanier, C.O., Canagaratna, M.R., Jayne, J.T., Worsnop, D.R., Pandis, S.N., Jimenez, J.L., 2004a. Insights into the chemistry of new particle formation and growth events in Pittsburgh based on aerosol mass spectrometry. Environmental Science & Technology 38 (18), 4797-4809.

Zhang, R.Y., Suh, I., Zhao, J., Zhang, D., Fortner, E.C., Tie, X.X., Molina, L.T., Molina, M.J., 2004b. Atmospheric new particle formation enhanced by organic acids. Science 304 (5676), 1487-1490.

Zhang, Y.X., Schauer, J.J., Shafer, M.M., Hannigan, M.P., Dutton, S.J., 2008. Source apportionment of in vitro reactive oxygen species bioassay activity from atmospheric particulate matter. Environmental Science & Technology 42 (19), 7502-7509.

Zhao, Y., Bein, K.J., Wexler, A.S., Misra, C., Fine, P.M., Sioutas, C., 2005. Field evaluation of the versatile aerosol concentration enrichment system (VACES) particle concentrator coupled to the rapid single-particle mass spectrometer (RSMS-3). Journal of Geophysical Research-Atmospheres 110 (D07S02), doi:10.1029/2004JD004644.

Zheng, M., Fang, M., 2000. Particle-associated polycyclic aromatic hydrocarbons in the atmosphere of Hong Kong. Water Air and Soil Pollution 117, 175-189.

Zhu, Y.F., Hinds, W.C., Kim, S., Sioutas, C., 2002. Concentration and size distribution of ultrafine particles near a major highway. Journal of the Air & Waste Management Association 52 (9), 1032-1042.

Appendix

Peer-reviewed Publications List

1. **Verma, V.**, Pakbin, P., Cheung, K.L., Cho, A.K., Schauer, J.J, Shafer, M.M, Kleinman, M.T., and Sioutas, C., 2010. Physicochemical and oxidative characteristics of semi-volatile components of quasi-ultrafine particles in an urban atmosphere. *Atmospheric Environment* doi:10.1016/j.atmosenv.2010.10.044 (in press).

2. **Verma, V.**, Shafer, M.M., Schauer, J.J. and Sioutas, C., 2010. Contribution of transition metals in the reactive oxygen species activity of PM emissions from retrofitted heavy-duty vehicles. *Atmospheric Environment*, 44 (39), 5165-5173.

3. Moore, K.F., **Verma, V.**, Minguillon, M.C., Sioutas, C., 2010. Inter- and intra-community variability in continuous coarse particulate matter ($PM_{10-2.5}$) concentrations in the Los Angeles area. *Aerosol Science and Technology* 44 (7), 526-540.

4. **Verma, V.**, Ning, Z., Cho, A.K., Schauer, J.J., Shafer, M.M., Sioutas, C., 2009. Redox activity of urban quasi-ultrafine particles from primary and secondary sources. *Atmospheric Environment* 43 (40), 6360-6368.

5. Biswas, S., **Verma, V.**, Schauer, J.J., Cassee, F.R., Cho, A.K., Sioutas, C., 2009. Oxidative potential of semi-volatile and non volatile particulate matter (PM) from heavy-duty vehicles retrofitted with emission control technologies. *Environmental Science & Technology* 43 (10), 3905-3912.

6. **Verma, V.**, Polidori, A., Schauer, J.J., Shafer, M.M., Cassee, F.R., Sioutas, C., 2009. Physicochemical and toxicological profiles of particulate matter in Los Angeles during the October 2007 southern California wildfires. *Environmental Science & Technology* 43 (3), 954-960.

7. Biswas, S., **Verma, V.**, Schauer, J.J., Sioutas, C., 2009. Chemical speciation of PM emissions from heavy-duty diesel vehicles equipped with diesel particulate filter (DPF) and selective catalytic reduction (SCR) retrofits. *Atmospheric Environment* 43 (11), 1917-1925.

8. Biswas, S., Hu, S.H., **Verma, V.**, Herner, J.D., Robertson, W.H., Ayala, A., Sioutas, C., 2008. Physical properties of particulate matter (PM) from late model heavy-duty diesel vehicles operating with advanced PM and NOx emission control technologies. *Atmospheric Environment* 42 (22), 5622-5634.